Report
P-17-04
July 2018

Hydraulic interaction between engineered and natural barriers

Task 8B-D and F of SKB Task Forces GWFTS and EBS

Klaus-Peter Kröhn

SVENSK KÄRNBRÄNSLEHANTERING AB

SWEDISH NUCLEAR FUEL
AND WASTE MANAGEMENT CO

Box 3091, SE-169 03 Solna
Phone +46 8 459 84 00
skb.se

SVENSK KÄRNBRÄNSLEHANTERING

ISSN 1651-4416
SKB P-17-04
ID 1589517

July 2018

Hydraulic interaction between engineered and natural barriers

Task 8B-D and F of SKB Task Forces GWFTS and EBS

Klaus-Peter Kröhn
Gesellschaft für Anlagen- und Reaktorsicherheit (GRS) gGmbH

Keywords: Crystalline rock, Fracture flow, Bentonite, Buffer, Re-saturation, Final repository, High-level waste, Long-term safety.

This report concerns a study which was conducted for Svensk Kärnbränslehantering AB (SKB). The conclusions and viewpoints presented in the report are those of the author. SKB may draw modified conclusions, based on additional literature sources and/or expert opinions.

Data in SKB's database can be changed for different reasons. Minor changes in SKB's database will not necessarily result in a revised report. Data revisions may also be presented as supplements, available at www.skb.se.

A pdf version of this document can be downloaded from www.skb.se.

© 2018 Svensk Kärnbränslehantering AB

Abstract

The Task Force on Groundwater Flow and Transport of Solutes (TF GWFTS) and the Task Force on Engineered Barrier Systems (TF EBS) both established by the Svensk Kärnbränslehantering AB (SKB) have defined the so-called Task 8 to investigate the hydraulic interaction of the granitic host rock at the Hard Rock Laboratory at Äspö and the bentonite clay buffer in a deep geological repository. Task 8 a–d ran parallel to the related BRIE-project (Bentonite Rock Interaction Experiment) at the Äspö Hard Rock Laboratory (HRL). The BRIE-project was concerned with an in-situ test where two boreholes were drilled from a tunnel floor and filled with compacted bentonite.

Task 8 encompassed obviously characterizing the groundwater flow field as well as simulating bentonite re-saturation. Described here is an approach to solve the problem by decoupling both aspects. Groundwater flow was simplified to a steady-state single-phase flow model including discretely described large fractures. Modelling was performed with the code d^3f. Outflow data from the rock was then assigned to the inflow boundary of the alternative re-saturation model realized in the experimental code VIPER.

With increasing knowledge about the site the upcoming data and the accompanying flow modelling indicated an inherent problem with predictions for the site and borehole characterization. Specific (deterministic) answers were sought from a flow domain that contains a relevant water-bearing fracture network which is only known in terms of geostatistics. While the overall flow regime could be represented in the final model the results were therefore not detailed below the scale of the boreholes.

Early data from the flow model had indicated that water uptake of the bentonite at the bentonite-matrix contact would occur under restricted access to water. This had not been considered in laboratory tests up to then and also not in VIPER. A new appropriate boundary condition was developed and implemented. The time until full saturation in a horizontal disk was calculated for low inflow from the matrix and high inflow from a fracture. Also the sensitivity of the re-saturation model against uncertainties in the inflow data from a flow model was analyzed.

In the framework of Task 8f the bentonite re-saturation model was finally checked against sensor data and the extensive post-test data of the BRIE. The water uptake at water bearing fractures which follows the uptake under unrestricted access of bentonite to water could be reproduced satisfyingly in the model. However, no unambiguous interpretation of data concerning uptake from the matrix which was assumed to provide insight into uptake under a limited water supply from the rock was possible.

Executive summary

The Task Force on Groundwater Flow and Transport of Solutes (TF GWFTS) and the Task Force on Engineered Barrier Systems (TF EBS) both established by the Svensk Kärnbränslehantering AB (SKB) have defined the so-called Task 8 to investigate the hydraulic interaction of the granitic host rock at the Hard Rock Laboratory at Äspö and the bentonite clay buffer in a deep geological repository. More precisely scientific understanding of the exchange of water across the bentonite-rock interface and better means of predicting the wetting of the bentonite buffer were asked for.

A concrete background for this exercise was construction and performance of the Buffer-Rock-Interaction-Experiment (BRIE). In the separate short TASO-tunnel boreholes were drilled for characterizing the flow field and for determining two suitable test boreholes. For the experiment one of these boreholes was supposed to be fracture-free while the other was intended to provide access to at least one water-bearing fracture. The test boreholes were then widened to accommodate test packages of pre-compacted bentonite so-called “parcels” including an array of sensors.

The Task was divided into subtasks 8a to 8d beginning with a theoretical study of the phenomenon (Task 8a) followed by three stages of modelling the BRIE based on increasing knowledge and data (Tasks 8b to 8d) as site characterization and the experiment itself progressed. However, at the end of Task 8d there was no data for the water uptake in the experiment available yet. In the course of activities for Task 8d it was also decided to add a modelling benchmark concerning a water uptake test performed in the laboratory. Even later yet Task 8f was defined as an exercise to check the developed models against the measurements.

Task 8 encompassed obviously characterizing the groundwater flow field as well as simulating bentonite re-saturation. Described here is an approach to solve the problem by decoupling both aspects. Groundwater flow was simplified to steady-state single-phase flow. Large fractures were incorporated as deterministic features in the model. The influence of background fractures was taken into account by an increased permeability value for the matrix. Generally it was looked to it that geometry and boundary conditions in the model were used as close as possible to the task description. Modelling was performed with the code d^3f.

Calibrating the flow model showed that there is a considerable contribution of background fractures to the effective matrix permeability. It had been increased by three orders of magnitude in comparison to the permeability values for the undisturbed matrix. While the overall result of the calibration was satisfying the measured outflow rates were not all captured by the model indicating significant inhomogeneities on the scale of the borehole field.

Outflow data from the rock was then assigned to the inflow boundary of a re-saturation model for the bentonite. Only three processes were considered here: vapour diffusion in the pore space, diffusion of water in the interlamellar space and an instantaneous exchange of water between these two spaces controlled by an adsorption isotherm. This conceptual model was realized in the code VIPER. The code is still experimental despite the fact that the validity of the alternative conceptual model has already been successfully demonstrated. It is therefore presently restricted to one-dimensional and axisymmetric geometries.

Water uptake rates for a bentonite with free access to water were calculated and compared with the outflow measurements at the BRIE-site showing clearly that a considerable part of the buffer material would re-saturate under restricted access to water. Restricting water inflow into the bentonite leads to highly non-linear model responses in terms of water content distributions and re-saturation times. Estimation of uncertainties ensuing from variations of the restricted inflow depends strongly on the reference inflow value. Axisymmetric water uptake was therefore predicted to take between 232 and 515 days. Using better adapted and calibrated models these values changed to 215 days and 11.3 years, respectively.

The model of the additional water uptake test showed a very good match with the measured data. It required only a little parameter adjustment showing that the envisaged buffer material had been well characterized for the VIPER-model. This gave also confidence in the predictive models for the BRIE.

Sammanfattning

Task Force on Groundwater Flow and Transport of Solutes (TF GWFTS) och Task Force on Engineered Barrier Systems (TF EBS), båda under ledning av Svensk Kärnbränslehantering AB (SKB), har definierat modelleringsuppgiften Task 8 för att undersöka den hydrauliska interaktionen mellan granitiskt berg- och bentonitlera för tillämpningen som bufferten i ett djupt geologiskt förvar. Task 8 a–d utfördes parallellt med det relaterade BRIE-projektet (Bentonite Rock Interaction Experiment) som utfördes vid Äspö Hard Rock Laboratory (HRL). BRIE-projektet handlade om ett in situ-test där två borrhål borras från tunnelgolvet och fylldes med kompakterad bentonit.

Task 8 omfattade karaktärisering av grundvattenflödesfältet samt simulering av bentonitmättnad. Det som beskrivs här är ett sätt att lösa problemet genom att ta bort kopplingen mellan dessa båda aspekter. Grundvattenflödet förenklades till en steady-state enfasflödesmodell som inkluderar diskret beskrivna stora sprickor. Modellering utfördes med koden d3f. Utflödesdata från berget tilldelades sedan till inflödesranden för den alternativa återmättnadsmodellen som implementerades i experimentkoden VIPER.

Med ökande kunskaper om experimentplatsen indikerade efterkommande data och den därmed följande flödesmodelleringen ett inneboende problem med prediktionerna av plats- och borrhålskaraktärisering. Specifika (deterministiska) svar söktes från en flödesdomän som innehåller ett relevant vattenförande spricknätverk som endast är känt när det gäller dess geostatistik. Medan den totala flödesregimen kunde representeras i den slutliga modellen var resultaten därför inte detaljerade under borrhålsskalan.

Tidiga data från flödesmodellen hade indikerat att vattenupptagning i bentoniten vid bentonit-matriskontakten skulle inträffa även under begränsad tillgång till vatten. Detta hade inte beaktats i laboratorietester fram till dess och inte heller i VIPER. Ett nytt lämpligt randvillkor utvecklades och implementerades. Tiden för full mättnad i en horisontell disk beräknades för låg tillströmning från matrisen och högt inflöde från en spricka. Dessutom analyserades känsligheten hos återmättnadsmodellen för osäkerheter i inflödesdata från en flödesmodell.

Inom ramverket för Task 8f jämfördes återmättnadsmodellen för bentonit slutligen mot erhållna sensordata och de omfattande data som erhölls efter BRIE. Vattenupptaget vid vattenförande sprickor kan reproduceras tillfredsställande i modellen. Det följer vattenupptaget som antas gälla under förutsättningen obegränsad tillgång av vatten till bentonit. Emellertid var det inte möjligt att tydligt tolka de data som avser vattenupptaget från matrisen. Det senare skulle ha kunnat ge en insikt i upptag under en begränsad vattentillförsel från berget.

Contents

1 Introduction

1.1 Background

The Swedish Svensk Kärnbränslehantering AB (SKB) has established the Task Force on Groundwater Flow and Transport of Solutes (TF GWFTS) in 1992 and the Task Force on Engineered Barrier Systems (TF EBS) in 2004. Each of these Task Forces builds a frame for an international group of participants to work on specific problems concerning flow and transport in crystalline rock and the behaviour of the bentonite buffer in a deep geological repository, respectively. In collaboration representatives of both Task Forces have come up with the definition of the so-called Task 8, a compilation of several subtasks – called 8a, 8b, etc. – with a view to the hydraulic interaction of the granitic host rock and the bentonite clay buffer (Vidstrand et al. 2017).

Task 8 a–d ran parallel to the related BRIE-project (Bentonite Rock Interaction Experiment) at the Äspö Hard Rock Laboratory (HRL). The BRIE-project was concerned with an in-situ test where two boreholes were drilled from a tunnel floor cutting supposedly at least through one large and one minor fracture and filled with bentonite. The objective of this experiment was to measure a) water uptake of the bentonite via different water flow paths – i. e. fractures and rock matrix – and b) the reaction of the flow system in the rock. The procedure for finding and characterizing a suitable site for the test was also part of Task 8. Task 8 included predictive as well as interpretive modelling parallel to the on-going BRIE. Task 8d was finalised, though, before the post-test investigations could produce conclusive experimental results. Task 8f was therefore defined to allow for checking the models against the test data and for modifications of the models where applicable.

While the option of granite as a host rock for a nuclear waste repository never had top priority in Germany there has nevertheless been considerable effort in the past to investigate hydraulic problems in crystalline rock. Quite recently, the development of the codes d^3f and r^3t originally designed to apply numerical cutting edge methods to modelling density-dependent groundwater flow and transport in the cap rock of salt domes was extended to incorporate fracture flow (Schneider 2012). For historical reasons this does not include multiphase flow, though.

Within the last 15 years clay stone has become a serious alternative to the originally favoured salt rock in Germany. Bentonite buffer and backfill has been envisaged for such a repository all the time. Much work has therefore gone into investigating the behaviour of bentonite, during re-saturation as well as in the post-closure phase.

Disagreeing with the established thermo-hydraulic-mechanical (THM) concept for the re-saturation of bentonite with respect to the hydraulic part, an alternative conceptual model had been derived and realized as the numerical code VIPER[1] (Kröhn 2011). Participation in research work that included fracture flow as well as bentonite re-saturation appeared thus to be a consequent step forward that would increase experience in both fields and contribute to the problem at hand. This report summarizes the work related to Task 8b to 8d and 8f.

1.2 Objectives

The overall objectives of Task 8 according to Vidstrand et al. (2017) are:

- Scientific understanding of the exchange of water across the bentonite-rock interface.
- Better predictions of the wetting of the bentonite buffer.
- Better characterisation methods of the canister boreholes.
- Better methods for establishing deposition hole criteria.

[1] VIPER is an experimental code that had been developed to test the alternative conceptual model and is thus presently still restricted to one-dimensional or 2d axisymmetric models.

These objectives were intended to be met by the following subtasks:

- Task 8a Initial – Scoping Calculation.
- Task 8b TASO – Scoping Calculation.
- Task 8c BRIE – Prediction for central deposition hole.
- Task 8d a) BRIE – Prediction of inflow and wetting of KO0017G01 and KO0018G01 based on detailed characterisation data.
  b) Water uptake test.
- Task 8e THM-modelling of the Prototype Repository.
- Task 8f Final BRIE modelling.

The subtasks were not all set up at once but one after another letting the experiences with the actual subtask influence the formulation of the next one. Definition of Task 8b made already clear that a good representation of the flow in the rock would be a prerequisite for a realistic model including the buffer. This was also reflected in the definition of the subtasks 8c1 and 8c2 as well as 8d1 and 8d2 later on. Task 8e refers to the Prototype Repository Experiment and is therefore treated in a separate report (Kröhn 2016). Task 8f in contrast concentrated exclusively on the re-saturation of the bentonite in the BRIE.

Work on Task 8 a–d was focused on the investigation of the interaction of buffer and rock. The last two objectives listed above are therefore not addressed here. The appealing aspects of Task 8 are listed below:

- Tackling a real hydraulic problem in fractured rock to test the advanced groundwater flow code. A successful model was to confirm the code as well as to contribute to the understanding of the flow regime at the BRIE site.
- Modelling of water uptake in the buffer was supposed to confirm the alternative conceptual re-saturation model.
- Coupling of both codes to investigate the influence of water uptake of the bentonite on the flow in the rock at the buffer-rock interface was intended but not executed.

As it turned out the focus of the work presented here lay more on interpretive modelling than on predictions.

1.3 Scope

Task 8a was a sensitivity analysis based on a simplified model of the BRIE test including only a tunnel section, one borehole and one fracture. Variations referred to parameters of the established THM-concept and did thus not apply to the conceptual model for re-saturation that was followed. This subtask was therefore skipped.

The formulated goals of **Task 8b** were quite detailed and appeared thus to be rather ambiguous. It was later stated in one of the meetings of the TF GWFTS that Task 8b was also simply intended to demonstrate the operational capability of the numerical tools to cope with a real case. This is what will be shown here.

During the work with Task 8b it had become apparent that there was little data referring to steady-state flow that could be compared to model results. Only consistency and plausibility of the results could therefore be checked. This unfortunate situation had improved a little for **Task 8c** where some outflow data had become available. A better representation of the fracture system as well as the geometry of the five probing boreholes called for a new flow model for the BRIE site.

With respect to the bentonite re-saturation a problem with VIPER emerged that had never been contemplated before. It had always been assumed that there would be enough water available for the water uptake process. A situation where water flow into the bentonite would be limited by the supply from the rock had not been envisaged in the conceptual model and could not be tackled

with VIPER. While working on the groundwater flow model the re-saturation concept for the bentonite was advanced to cope with this new situation so there was no contribution to the bentonite part of Task 8c.

For two reasons the flow model from Task 8c was revised again for **Task 8d**. Firstly, there were now 21 probing boreholes and the two expanded test boreholes, and, secondly, the outflow from the fractures calculated in the framework of Task 8c was too high. Since a skin-like narrow zone at drift walls that impedes flow had been observed at Stripa as well as at Äspö such a skin was included in the new model to check if it could explain the ill-fitting results from Task 8c.

The modified concept for bentonite re-saturation at restricted water supply from the rock had been implemented and become available for Task 8d. The time until full saturation defined as a minimum saturation of 95 % all over the model could therefore be predicted in an axisymmetric disk for the case of water from the rock matrix (restricted water supply) and for the case of water from a fracture (unrestricted supply). The model without uptake restrictions was also used to compare numerical results with the measurements in the **Water Uptake Test** that had been included in Task 8d.

The transient sensor data covering the test period as well as the spatial the end-of-test water content distribution in the two parcels formed the basis for interpretive modelling of the bentonite re-saturation in the framework of **Task 8f**. This work indicated a good understanding of the water uptake under unrestricted access to water but revealed at the same time some gaps in the knowledge about uptake under restricted access to water.

2 Task 8b: TASO – Scoping Calculation

2.1 Objectives

In the task description the objectives of Task 8b were stated in detail as follows: “Scoping calculations

- to determine means of incorporating unsaturated rock. Examine effects of different concepts and properties (K, K_{rel}, retention curves).
- to evaluate effects of different implementations of the rock as being fracture and matrix. Examine effects due to contrasts between matrix and fracture properties. Examines bounds for contrasts in order to reveal the significance of fractures.
- to evaluate effects of the fracture location along the deposition hole on the resulting wetting of the bentonite.
- to evaluate effects of different implementations of different boundary conditions. Examines whether the deposition tunnel is best described as a specified pressure boundary, no-flow boundary, or as a general head/flow boundary.
- to supply guidance to the field experiment on importance of bedrock fractures and matrix and where to place measurement instrumentation. “ (Vidstrand et al. 2017).

These objectives except the last one asked for the effect of variations. This suggests that a reference model including a bentonite-filled borehole had been taken for granted. However, to come up with a groundwater flow model alone proved to be a task in itself. Later at one of the TF GWFTS meetings it was stated that this task was originally intended to make the modellers from the TF EBS familiar with the influence of a real groundwater flow system, and it was acknowledged that it could also be used as a platform for testing the fracture flow capabilities of the codes involved. This is also reflected in the simple geometry that was considered in Task 8b.

Task 8b was therefore seen as an opportunity to gain experience with the groundwater flow code d^3f that had just been advanced to cope with fractured porous media. The intention was to set up a flow model for a well described domain in near-field scale, to adapt the code to a “real world” application, and thereby to contribute to characterizing the flow system at the BRIE site. However, during the active phase of Task 8b there were virtually no data from the field available that could be compared with the modelling results. Consequently, no calculations concerning the wetting of the bentonite were performed at this stage.

2.2 Approach

2.2.1 Model concept

Task 8 had apparently two aspects: water flow in the host rock and water uptake of the bentonite. Both phenomena are often described on the basis of two-phase flow. This allows formally a simultaneous calculation of flow in the rock and in the bentonite with the same numerical tools which is usually based on coupled thermo-hydro-mechanically (THM) balance equations. However, the two-phase flow concept appears to be not entirely consistent with the observed phenomena in the bentonite (e.g. Kröhn 2011). It was therefore a natural choice to use separate tools for fracture flow and for bentonite re-saturation. The concepts for both models are described in the following even if bentonite re-saturation is only simulated in Tasks 8c and 8d.

Groundwater flow

All groundwater flow models used for Task 8 contain three features: matrix, large deterministic fractures and background fractures. A hybrid approach that allows to describe discrete fractures embedded in a continuum was chosen for this problem. Since the contribution of the so-called “undisturbed matrix”

or "intact rock"[2] to the flow model is not clear it was considered necessary to include the **matrix** in a groundwater flow model as a continuum.

Large deterministic fractures are deterministically known and have a size comparable to the model domain or larger. These fractures split the continuum occupied by the matrix. Their aperture is extremely small in comparison to the model size while they are producing large amounts of water. A discrete representation of these fractures appeared to be appropriate for the flow model, especially since the flow code intended for use meets the challenge of reproducing high flow rates in the fractures in direct vicinity of slow flow in a low conducting matrix. A new approach to this effect (Grillo et al. 2010, Reiter et al. 2014, Stichel et al. 2012) had just been developed and implemented. For the lack of better knowledge the large deterministic fractures are simplified to features with constant properties within their plane.

Background fractures in contrast are defined here as fractures that are of significantly smaller scale than the model domain and are only described in terms of stochastic mathematical relations. Visual inspection of the background fractures in the TASO-, the TASD- und the TASK[3]-tunnel as well as in the two deposition boreholes had formed the bases for a statistical analysis of the local fracture network. Three fracture sets were identified this way. The results in terms of Fisher distributions are compiled in Table 2-1. Due to the rather pragmatic ad-hoc approach to gathering the necessary data the authors of the task description concede that the data leaves room for different interpretations. Uncertainties in the parameters are given as follows: Mean pole 15° (dihedral angle) and $k_r \pm 0.15$. Plots and descriptions concerning data and interpretation are given in Vidstrand et al. (2017). A basic introduction to fracture network statistics can be found in Appendix B.

Table 2-1. Fracture statistics for the TASO-tunnel; from Vidstrand et al. (2017).

Set	Orientation			Size		Spatial distribution	Intensity
	Trend	Plunge	Fisher konc.	r_0	k_r		P_{32} (r_0,∞)
set 1	280	20	10	0.25	2.6	Poisonian	1.1
set 2	20	10	15	0.25	2.6	Poisonian	2
set 3	120	50	10	0.25	2.6	Poisonian	0.75

With a view to the numerical modelling two types of background fractures can be distinguished: those who are in the order or larger than the typical element size and those who are smaller. The contribution of the smaller ones to the flow can be taken into account by increasing the matrix permeability accordingly which can introduce inhomogeneities in the permeability.

Note that for those participants in the Task Forces who had not the capability of creating an own fracture network, stochastically generated fractures in the vicinity of the first five probing boreholes were provided as depicted in Figure 2-1. This picture indicates a rather poor connectedness of the fractures and thus only little influence of the small background fractures on the flow field.

The larger background fractures pose a problem, though, in that they need to be represented by several elements. This cannot be done by an inhomogeneity within an element but requires either a discrete description or a heterogeneous permeability field. A method to convert a stochastically described fracture network to an equivalent heterogeneous continuous medium had therefore been foreseen for the flow code d^{3}f and had been envisaged to be used for Task 8. However, this method had not been available in time so that no use could be made of the statistical data. The matrix including all background fractures was therefore represented by a homogeneous medium.

[2] It is a common assumption that fractures exist on all length-scales. In Dershowitz et al. (2003) for instance it is claimed that "The connected porosity in crystalline rock is mainly made up of micro fractures …". This means there are always fractures that are smaller than any reasonably sized REV.

[3] Outside the model domain

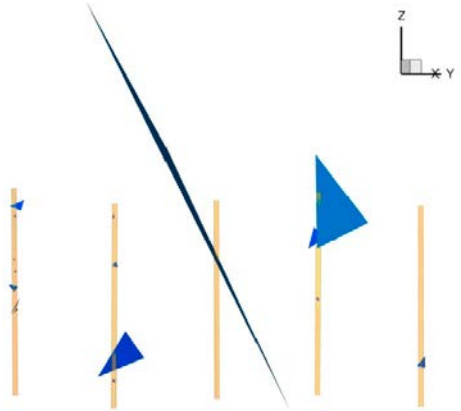

Figure 2-1. *Stochastically generated fractures at the probing boreholes (Task 8c); from Vidstrand et al. (2017).*

Bentonite re-saturation

For the re-saturation of bentonite a new approach had been developed at GRS. Here, advection of liquid water occurs only within a very narrow zone of a few millimetres at the bentonite-water contact after which evaporation is assumed. The main water transport mechanisms are then vapour diffusion in the pore space and diffusive transport of hydrated water in the interlamellar space of the clay particles. Since the particles are tightly connected it is believed that the interlamellar space of the individual particles forms a more or less continuous space parallel to the pore space. Water uptake is thus mathematically described in a double-continuum where both continua are hydraulically connected through the process of water exchange (hydration/dehydration) as depicted schematically in Figure 2-2. The experimental code VIPER was developed to test the resulting mathematical model. Theory and model qualification are described in detail in Kröhn (2011).

Water uptake of compacted bentonite directly from the vaporous phase is also a powerful re-saturation process. An increase from the initial water content of 10 % up to 17 % and a penetration depth of hydrated water to almost 3 cm within 5 days of contact with vapour saturated air has been observed in the laboratory (Kröhn 2004). This process would have been of interest for Task 8 if the rock was dried out to a certain extent.

Two-phase flow model calculations for granodiorite at the Grimsel site had shown, tough, that the water saturation in the rock drops below 50 % already at a distance of a few centimetres from the tunnel wall if the relative humidity in the tunnel is kept at 75 % (Finsterle and Pruess 1995). Relative Humidity in the TASD-tunnel from which the TASO-tunnel branches off had been monitored in 2008 and shown values between 65 % in winter up to 85 % in summer (Wass and Nyberg 2009). Direct on-site observation underpins these results in that the tunnel system at Äspö appears to be very wet with open water present along the tunnels at all times. It is therefore highly probable that the unsaturated zone in the rock at the tunnel walls is also quite narrow at the BRIE-site.

As a consequence vapour transport through the rock would only be a secondary water transport mechanism for bentonite re-saturation. The data uncertainty concerning the two-phase flow properties of the rock (cp. Appendix C) introduced considerable additional difficulties so it was decided to neglect two-phase flow effects at all and to model groundwater migration exclusively as steady-state single-phase flow.

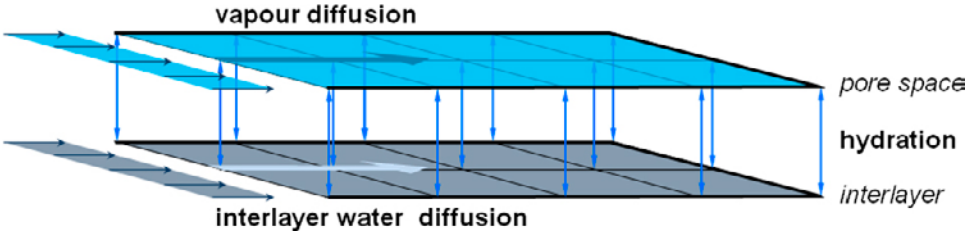

Figure 2-2. *Double-continuum approach for re-saturating bentonite; from Kröhn (2011).*

2.2.2 Approach to modelling Task 8

A wide range of models had been used in the Task Force during the work on Task 8. At the end it was therefore tried to do comparative analyses and to evaluate conceptual uncertainties. To prepare grounds for discussions a questionnaire encompassing 26 questions was sent out to each participant. It turned out that answering the questions required some additional explanations as the GRS model was somewhat off the mainstream. Since answers to these questions reflect the presently deepest insight into the conceptual approach they are compiled in Appendix G for completeness.

Since the model concept that is followed here describes flow processes in the rock and in the bentonite rather differently the hydraulic interplay of rock and buffer needed special attention. A detailed discussion of the related processes involved can be found in Section G1.1 of Appendix G. It shows that groundwater flow in the rock and bentonite re-saturation can be calculated separately provided that adequate boundary conditions are chosen. Modelling Task 8 was therefore tackled in two steps.

In the first step the flow field in the rock was characterized including the geotechnical openings in order to provide a realistic basis for calculating the water supply from the rock.

The second step was concerned with modelling water-uptake in the bentonite. A one-dimensional axial symmetric model for the bentonite in the plane at mid-height of the borehole was set up and water uptake was calculated as if the rock could supply all water that was demanded by the bentonite. This case leads to the minimum time to reach full water saturation in the bentonite.

In case maximum inflow into the bentonite exceeded the steady-state outflow from the rock the re-saturation model was rerun with a modified boundary condition where inflow into the bentonite was limited according to the calculated outflow rate from the rock. This led of course to longer re-saturation periods.

2.3 Model setup

2.3.1 Coordinates

The coordinate system used for location data in Task 8 is the Swedish RT90 system. At Äspö this system lead nevertheless to large numbers. It was therefore recommended to cut off the leading 4 digits of the x- and y-coordinates.

All coordinates provided in the task description (Vidstrand et al. 2017) and in the supplementing data-files were given as integers meaning that they were resolved only in the meter-scale. For the model some adjustments were thus necessary.

2.3.2 Model domain

The suggested model domain was cube-shaped with a side length of 40 m. The relation of the model domain to the other geotechnical structures at Äspö at a larger scale can be seen in Figure 2-3.

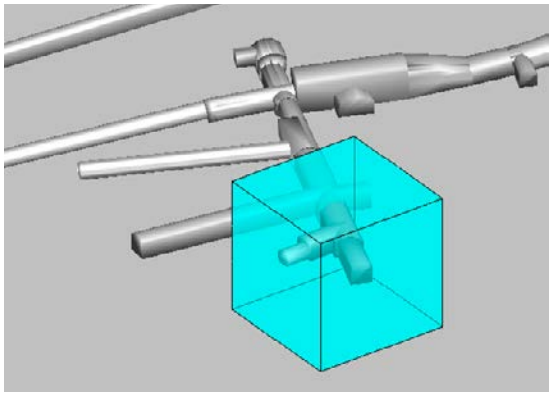

Figure 2-3. *Geometry of geotechnical structures at Äspö at a larger scale; from Vidstrand et al. (2017).*

The coordinates of the bounding eight corners are compiled in Table 2-2. The coordinates given in the task description lead to slightly off-orthogonal angles for the top and bottom quadrilaterals. In order to provide a better approximation to a cube-shaped boundary corrected values with a precision of millimetres instead of meters were calculated and listed in Table 2-2.

Table 2-2. Original and corrected coordinates for the corners of the model domain.

From task description			Corrected		
x [m]	y [m]	z [m]	x [m]	y [m]	z [m]
1551603	6367769	−396	1551572.716	6367797.500	−396
1551629	6367799	−396	1551601.000	6367825.784	−396
1551600	6367826	−396	1551629.284	6367797.500	−396
1551573	6367796	−396	1551601.000	6367769.216	−396
1551603	6367769	−436	1551572.716	6367797.500	−436
1551629	6367799	−436	1551601.000	6367825.784	−436
1551600	6367826	−436	1551629.284	6367797.500	−436
1551573	6367796	−436	1551601.000	6367769.216	−436

2.3.3 Drifts and boreholes

In the model domain two drifts had been excavated: the TASD- and the TASO-tunnel. The drifts have a plane floor and plane walls but a domed roof. The TASD-tunnel begins outside the model domain but ends within. The TASO-tunnel branches off from the TASD-tunnel and also ends within the domain. The cross-sections of both drifts are reduced at the last meters towards the end of the respective drift. Contrary to the task description these changes in the cross-section are not considered here because they are considered to be negligible in comparison to the uncertainties introduced by other factors especially permeabilities and boundary conditions.

There are two boreholes at the bottom of the TASD-tunnel representing boreholes from the previously performed Temperature Buffer Test (TBT) and the Canister Retrieval Test (CRT), respectively. They are labelled here “deposition borehole 2” and “deposition borehole 3”. Their size is not directly given but from the data it can be assumed that they have a diameter of 1.60 m and a depth of 9 m. An additional “user-defined” borehole at bottom of the TASO-tunnel with a diameter of 30 cm and a depth of 3 m, called “deposition borehole 1” is also requested by the task description but did not exist in reality.

The geometry data is provided in stl-files as ensembles of triangles representing the surface of the drifts. In case of the TASD-tunnel the description covers also the part outside the model domain. The intersection of TASD- and TASO-tunnel is not resolved. Instead, the describing triangles for the TASO-tunnel reach into the TASD-tunnel.

As with the definition of the model boundaries, the electronically provided data resolved the coordinates only with an accuracy of 1 m. This led to strange structures as shown in Figure 2-4 a). The given structures were therefore replaced by geometrical descriptions that encompass only a minimum of bounding faces as in Figure 2-4 b). The curvature of the roof was simplified to a polygon with five nodes. Boreholes were represented by hexagonal prisms. Additionally, the part of the TASD-tunnel that lies outside the model boundaries was cut off.

The remaining geometrical model contained some inaccuracies that were not considered to be important and were thus corrected in what was seen as a sensible way:

- The intersection of TASD- and TASO-tunnel was still not resolved.
- There was a little slope in the TASD-tunnel leading to an initial slanting of the floor of the TASO-tunnel.
- The top of the boreholes was only approximately consistent with the floor of the drifts.

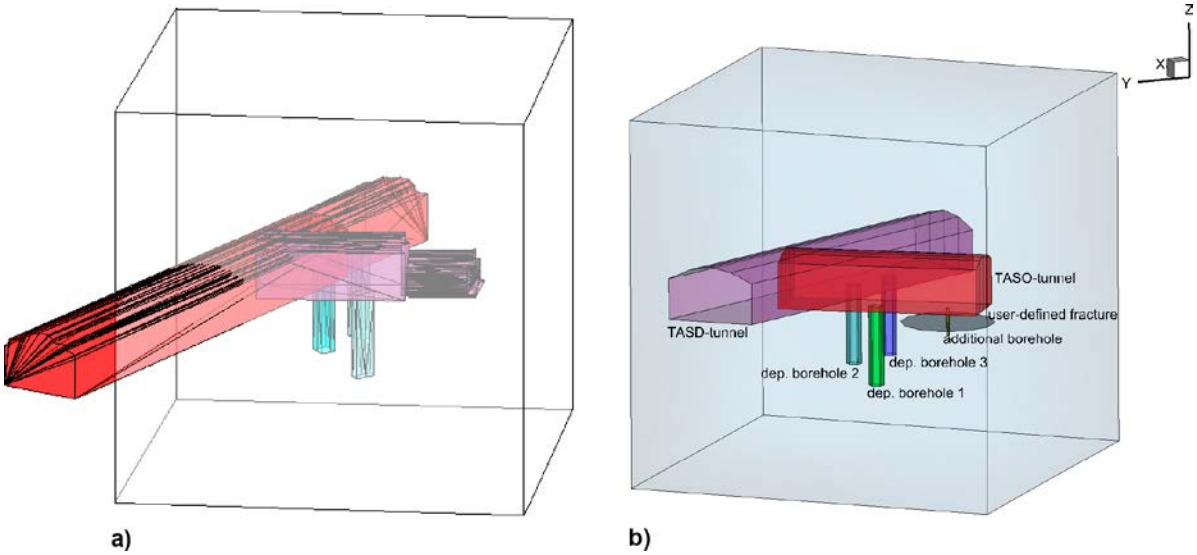

Figure 2-4. *Geometry of the openings; a) original data, b) modified data; from Kröhn (2012).*

2.3.4 Fractures

By visual inspection seven large deterministic fractures had been identified. They were assumed to be larger than the 40 m model domain. The edges of the fractures were therefore defined by the interception of fractures and the model boundaries.

Data from the task description showed that the fractures were almost but not quite plane features (see Figure 2-5 a). At a closer look they showed actually a polyhedral structure. However, the fractures were treated as planes in the model as shown in Figure 2-5 b). Due to inclination of the fractures and position within the model domain some fractures were represented by pentagons.

Additionally, a so-called user-defined single rock fracture was assigned to the model as a circular (or equivalent) feature of a diameter of 10 metres with its centre at the centre axis of the additional borehole (see Figure 2-4). This single fracture lay horizontal and was located 1.5 m below the floor of the TASO-tunnel.

Note that some interceptions of different fractures lead to geometries that provoked initial difficulties for the grid generation as well as for the numerical simulation.

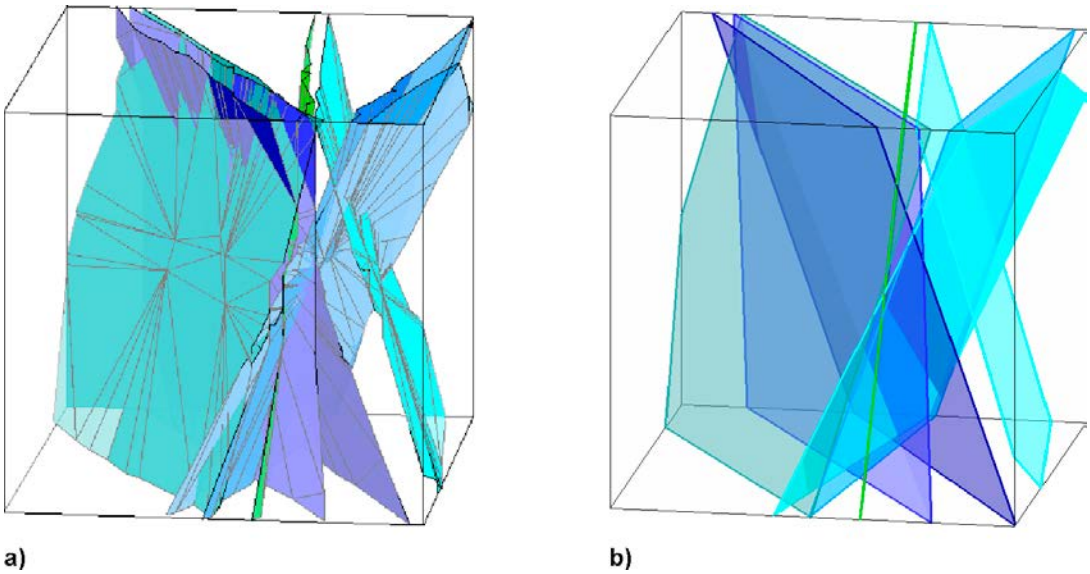

Figure 2-5. *Fracture geometry; a) original data, b) modified data; from Schneider (2012).*

2.3.5 Hydraulic properties

Three different hydraulic features had to be characterized: the rock matrix, the large deterministic fractures and the user-defined fracture. While the data for the rock was given in terms of hydraulic conductivity, transmissivity had been measured for the fractures. An aperture was assigned to the fractures in the task description to enable modelling in discrete fracture networks (DFN). If this transport aperture was also applicable for flow simulations was not clear. Nevertheless, it was used here to derive the fracture permeability. All the data are compiled in Table 2-3. Derived values are given in italics. Note that the matrix conductivity was later reduced by two orders of magnitude in the description for Tasks 8c and defined as something between 6×10^{-21} and 5.5×10^{-19} for Task 8d (cf. Vidstrand et al. 2017).

Table 2-3. Hydraulic properties of the hydraulic features.

Property	Rock matrix	Large-scale fractures	User-defined fracture
Hydraulic conductivity [m s^{-1}]	1×10^{-12}		
Permeability [m^2]	1×10^{-19}	5×10^{-7}	5×10^{-8}
Porosity [-]	1×10^{-5}	1×10^{-3}	1×10^{-3}
Transmissivity [m^2 s^{-1}]		5×10^{-8}	5×10^{-10}
Transport aperture [m]		1×10^{-5}	1×10^{-6}

Since transport of salt could be neglected (cp. Section 2.3.7) solute transport was not accounted for in the model. Concerning flow, only Darcy velocities were calculated. The porosity was therefore not of interest. As a steady-state model was considered no use was made of the storativity data.

2.3.6 Hydraulic boundary conditions

Atmospheric pressure is assigned to the surface of the drifts and boreholes. For the conditions on the outer surface of the model, an excel-file with the results of a large-scale flow simulation at Äspö was provided. Results of the large-scale model are given in terms of porosity and a pressure plots that are given in Figure 2-6.

The excel-file contained information about dynamic pressure[4], salinity and flow velocity. The data was given as point wise information from the nodes of an irregular grid which was then projected bit by bit on the outer model surface by a procedure described in Appendix A. The whole model surface is shown in Figure 2-7 including the interception of fractures and boundary faces.

The resulting pressure distribution showed a certain trend but was rather erratic on a small scale. The adopted projection procedure apparently introduced some "noise" in the results of the large-scale simulation. Flow simulations based on these boundary conditions were expected to show numerical difficulties and unphysical results. An inverse distance weighing procedure for smoothing the dynamic pressure on the boundaries was therefore implemented in the flow code. The effect of this smoothing procedure can be seen in Figure 2-8.

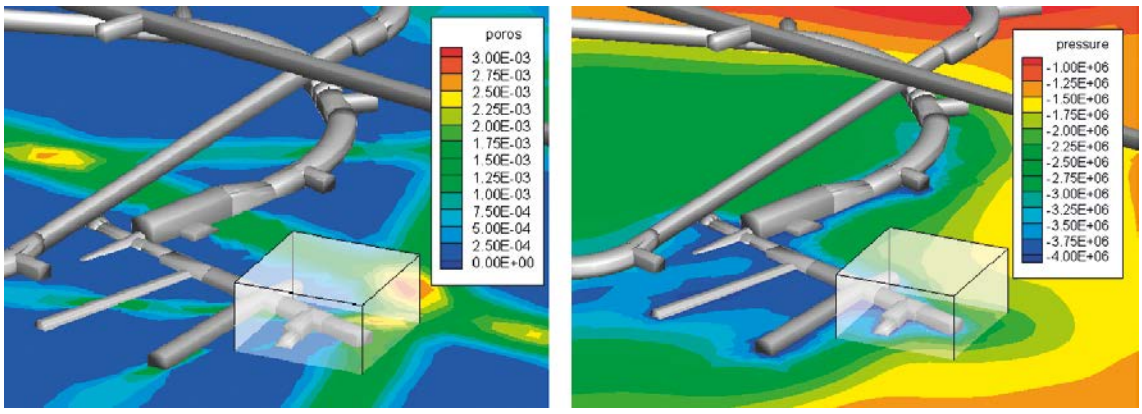

Figure 2-6. *Porosity and pressure in the large-scale Äspö model; from Vidstrand et al. (2017).*

[4] The difference between absolute pressure and hydrostatic pressure.

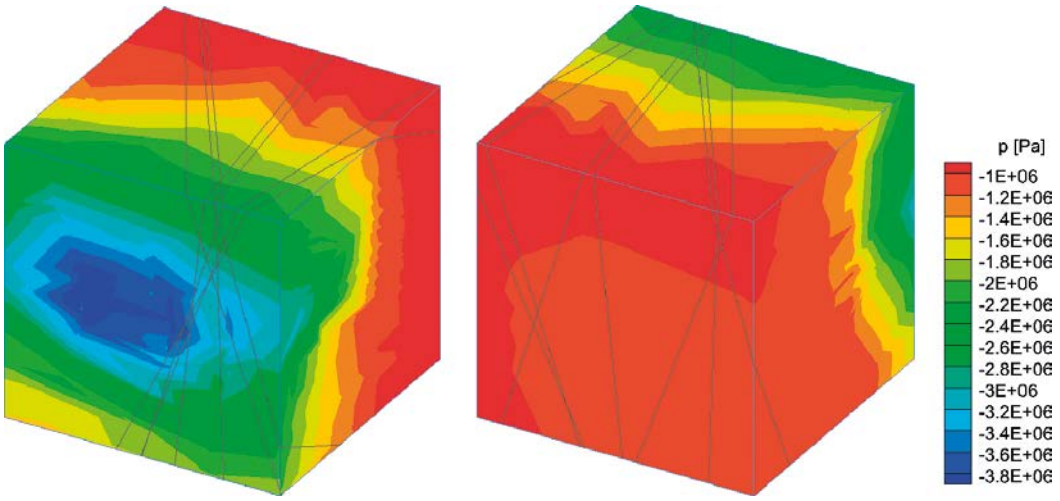

Figure 2-7. *Dynamic pressure on the model boundaries; from Kröhn (2012).*

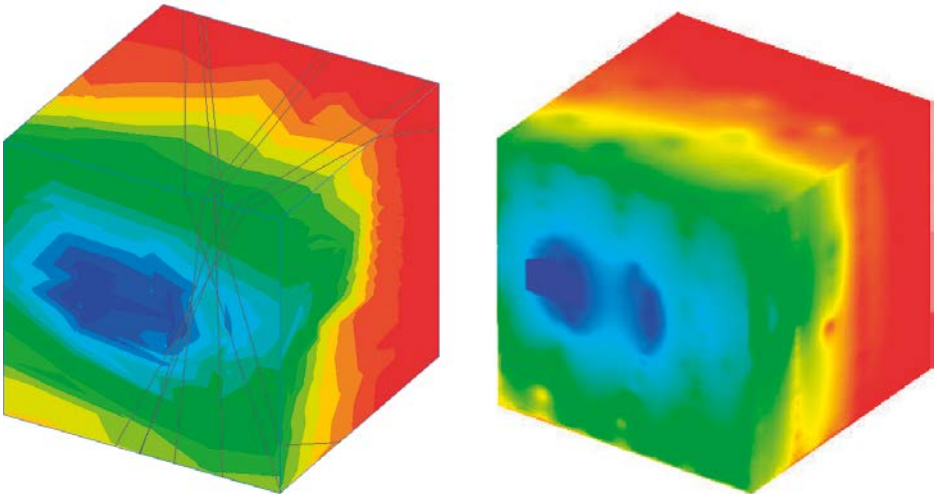

Figure 2-8. *Initial and smoothened pressure distribution on the model boundaries; from Schneider (2012).*

Note that the pressure distribution of the original simulation accounts apparently only rather loosely for the influence of the open TASD-tunnel and the fractures. Some inaccuracies concerning the local flow rates at the tunnel opening were therefore expected.

2.3.7 Influence of salinity

There is a noticeable trend in the salinity data provided by the data file as depicted in Figure 2-9. However, the maximum difference amounts to less than 0.1 % salinity. In the light of the overall model uncertainties the effect from the varying density can therefore safely be neglected.

2.3.8 Numerical grid

The first attempt on the grid for the coarse grid solver was performed with the ProMesh3-Tool (Reiter et al. 2012). The grid consisted of 12 634 nodes and 62 175 elements. Figure 2-10 a) shows the model surface where the TASD-tunnel cuts through the model surface. The intersections of the fractures with the model boundary are visible as straight lines on the surface. A vertical cross-section through the model is shown in Figure 2-10 b). Both drifts can be identified by the characteristic cross-sections as well as the coloured fractures. Figure 2-10 c) and Figure 2-10 d) represent horizontal cross-sections in the plane of the drifts, one including the 3d-elements for the rock matrix and one showing only fractures and surfaces.

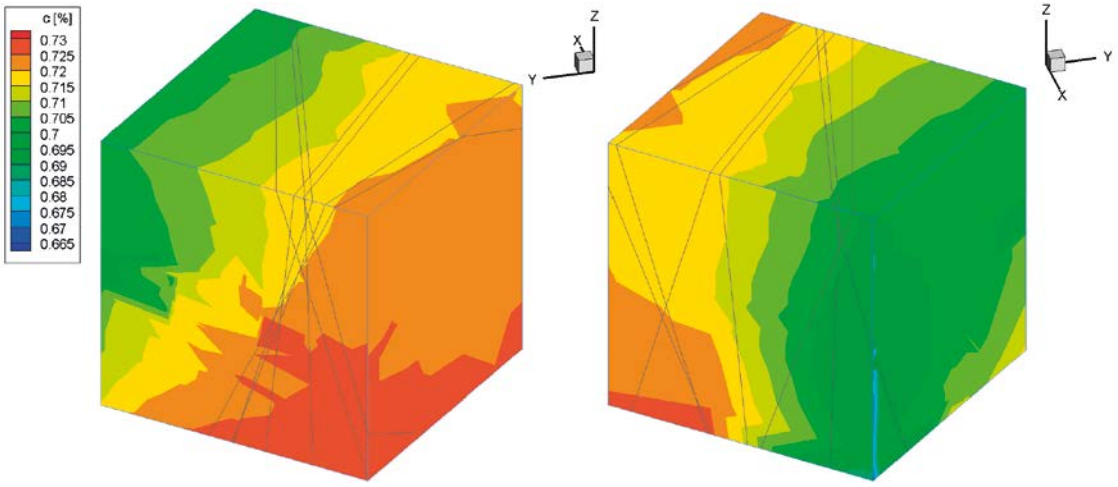

Figure 2-9. *Salt concentration on the model boundaries; from Schneider (2012).*

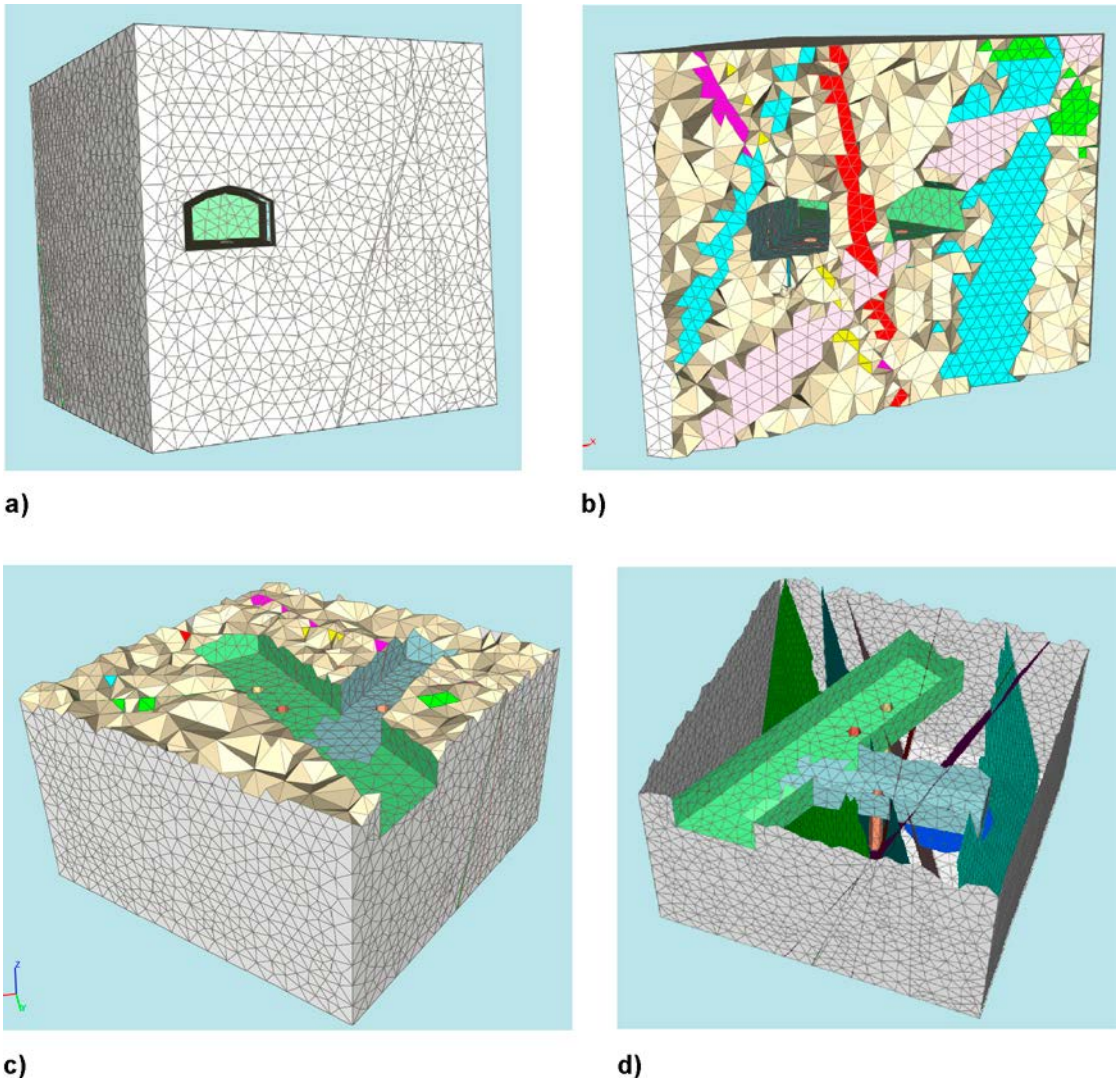

Figure 2-10. *First attempt on the coarse grid; a) view of the model surface, b) vertical cross-section, c) and d) horizontal cross-sections; from Schneider (2012).*

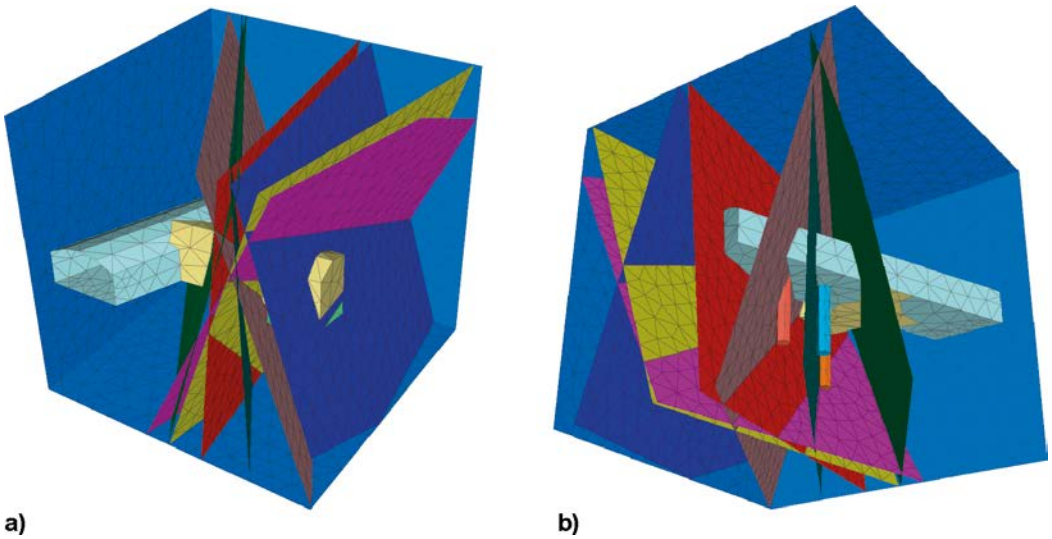

Figure 2-11. *Ultimately used coarse grid for the model; a) view from above, b) view from below; from Kröhn (2012).*

The reason for this comparatively fine discretization lay in the fracture geometry which included several subparallel fractures intersecting in close vicinity and thus required a rather fine grid resolution. This led to problems with the multigrid solver because the coarse grid solver did not work economically anymore. At a later stage a coarser grid was developed as shown in Figure 2-11 that consisted only of about 25 000 elements which improved the computational performance considerably. The finest grid used during the calculation contained 140 296 nodes and 588 776 elements.

2.4 Results

Results are given in terms of dynamic pressure distributions, flow fields, and water outflow at the model boundary. However, there was no data from the field available to compare with.

2.4.1 Pressure distribution

Figure 2-12 shows isoplanes in a vertical cross-section through the TASD-tunnel representing the dynamic pressures of −3.5, −3.0, −2.5, −2.0, and −1.5 MPa. The pressure decreases from the cube surface in the direction of the openings showing the highest gradient at the end of the TASD-tunnel. The contour plane of lowest pressure (blue) follows loosely the surface of the openings. This is evident at the deposition boreholes 2 and 3.

The part of the model shown in Figure 2-12 is only little disturbed by fractures. The isoplanes thus have a rather smooth look. If the vertical cross-section is slightly turned clockwise, though, several fractures are located in the remaining volume of the model which results in wave-like disturbances especially at a distance to the geotechnical openings as shown in Figure 2-13.

2.4.2 Flow velocity

Exemplary for the calculated flow field in a fracture Figure 2-14 depicts a wire plot of the model including a fracture highlighted in red. Direction and flow velocity in the fracture are indicated by equally spaced vectors of varying length. Flow occurs from the cube surface towards the tunnels and boreholes as expected from the pressure plots. A significant influence on the flow field from other fractures is not expected, and in fact cannot be observed, because all fractures are of comparable orientation. All of them are assumed to be larger than the model domain, and therefore all of them simply connect the surfaces of the model with the geotechnical openings resulting in comparable pressure gradients.

The situation is different for the flow field in the matrix. Here, the fractures provide hydraulic short-cuts for the water on its way from the cube surface to the openings. The plot of the velocity field in a horizontal cross-section through the matrix provides a meaningful example. In Figure 2-15 the flow direction is indicated by vectors and the flow rates are visualised by an underlying contour plot. The position of the intersections with the fractures can clearly be determined by the abrupt colour changes in the contour plot. Where this happens the fractures influence the flow field in the matrix by deflecting the stream lines. At some locations the colour changes are accompanied by visible changes in the flow direction as well.

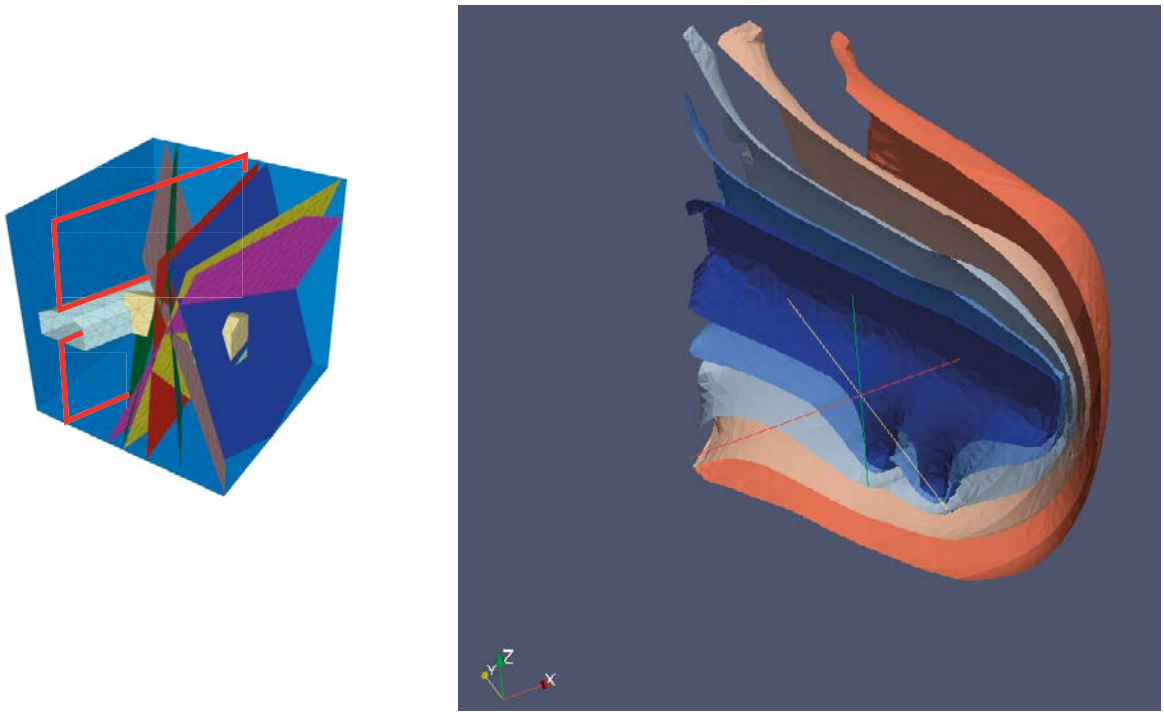

Figure 2-12. *Isoplanes of the dynamic pressure at the TASD-tunnel; from Schneider (2012).*

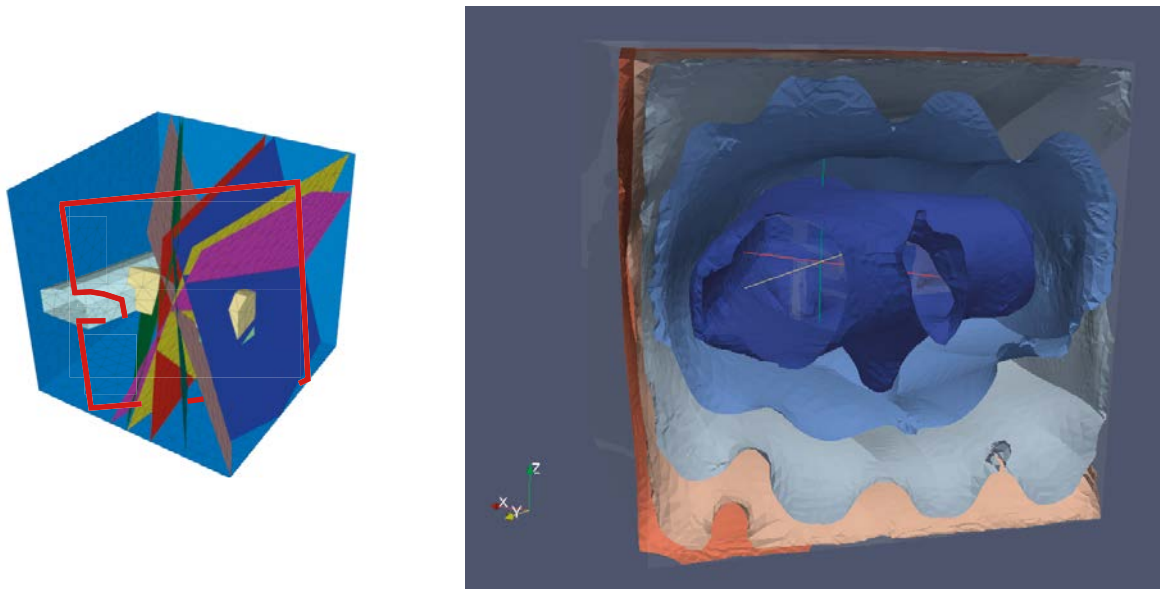

Figure 2-13. *Influence of fractures on the isoplanes of the dynamic pressure; from Kröhn (2012).*

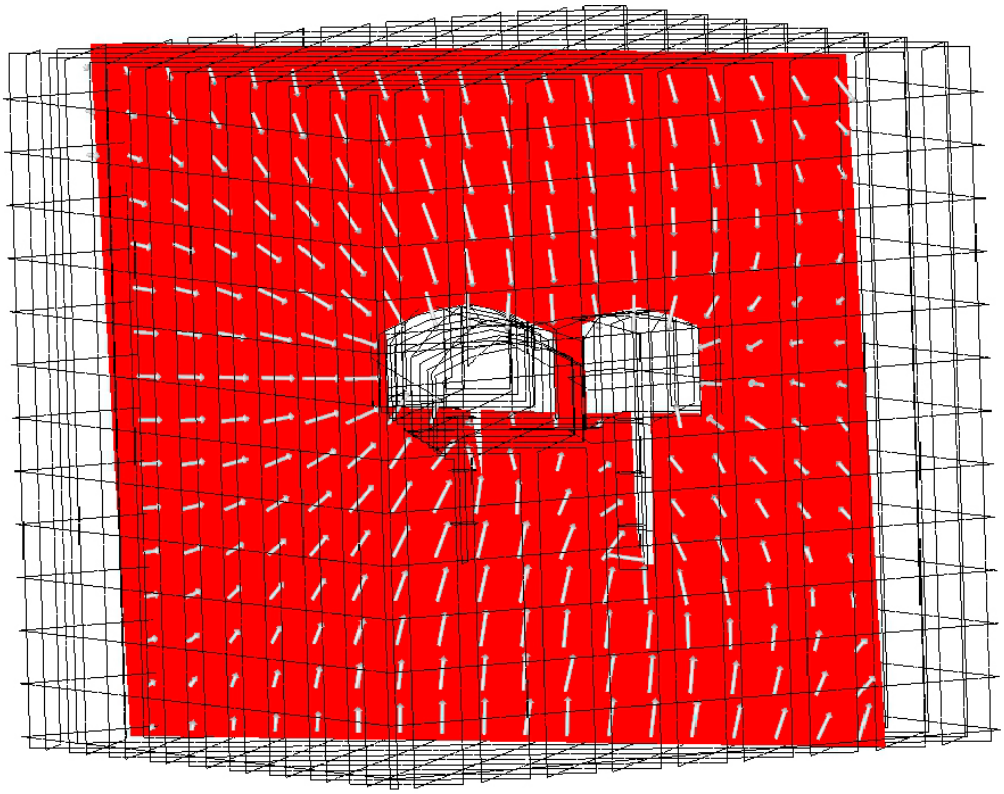

Figure 2-14. *Flow field in a fracture; from Schneider (2012).*

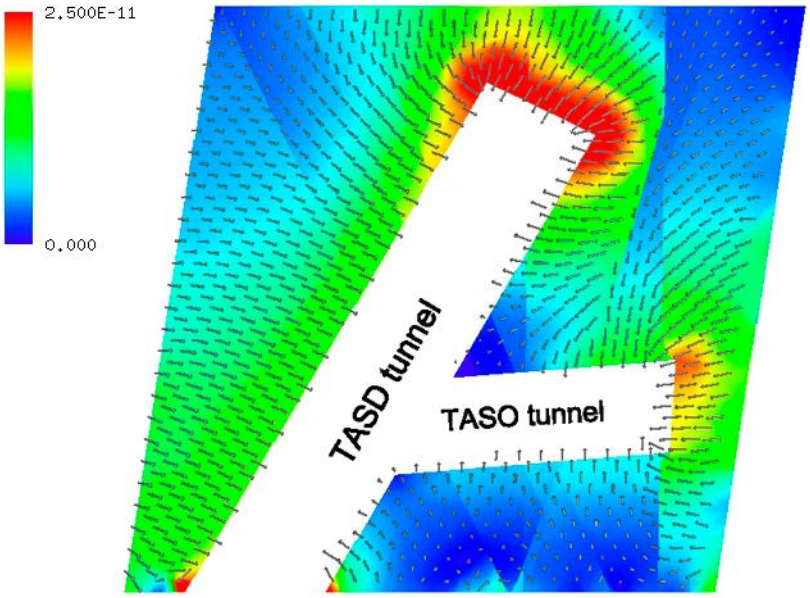

Figure 2-15. *Flow field in the matrix; from Kröhn (2012).*

The highest flow velocities can of course be found where the openings are closest to the cube surface, most obvious at the end of the TASD-tunnel. Interestingly, the area showing the highest velocities appears to be more or less symmetrically arranged around the tunnel face despite the fact, that the tunnel face is not parallel to the cube surface. In a homogeneous domain the location with the highest flow velocity would have been expected at the tunnel edge closest to the surface. But apparently, the fracture system lowers the flow resistance to the other edge in such a way that inflow into the tunnel is more or less equally distributed along the tunnel face.

2.4.3 Water outflow

Since the task description provides no means of comparing the results described above with data from the HRL at least a rough check was devised. Water flow into the openings was calculated to be compared with flow data from a different location in the HRL. The V2-fracture system at niche 2715 in the HRL had been found to be highly permeable and to produce about 50 ml s^{-1} (Kull et al. 2002). This compared nicely to the amount of water flowing out of tunnels and boreholes which amounts to approx. 180 g s^{-1} in the model especially considering that this value comes from the first and uncalibrated model.

Note that outflow out of the TASO-tunnel was estimated during the active time of Task 8c to amount only to 10 ml s^{-1} (Fransson Å 2012, personal communication). An estimation for the outflow from the tunnel surface without large fractures was even later given in Task 8d as 1.7 ml/s based on a test with sorbing mats that had been attached to the walls of the TASO-tunnel (Vidstrand et al. 2017). Figure 2-16 shows location and size of the mats as well as the referring measured outflow. Mats were installed wherever water flow had been detected by visual inspection. Compared to the calculated total outflow of 180 g s^{-1} for TASO- and TASD-tunnel it has to be concluded that the actual total outflow is considerably overestimated in the model.

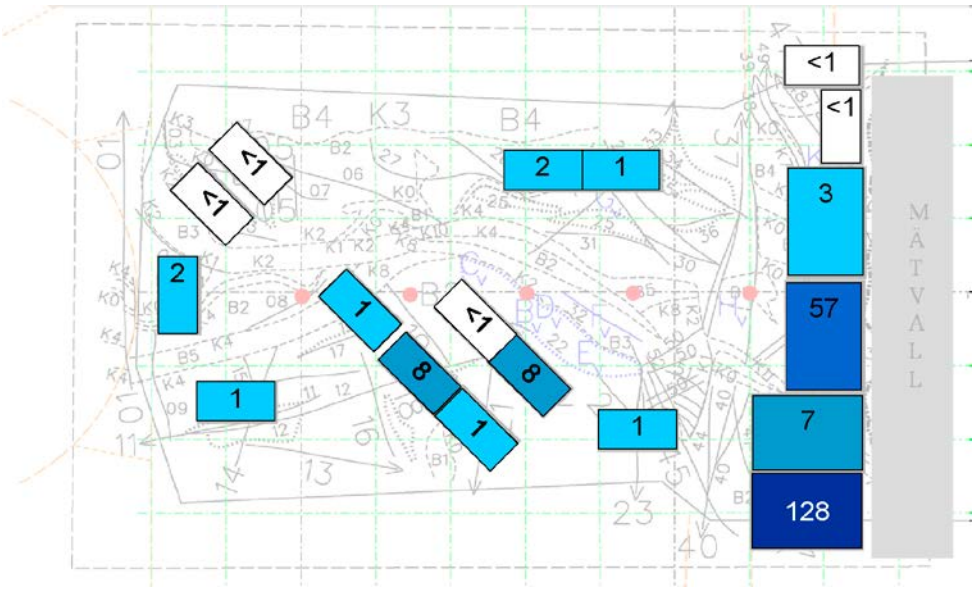

Figure 2-16. *Location of sorbing mats in the TASO-tunnel; flow rates in ml/min; modified from Vidstrand et al. (2017).*

2.5 Discussion

In the absence of any means for checking the model against measured data the only thing to do were plausibility checks. This has been done using the outflow data (which was not part of the test case description) and by looking at the flow field which showed the expected fracture-induced discontinuities and hydraulic shortcuts. Most obvious is the effect at the front of the TASD-tunnel over which the flow velocity is more or less equally high despite the fact that the front is not nearly parallel to the closely located model boundary.

From the model set-up follows that groundwater flow is basically directed from the outer model surface to the geotechnical openings. This applies to flow in the matrix as well as to flow in the fractures since all the fractures connect the cube surfaces with the tunnel system. But the considered deterministic large-scale fractures are distinctly more conductive than the surrounding matrix. These fractures have an impact on the flow pattern and thus on the resulting pressure field as they change the flow path of the least hydraulic resistance. The inconsistency of the fractures in the large-scale model with the fractures defined for Task 8b thus introduces an error in the pressure boundary conditions for the BRIE-model giving rise to another uncertainty in this model.

2.6 Conclusions and recommendations

Judged by the plausibility checks two conclusions can be drawn. Firstly, they indicate convincingly that the option of fracture flow in d^3f is fully operational after some shortcomings in the pre- and post-processing tools as well as in the solver had been resolved accordingly. The code was able to cope with the complex model that included tunnels, boreholes and seven large deterministic fractures. Most prominent here is the refined approach to fracture flow and transport in d^3f that results in sharp discontinuities across the fracture.

Secondly, in hindsight it appears that Task 8b could have been better posed. There was no way to check the proposed steady-state model. Not even a reference model could be developed beyond a state of considerable arbitrariness which became apparent when a check with measured outflow data became available. The assumption of the same constant transmissivity for all seven large deterministic fractures is also rather questionable. In the light of the radically different set of discrete large deterministic fractures defined for Task 8c concrete recommendations for the BRIE as well as a discussion of variations of the model on the basis of Task 8b would have been therefore more or less futile.

3 Task 8c: BRIE – Prediction for central deposition hole

3.1 Objectives

Task 8c addressed confirming the general set-up of the TASO site model and first predictive calculations. It was then found that Task 8c should be subdivided into two subtasks (Vidstrand et al. 2017):

- Task 8c1
  - "… predict inflows and inflow characteristics to deposition holes."
  - "… set up the main features of the TASO site."
  - "… test the adopted boundary conditions in relation to the site-specific deformation zones (wfracture_01,wfracture_02 and NNW4)."
  - "… supply guidance to the field experiment on importance of bedrock fractures and matrix and where to place measurement instrumentation."
- Task 8c2: Predict wetting of bentonite based on Task 8c1
  - "… evaluate effects of the fracture locations along the deposition hole on the resulting wetting of the bentonite."
  - "… serve as a base case for comparison with later results based on more elaborated hydro-geological models."

Task 8c1 referred to setting up a groundwater flow model of the site using data from five probing boreholes. On the basis of such a model the effect of expanding two of the five boreholes was then to be predicted but another model with expanded boreholes could unfortunately not been set up within the active time of Task 8c.

Task 8c2 focused on the simulation of wetting the buffer material based on the groundwater model from Task 8c1. It had become apparent, though, that the concept behind the re-saturation code VIPER did not cover the case where less water is available than the buffer demands. During the active phase of Task 8c a referring conceptual approach was developed and implemented in the code but there was no time left for model calculations. Modelling could therefore not be completed but was performed with the old version based on unrestricted access to water which provided of course only part of the work intended for task 8c2.

3.2 Approach

The approach described in Section 2.2 was used for Task 8c again with one modification. In the five probing boreholes that were drilled in a row with a distance of 1.5 m extremely different outflow rates had been observed (see Table 3-4). To account for this phenomenon the vicinity of the boreholes was treated differently from the rest of the model as shown in Figure 3-1. A box-like zone (depicted in yellow) was defined in such a way that the minimal distance of the boreholes to the zone boundary amounted to 1 m. The box was assumed to contain only undisturbed rock except for two fractures that where assumed to cross the two comparatively strong water producing probing boreholes and connected them to the outside of the box. Outside of the box increased matrix permeability was assumed to account for the network of smaller background fractures.

An axisymmetric re-saturation model for unrestricted water supply was set up to provide a reference value for the maximum water uptake rate that is demanded by the bentonite. In comparison with outflow data from the flow model the applicability of the boundary condition was to be evaluated and if need be a new boundary condition considering limited water access was to be formulated and implemented.

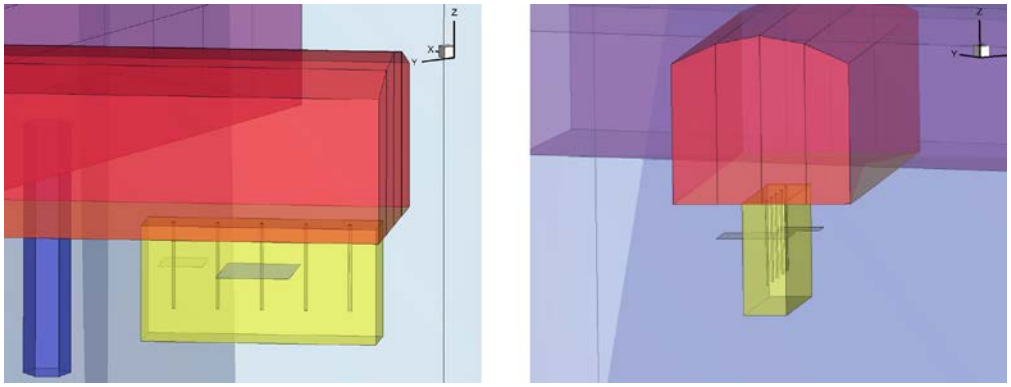

Figure 3-1. *Close-ups of the small box of undisturbed rock and the assumed fractures.*

3.3 Model setup

3.3.1 Coordinates

(See related Section 2.3.1 for Task 8b.)

3.3.2 Model domain

(See related Section 2.3.2 for Task 8b.)

3.3.3 Drifts and boreholes

The geometry of the TASD- and the TASO-tunnel as well as the boreholes for the TBT and the CRT in the TASD-tunnel (see related Section 2.3.3 for Task 8b) remained the same for Task 8c. The five new probing boreholes in the TASO-tunnel replaced the user-defined borehole and the artificial circular fracture from Task 8b.

Geometry data for the probing boreholes was given in dxf-files. However, retrieving the location data for the probing boreholes from these files became a severe problem since the coordinates were given in a local coordinate system automatically set up by the generating CAD program. The location was therefore not taken from the provided dxf-files. Pictures from the test site indicated that the closest borehole to the tunnel front (borehole KO0020G01) had been placed at a distance of 1.5 m to this front. The distance between the boreholes amounted also to 1.5 m. The row of probing boreholes was estimated to be aligned to the middle axis of the TASO-tunnel. All boreholes are represented by octagonal prisms with a distance of 10 cm between opposing corners. Sketches of the geometry of the openings are given in Figure 3-2.

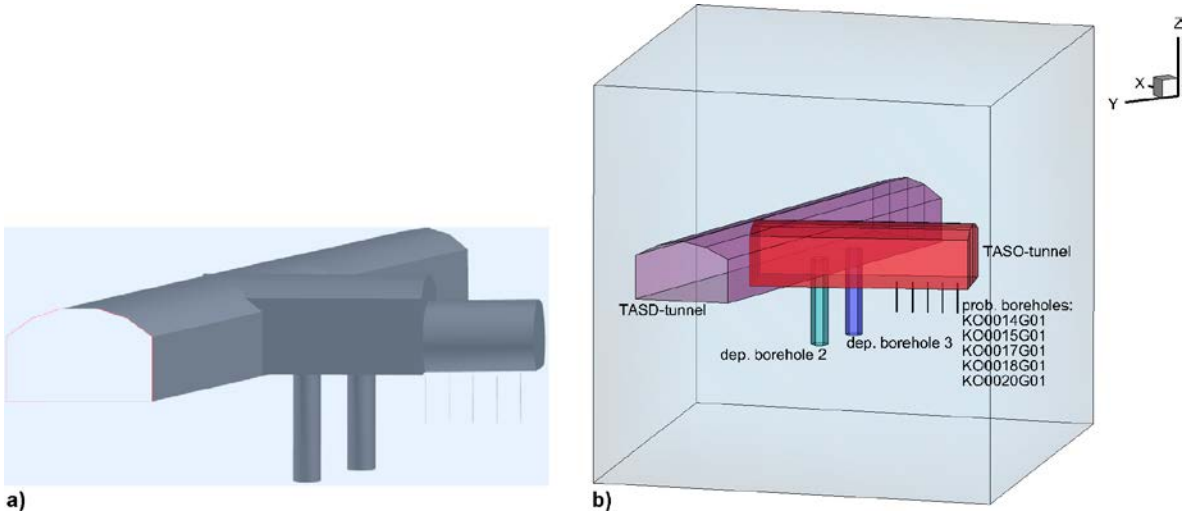

Figure 3-2. *Geometry of the openings; a) from task description, b) model.*

3.3.4 Fractures

Different from Task 8b there are only three large deterministic fractures located in the model domain which are again larger than the 40 m domain. The edges of the fractures in the model are therefore again defined by the interception of fractures and the model boundaries.

In contrast to the coordinates for the probing boreholes the coordinates of the vertices of the deterministic fractures are interpretable in the provided dxf-files. As far as can be seen from visualizing the fractures the vertices actually span a plane. In Figure 3-3 the fractures are shown in relation to the geotechnical openings. The fracture coordinates are compiled in Table 3-1.

Table 3-1. Coordinates for the corners of the deterministic fractures.

Fracture	x-coordinate [m]	y-coordinate [m]	z-coordinate [m]
wfracture_01	581.811	806.595	−396.000
	613.845	782.061	−396.000
	613.374	781.590	−436.000
	581.340	806.124	−436.000
wfracture_02	618.865	806.946	−436.000
	620.395	802.859	−396.000
	590.144	800.213	−396.000
	584.224	803.915	−436.000
NNW4	624.278	792.494	−436.000
	624.278	792.494	−396.000
	618.281	808.503	−396.000
	618.281	808.503	−436.000

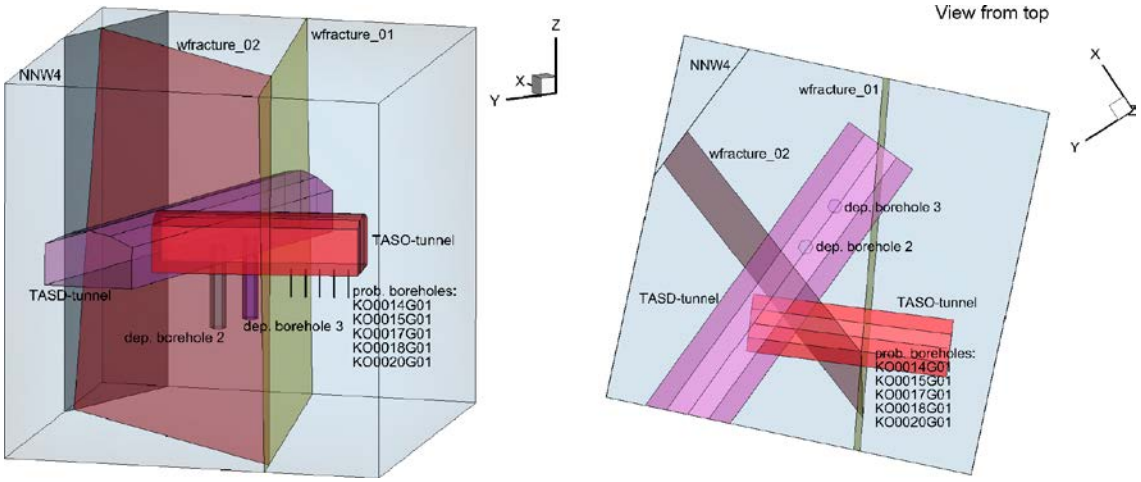

Figure 3-3. *Two views of the fracture geometry in relation to the openings.*

3.3.5 Hydraulic properties

Matrix conductivity as low as 10^{-14} m/s was defined in the task description. This value translates into a permeability of 10^{-21} m^2. Six core measurements presented by Vilks (2007) for the rock matrix at the Forsmark site which is believed to be comparable to the rock at Äspö indicated a spectrum for the permeability roughly ranging from 10^{-21} m^2 to 10^{-19} m^2. A fracture network model for the undisturbed rock pointed in the direction of slightly less than 10^{-20} m^2. The value from the task description thus appears to represent the lowest value in a possible range of one to two orders of magnitude.

According to the approach described in Section 3.2 there were two different permeability values required, one for the undisturbed rock and one for the rock including a network of small background fractures. This network was assumed to increase the matrix permeability in the reference case by one order of magnitude to 10^{-20} m^2.

The task description assigned different transmissivity values to the three large deterministic fractures: 2×10^{-8} m^2/s for wfracture_01, 2×10^{-9} m^2/s for wfracture_02, and 6.5×10^{-7} m^2/s for NNW4. Since the code d^{3}f treats fractures as porous media (Schneider 2012) the transmissivities had to be converted to equivalent permeabilities which required also the definition of related fracture apertures. Note that these apertures have no actual physical meaning but are just defined for numerical purposes to derive equivalent permeabilities. For the sake of simplicity the transmissivity values were taken as conductivities for fractures with an aperture of 1 m since standard measurements of the transmissivity had been performed in a packered interval of approximately one metre length (Vidstrand P 2011, personal communication). Then conductivity was transformed into permeabilities of 2×10^{-15} m^2, 2×10^{-16} m^2, and 6.5×10^{-14} m^2, respectively.

The effect of background fractures on the rock permeability depends not only on transmissivity and frequency of the fractures but also on the connectivity. The lower the connectivity the less is the impact on the overall rock permeability. An indication for the connectivity at the BRIE site on tunnel scale is provided by measurements in the five probing boreholes that were drilled in a row in early 2011. Despite the fact that they were positioned at a distance of just 1.5 m from each other only the first and the third borehole (KO0014G01 and KO0017G01) cut through significantly water bearing fractures. And even these fractures did not appear to be hydraulically connected. Qualitatively, only a limited impact of the background fractures on the rock permeability was thus expected.

The assumed fractures at KO0014G01 and KO0017G01 were square-shaped and had a side length of 1.5 and 2.5 m, respectively. The size was geometrically limited by the condition that they should not cut through the neighbouring boreholes. According to the transmissivity-size relation of fractures at Äspö provided in the task description (cp. 0) this size falls into the range of the background fractures encountered in the TRUE Block Scale exercise. A transmissivity of approximately 10^{-10} m^2/s up to 10^{-9} m^2/s can typically be assigned to such fractures. For modeling purposes this translated into a permeability of 10^{-17} m^2 up to 10^{-16} m^2 at an aperture of 1 m.

All the model-relevant data is compiled in Table 3-2. Derived values are given in italics.

Table 3-2. Hydraulic properties of the hydraulic features.

Feature	Conductivity [m/s]	Permeability [m^2]	Transmissivity [m^2/s]
Undisturbed rock matrix	1×10^{-14}	1×10^{-21}	
Rock matrix incl. background fractures		1×10^{-20}	
wfracture_01		2×10^{-15}	2×10^{-8}
wfracture_02		2×10^{-16}	2×10^{-9}
NNW4		6.5×10^{-14}	6.5×10^{-7}
Assumed fracture at KO0014G01		1×10^{-17}	1×10^{-10}
Assumed fracture at KO0017G01		1×10^{-16}	1×10^{-9}

3.3.6 Hydraulic boundary conditions

The same boundary conditions were applied as described in the related Section 2.3.6 for Task 8b. Where the boreholes KO0014G01 through KO0020G01 were packered off no-flow boundaries were assigned to mimic the installed packers. Otherwise atmospheric pressure was assigned to the borehole surfaces. In the reference case all five probing boreholes were closed.

The fact that a more realistic set of large deterministic fractures was considered for Task 8c calls for repeating the comment in Section 2.5 on the boundary conditions proposed in the task description. If the total number of large-scale fractures as well as position and orientation of the remaining fractures changes without changing the pressure boundary conditions a certain error must be expected in the resulting outflow rates. Due to the high conductivity of the large deterministic fractures compared to the matrix these errors in terms of absolute flow rates are most pronounced in the fractures.

3.3.7 Effects from groundwater salinity

(See related Section 2.3.7 for Task 8b.)

3.3.8 Calibration of the flow model

Calibration parameters

In order to fit the outflow rates of the model to the measurements the quantities listed in Table 3-3 were open to be varied within the also in Table 3-3 indicated parameter ranges. Technically, also the aperture of the fractures could be varied but the aperture had simply come into play in the course of transforming transmissivity into permeability. It is thus sufficient to vary just the permeability.

Table 3-3. Calibration parameters and possible ranges (where applicable).

Quantity	Value range
Permeability	
Undisturbed rock (small box)	10^{-21} to 10^{-19} m^2
Rock including background fractures	(higher than undisturbed rock)
Large deterministic fractures	after Vidstrand et al. (2017) ± one order of magnitude
Assumed fractures	< 1/10 of the least conductive large fracture
Boundary conditions (not performed; see text)	

It was also tried to lower the boundary pressure along the intersections of fractures and model surface. A first try revealed that considerable work in the code would have been required so that the effort was aborted in the end.

Control quantities and data for checking the model

There were two measurement campaigns that could be used for checking the flow model. Both were performed at the probing boreholes. Firstly, the five probing boreholes were packered off below the top metre allowing hydraulic pressure to build up. Even without taking the transient pressure development into account – only steady-state is considered in the model – the maximum pressure build-up can nevertheless be used for comparison. When the boreholes were packered off the fluid pressure in KO0014G01 and KO0017G01 was measured to reach 0.3 and 0.6 MPa, respectively.

Secondly, the inflow rates into the boreholes after opening one of the packers at a time were also measured. For calibrating the steady-state flow model only the outflow rates of 1.7×10^{-8} m^3/s and 8.5×10^{-9} m^3/s for boreholes KO0014G01 and KO0017G01, respectively could be used because no outflow could be measured in the other three boreholes. The outflow rate into these three boreholes had been below the detection limit and must therefore have been substantially lower than the rates for KO0014G01 and KO0017G01. The results for pressure build-up and inflow rates are given in Table 3-4.

Additionally, at the time of Task 8c there was the estimation of the total outflow out of the TASO-tunnel as 1.0×10^{-5} m^3/s (Fransson Å 2012, personal communication).

Table 3-4. Maximum pressures and outflow rates in the probing boreholes, from Vidstrand et al. (2017).[5]

	KO0020G01	KO0018G01	KO0017G01	KO0015G01	KO0014G01
Inflow, Q Built-up pressure, P	**Yes, but below the measurement limit**	**No**	**Yes** Q ≈ 0.5 ml/min P ≈ 6 bar	**No**	**Yes** Q ≈ 1 ml/min P ≈ 3 bar

Strategy

At first the model described in the previous sections was set up as a reference case – also called case A in the following. After checking the output of the model against measured data (control quantities) variants called cases B, C, D, and E were defined to adjust the input of the model (calibration parameters) varying the reference values preferablywithin the ranges given in Table 3-3. The target values of the control quantities were considered to be matched if they were calculated with a deviation of less than a factor of 5. These variations of the reference case provided also some information about the sensitivity of the model to the specified changes.The last case includes the final set of hydraulic parameters and thus represents the hydraulic model for Task 8c.

3.3.9 Re-saturation model

Geometry

The BRIE was to be installed in a testing borehole with a depth of 3 m and a diameter of 0.30 m. A homogeneous host rock could be assumed at mid-height of the borehole. The re-saturation process at the bentonite-matrix contact could therefore be described in an axial symmetric one-dimensional model domain that originated at the borehole axis and has a length of 0.15 m.

A bentonite-fracture contact can also be simulated with such a model but requires additional simplifying assumptions such as neglecting water migration in the third dimension. The results can thus only be seen as bounding cases.

Bentonite

MX-80 bentonite was used for the experiment with a dry density of 1 560 kg/m^3. Grain density amounted to 2 780 kg/m^3 (Vidstrand et al. 2017).

The adsorption isotherm which is the most critical material data in the framework of VIPER was taken from Kröhn (2011) where it had been applied to a model of the Canister Retrieval Test (CRT) at the Hard Rock Laboratory Äspö.[6] The isotherm was a composite of adsorption and desorption data from re- and de-saturation experiments with an initial water content of 17.5 % (Dueck 2004). As Figure 3-5 shows this curve fits also data from Dueck (2004) with an initial water content of 10 % quite well. It should be mentioned, though, that adsorption and desorption data from Dueck (2004) differ in several aspects from the data of other authors.

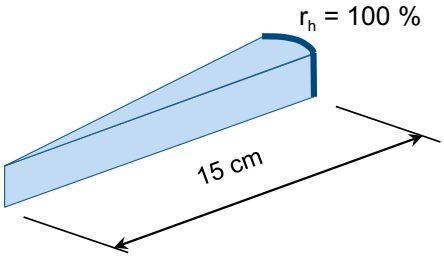

Figure 3-4. *Geometry and boundary condition for the re-saturation model.*

[5] The flow rates for KO0017G01 and KO0014G01 are equal to 8.3×10^{-9} m^3/s and 1.7×10^{-8} m^3/s, respectively.

[6] All other material parameters were also chosen as for the CRT.

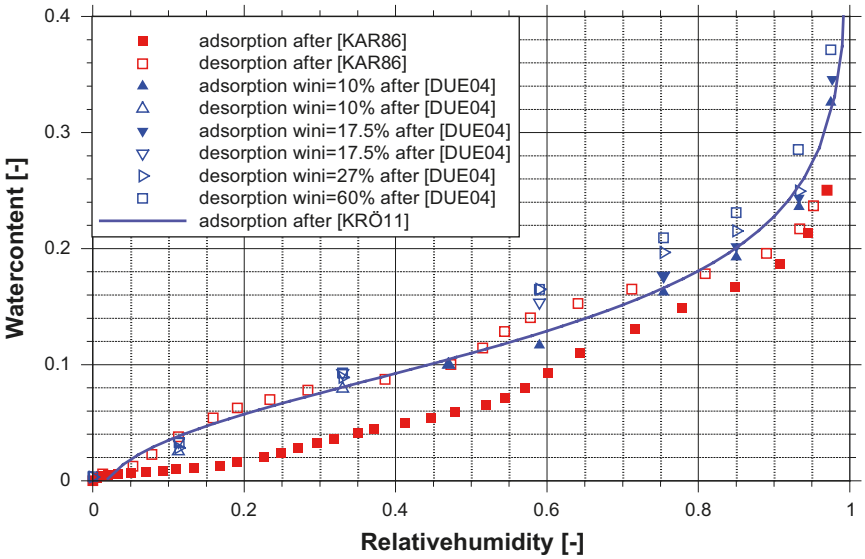

Figure 3-5. *Adsorption isotherms; modified from Kröhn (2011).*

Most prominent are the comparatively high water contents in the desorption curve and the test procedure that included initial water contents between 0 and saturation content (without explaining the saturation history of those samples). A more detailed comparison and discussion is given in Kröhn (2011). For reference the very detailed measurements from Kahr et al. (1986) are included in Figure 3-5. For the actual modeling the isotherm was modified according to Dueck and Börgesson (2007) to account for the effect of swelling in a confined space.

Initial and boundary conditions

The initial water content of the bentonite was 10 %. Temperature in the model was set to 14 °C and water density to 1 000 kg/m^3. Since flow rates into the bentonite under unrestricted water supply were investigated the relative humidity at the inflow boundary was set to 100 %.

3.4 Results

3.4.1 Flow model

Case A: Reference case

Pressure is generally decreasing from the outer model surface (surface of the cubic domain) towards the tunnels and boreholes. This is exemplarily shown in Figure 3-6 for the vertical cross-section through the TASO-tunnel. Noticeable is how little influence wfracture_01 exerts on the pressure field in the vicinity of borehole KO0014G01. A comparison of Figure 3-6 a) and Figure 3-6 b) reveals that opening the boreholes has only an influence in the immediate vicinity of the boreholes. Also observable in the borehole field is a slight trend to less pressure along the TASO-tunnel towards the TASD-tunnel (to the right in Figure 3-6). Taking the maximum pressure in a borehole to be the measured pressure in the test the model gives 6.3 bar for KO0014G01 and 7.7 bar for KO0017G01 which relates loosely to the measured values of 3 bar for KO0014G01and 6 bar for KO0017G01.

Flow rates out of the rock into the probing boreholes as well as into the TASO-tunnel were also calculated. They are compiled as well as the results from the other cases in Table 3-5.

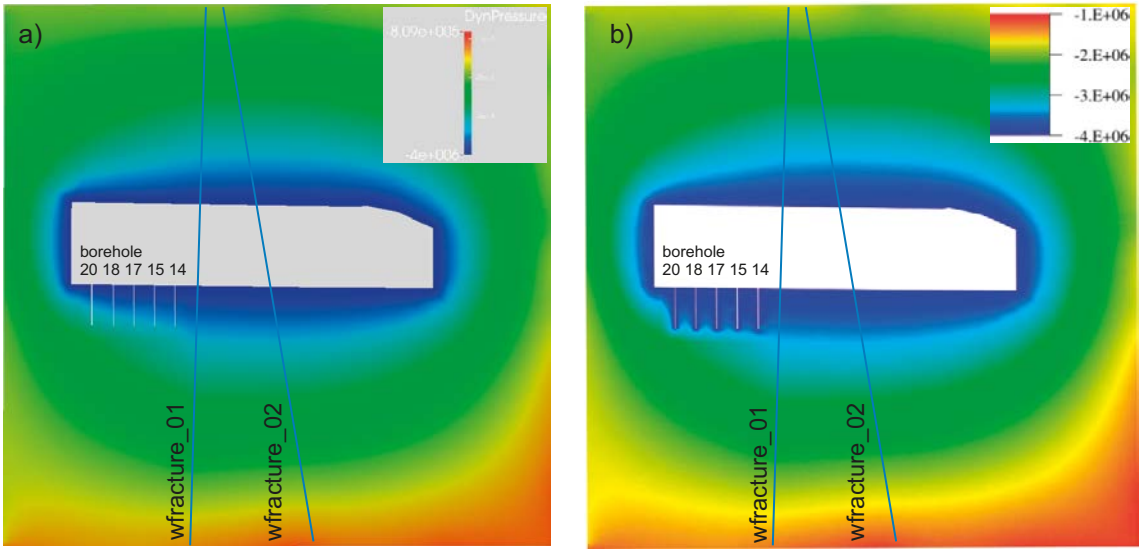

Figure 3-6. *Dynamic pressure in a vertical cross-section through the TASO-tunnel; a) all boreholes closed (reference case), b) all boreholes open*

Total flow through the whole tunnel surface in the model exceeds the estimated total outflow of 10^{-5} m^3/s (Fransson Å 2012, personal communication) only by 40 %. Additionally, outflow from the two fractures and outflow over the remaining tunnel surface were distinguished in the model results. From this data it became clear that total outflow into the tunnel is dominated by w_fracture_01 for case A as well as all other cases shows.

An outflow value of 5.0×10^{-11} m^3/s chosen as an ad-hoc criterion for unobservable outflow into the boreholes was nowhere nearly exceeded.

Case B: Only borehole KO0014G01 opened

Opening borehole KO0014G01 in the reference case showed clearly that the permeability values adopted for the matrix were far too low. The target value was missed by a factor of about 2000. Flow from the fractures and over the tunnel surface proved to be virtually insensitive to opening the borehole. Note that all changes in the boundary conditions and the permeability values referring to case A are indicated in Table 3-5.

Case C: Borehole KO0014G01 opened and increase of permeability in the matrix

For case C it was assumed that a network of background fractures would increase the matrix permeability by three orders of magnitude. This increased outflow into borehole KO0014G01 by two orders of magnitude and brought the resulting value of 1.0×10^{-9} m^3/s almost in an acceptable range.

Case D: Increasing the permeability in the box and the assumed fractures

The increase in outflow rate for borehole KO0014G01 had not been proportional to the increase in matrix permeability as case C had shown. Therefore the permeability of the box that was supposed to represent the undisturbed matrix adjacent to the boreholes was increased. As this proved not to be sufficient yet the permeability for the assumed fracture at KO0014G01 was increased also. The resulting model showed a permeability contrast between the matrix and the box of two orders of magnitude that provided a satisfying contrast in the outflow rates between the high and low water producing boreholes, KO0014G01 and KO0017G01 on the one hand and KO0015G01, KO0018G01, and KO0020G01 on the other hand. The assumed permeability of the fractures in the box needed indeed to be higher than the matrix permeability in order to attract a sufficient amount of water to KO0014G01 and KO0017G01. The calculated outflow rate for KO0014G01 lay eventually by less than a factor of 5 off the target value.

Table 3-5. Input parameters and calculated flow rates for the cases A to E.

Case	Property	Rock	Small box	Fractures					Boreholes					TASO tunnel	
				wf_01	wf_02	NW4	ass.fr. KO 14	ass.fr. KO 17	KG14	KG15	KG17	KG18	KG20	Surface	Total
Meas.	Q_t [m^3/s]								1.7×10^{-8}	–	8.3×10^{-9}	–	–	–	10^{-5} *
A	k [m^2]/b.c. bore.h.	10^{-20}	10^{-21}	2×10^{-15}	2×10^{-16}	2×10^{-14}	10^{-17}	10^{-17}	closed	closed	closed	closed	closed		
	Q_c [m^3/s]			1.4×10^{-5}	9.0×10^{-7}		2.7×10^{-14}	6.8×10^{-14}	8.1×10^{-14}	6.9×10^{-14}	1.6×10^{-13}	2.1×10^{-13}	1.4×10^{-13}	9.3×10^{-10}	1.4×10^{-5}
B	b.c. bore.h.								open	closed	closed	closed	closed		
	Q_c [m^3/s]			1.4×10^{-5}	9.0×10^{-7}		7.6×10^{-12}	8.2×10^{-14}	8.4×10^{-12}	1.1×10^{-13}	1.7×10^{-13}	2.1×10^{-13}	1.4×10^{-13}	9.2×10^{-10}	1.4×10^{-5}
C	k [m^2]/b.c. bore.h.	10^{-17}							open	closed	closed	closed	closed		
	Q_c [m^3/s]			1.4×10^{-5}	9.3×10^{-7}		1.0×10^{-9}	3.3×10^{-11}	1.0×10^{-9}	8.8×10^{-14}	3.3×10^{-11}	2.2×10^{-13}	1.4×10^{-13}	9.3×10^{-7}	1.6×10^{-5}
D	k [m^2]/b.c. bore.h.	10^{-17}	10^{-19}				10^{-16}		open	closed	closed	closed	closed		
	Q_c [m^3/s]			1.4×10^{-5}	9.3×10^{-7}		4.0×10^{-9}	3.5×10^{-11}	4.0×10^{-9}	1.0×10^{-11}	4.4×10^{-11}	2.2×10^{-11}	1.4×10^{-11}	9.3×10^{-7}	1.6×10^{-5}
E	k [m^2]/b.c. bore.h.	10^{-17}	10^{-20}				10^{-16}		open**	open**	open**	open**	open**		
	Q_c [m^3/s]			1.4×10^{-5}	9.3×10^{-7}				4.0×10^{-9}	1.5×10^{-11}	8.6×10^{-9}	2.3×10^{-11}	2.5×10^{-11}	9.3×10^{-7}	1.6×10^{-5}

Colour coding

Open borehole: 1/5 × target value < calculated value < 5 × target value

Closed borehole: calculated value < 5.0×10^{-11}; ad-hoc criterion for unobservable outflow

Open borehole: calculated value < 1/5 × target value or calculated value > 5 × target value

Closed borehole: calculated value > 5.0×10^{-11}; ad-hoc criterion for unobservable outflow

* This data refers to the estimations that were valid at the time of calculation.
** Exclusively this borehole opened.

Case E: Final model – all boreholes successively just opened once

With the permeability set derived for case D outflow rates for all five probing boreholes were checked. As Table 3-5 shows all flow rates were reproduced within the adopted uncertainty of a factor of 5. The calculated values deviated by factors of 0.24, 1.04 and 1.6 from the measurements for KO0014G01, KO0017G01 and the tunnel, respectively.

The contrast of flow rates for KO0014G01 and KO0017G01 in comparison to the rates for the other boreholes showed that the assumed fractures contributed substantially to the outflow. However, the calculated values for KO0018G01 and KO0020G01 were disturbingly high. This reflects a related increase of the pressure gradients along the TASO-tunnel towards its end which is consistent with the pressure distribution discussed above.

Note that variations in the permeability of the three large fractures resulted in significant changes of outflow rates only in these fractures. The rest of the flow system remained largely unaffected by such changes.

3.4.2 Re-saturation model

At the time of modelling using the re-saturation model for Task 8c implied unrestricted water supply from the rock (cf. Section 2.2.2). To check this assumption flow from the rock was compared with the calculated maximum uptake rate for the bentonite. The re-saturation model yielded a maximum flux density of 2×10^{-7} m^3/(m^2 s) which is defined here as the flow rate divided by the related cross-sectional area. Inflow decreases strongly over time as depicted in Figure 3-7. Some values are indicated explicitly in the graph. The development of the water content distribution in the bentonite is shown in Figure 3-8.

Comparison of the water demand by the bentonite which is expressed in Figure 3-7 and the outflow data from the rock can be done straightforward in terms of flux densities. As all flow rates are given by measurements and model calculations, respectively, the related areas have to be defined yet.

Concerning inflow two extremes were considered in this respect. One of them was the assumption that all inflow was concentrated in a horizontal fracture with an aperture of 0.1 mm putting up a case of local high inflow. Inflow via such a fracture was attributed to KO0017G01 and KO0014G01 where fracture flow had indeed been observed. The three-dimensional nature of water uptake by the bentonite was neglected here. This might be seen as a compensation for the rather stringent assumption of concentrating all outflows to just one fracture. Migration in the not considered third dimension would slow down the progress of the wetting front into the buffer not unlike reducing the hypothetical inflow rate from just one fracture by distributing a certain fraction over the borehole surface.

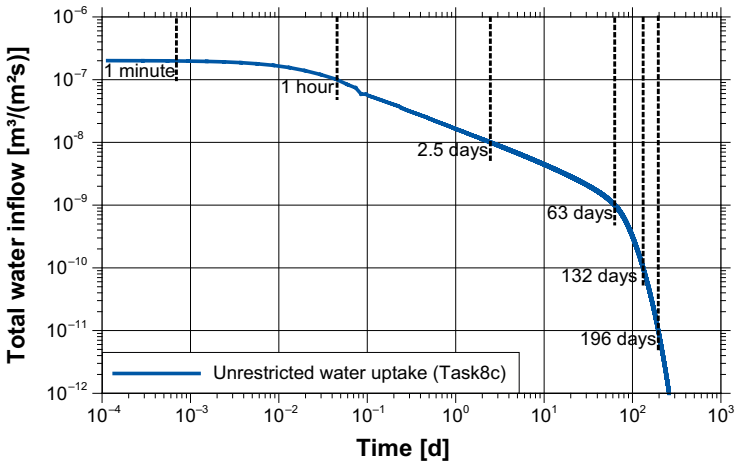

Figure 3-7. *Inflow into the bentonite at unrestricted access of water (Task 8c).*

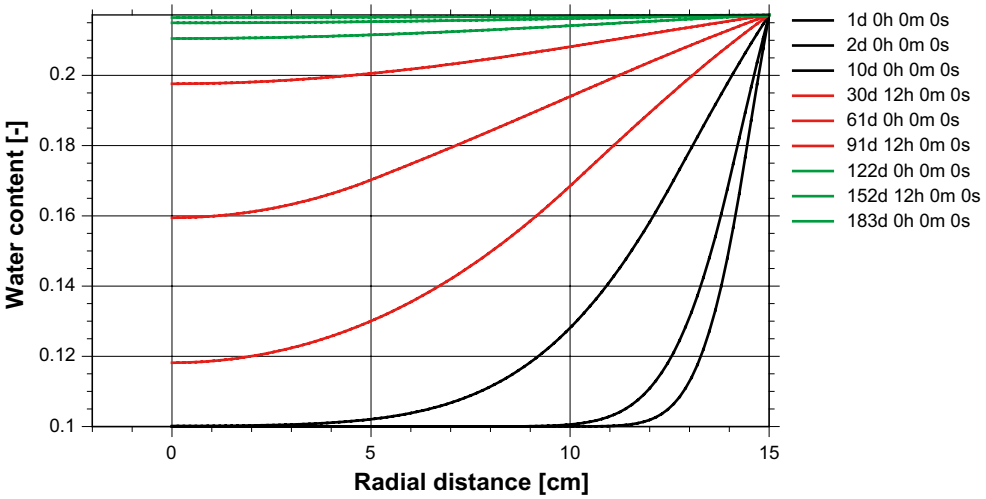

Figure 3-8. *Re-saturation dynamics at unrestricted water access (Task 8c).*

The other extreme was distributing inflow over the whole surface of the test borehole. Unfortunately no hard data was available for the case of distributed inflow via rock matrix. As a first approximation outflow from the unfractured rock surface of the TASO-tunnel was used instead. The outflow of 9×10^{-7} m^3/s calculated with the flow model d^{3}f (cf. Table 3-5) was distributed over the estimated tunnel surface area of 460 m^2.

Flow rates, related areas and the resulting flux densities are compiled in Table 3-6. Flux densities for fracture-bentonite contacts as formulated for the test boreholes exceed the water demand of the bentonite by several orders of magnitude which fulfills the condition of unrestricted water access for the bentonite.

For the bentonite-matrix contact it is the other way round. Demand exceeds the supply by 2 orders of magnitude. At a bentonite-matrix contact a restricted water access is therefore to be expected.

Table 3-6. Flow rates and flux densities.[7]

Location	Bentonite column	KG0017G01	KG0014G01	Tunnel surface
Flow rate [m^3/s]	–	8.3×10^{-9} **	1.7×10^{-8} **	9.0×10^{-7} **
Related area [m^2]	–	9.4×10^{-5}	9.4×10^{-5}	460
Flux density [m^3/(s m^2)]	2.0×10^{-7} *	8.8×10^{-5}	$1{,}8 \times 10^{-4}$	2.0×10^{-9}
Source	VIPER	Measured	Measured	d^{3}f

* Maximum value for the bentonite cylinder of 1 m height.
** cf. Table 3-5.

3.5 Discussion

3.5.1 Modelling results

Flow model

The flow model for Task 8c was able to reproduce the trend of a pressure decrease along the TASO-tunnel towards the TASD-tunnel which had been observed in the series of five probing boreholes

The calculated flow rates for all boreholes lay within a factor of 4 of the measured values. Parameter variations confirmed that inflow rates are mainly depending on matrix permeability and on additional water-bearing fractures that were opened by these boreholes. The large deterministic fractures wfracture_01, wfracture_02 and NNW4 had apparently little influence on these flow rates.

[7] The codes d^{3}f and VIPER calculate mass fluxes while the measurements are given as volume fluxes. For the sake of comparability model results and measured data were transformed to volume fluxes in [m^3/s].

However, boreholes KO0018G01 and KO0020G01 were producing too much water when opened in the model. This is because these boreholes reach deeper into the zone of higher pressures around the tunnel. Therefore these boreholes attract more water than those which are almost totally located in the low pressure zone created by the tunnel. It is not clear if this has to do with the location of the model boundary that lies rather close to the end of the TASO-tunnel or with the heterogeneities introduced by the network of background fractures. Note that the borehole field generally lowers the pressure within its perimeter.

Parameter variations indicated an effective permeability of the rock matrix including background fractures of about 10^{-17} m^2. This value is surprisingly high in comparison to the values of 10^{-21} to 10^{-19} m^2 for the undisturbed matrix. It suggests on a larger scale a somewhat homogeneous fracture network consisting of rather well-connected smaller fractures.

Flow into the tunnel was dominated by outflow from wfracture_01. Outflow from wfracture_02 and the tunnel surface contributed less than 10 % each to the total outflow.

From the measured outflow rates into the probing boreholes can be concluded, though that the flow field is very inhomogeneous on the scale of these boreholes. Larger local background fractures provide apparently inflow for some of the probing boreholes. Connectivity of the larger background fractures is thereby rather low since there is little if no hydraulic connection between the five probing boreholes despite the fact that they are located only 1.5 m apart from each other.

The source of the outflowing water is therefore not quite clear. A hydraulic connection by a few background fractures to one of the strongly water conducting large deterministic fractures is as likely as a connection of just one fracture to a better connected network of smaller fractures that are more homogeneously distributed in the matrix. Considering the low connectivity of the larger background fractures it is quite probable that the water producing boreholes KO0014G01 and KO0017G01 are drawing the water from different sources.

Re-saturation model

Bentonite-rock interactions can theoretically be divided into two types depending on the ratio of water supply from the rock and water demand by the bentonite. In other words there can either be more water coming from the rock than the bentonite can take up or less. The first case is the one that has been addressed numerous times in the past by water uptake tests in the laboratory which is to say the re-saturation dynamics to be expected in this case are rather well known. For all practical purposes an instantaneously fully water saturated bentonite at the bentonite-rock interface can be assumed for the re-saturation model in this case. Research on bentonite re-saturation has shown that the uptake of water is more or less independent of the applied hydraulic pressure at the bentonite surface (Pusch and Kasbohm 2001). The only impact seems to be the thickness of the fully saturated zone which might increase to the centimetre range. If this condition prevails the re-saturation process is thus independent of the groundwater flow in the rock.

In the second case however the re-saturation process depends also on the outflow from the rock. The lower the outflow from the rock the lower is the inflow into the bentonite since water is readily taken up by the bentonite at any rate up to the maximum.

Since the water demand of the bentonite is a crucial quantity for deciding about the mode of re-saturation it was calculated by a re-saturation model for the buffer at the BRIE. A comparison of the model results with the measured or calculated outflow rates from the rock indicated that both modes of re-saturation and thus both types of bentonite-rock interactions occur at the BRIE-site. According to the models fractures provide locally sufficient water to justify a fully saturated boundary condition for the bentonite while the rock matrix is not able to do so.

3.5.2 Uncertainties

Conceptual uncertainties

The location of the geotechnical openings is well known as well as the location of the intersections between these openings and significantly water bearing fractures. Orientation of these fractures is given by the trace at the tunnel/borehole surface, and their size can be estimated from the aperture-size

relation in the task description. But of course there are fractures that are not observed directly even if they are located close to tunnels or boreholes. For the description of those fractures no other means than statistical methods are available.

A problem stems therefore from the inherent contradiction of seeking deterministic results for pressures and fluxes in the probing boreholes from a fracture network that is known only in terms of geostatistics. The measurements indicate that the water-bearing fractures that were encountered in boreholes KO0014G01 and KO0017G01 are only loosely hydraulically connected at best. Where they actually draw the water from remains totally unclear. Since there is no information about the fracture network in the vicinity of the probing boreholes there exist no possible means either for setting up a local deterministic discrete fracture network or for validating a realization of a statistical model. The resulting uncertainty for predictions concerning outflow into the testing boreholes especially for changing flow conditions in the presence of water attracting bentonite appears to be rather high in any case.

Fractures and boundary conditions

The large-scale model from which the pressure boundary conditions were derived had the fractures apparently taken into account by 3D-elements with a modified hydraulic properties (Figure 3-9 a). The impact of these fractures on the pressure field can hardly be recognised though. Only a pressure decrease in the corner between the TASK- and the TASD-tunnel can apparently be attributed to wfracture_01 (Figure 3-9 b).

A comparison of the high porosity features in Figure 3-9 a) with the fracture locations given by Vidstrand et al. (2017) (Figure 3-9 c) reveals a rather loose relation between these two fracture locations (Figure 3-9d). wfracture_01 has been rotated while wfracture_02 was shifted and shortened. According to the large-scale model the feature NNW4 would not be part of the BRIE-site model at all.

In the large-scale model that had provided the pressure boundary conditions wfracture_02 was located in such a way that the fracture would have been hydraulically directly connected to the boundary of the BRIE-site model (cp. Figure 3-9 a)). The task description in contrast prescribes a shorter version of wfracture_02 that is connected via NNW4 with the model boundary (cp. Figure 3-9 a)). Only a small impact on the flow field is expected from this difference though.

However, these changes introduce an inconsistency between fracture locations in the BRIE-site model and the pressure field from the large-scale model. More precisely, the pressure boundary conditions derived from the large-scale model are not consistent with the fracture locations in the BRIE-site model. Judging from the calibration procedure described in Section 3.4.1 it can be concluded that a noticeable influence of this inconsistency on the flow field would only be observed in the fractures. However the effect of this inconsistency was not investigated due to serious difficulties with modifying the boundary conditions in the model.

Hydraulic parameters

Besides the model geometry and the hydraulic boundary conditions which were discussed above, the flow field of the model is controlled by the permeability of the hydraulic features. There are only four distinct hydraulic features in the model, namely undisturbed rock, rock including background fractures, large deterministic fractures, and assumed fractures. How the permeability for these features varied during the calibration process provides a feeling for the degree of understanding the flow system.

The permeability for the large deterministic in the reference fractures lead directly to matching results for the estimated total outflow rate from the tunnel. This rate was only marginally affected by any model variations. Since the outflow was dominated by these fractures it can be concluded that the hydraulics of the large deterministic fractures were more or less captured.

Much more degrees of freedom are attributed to the other three features. The comparatively high permeability value for the rock including background fractures had not been anticipated. The result of the calibration appears therefore to be reasonable but not unique. The related uncertainties are thus much higher than those for the large fractures.

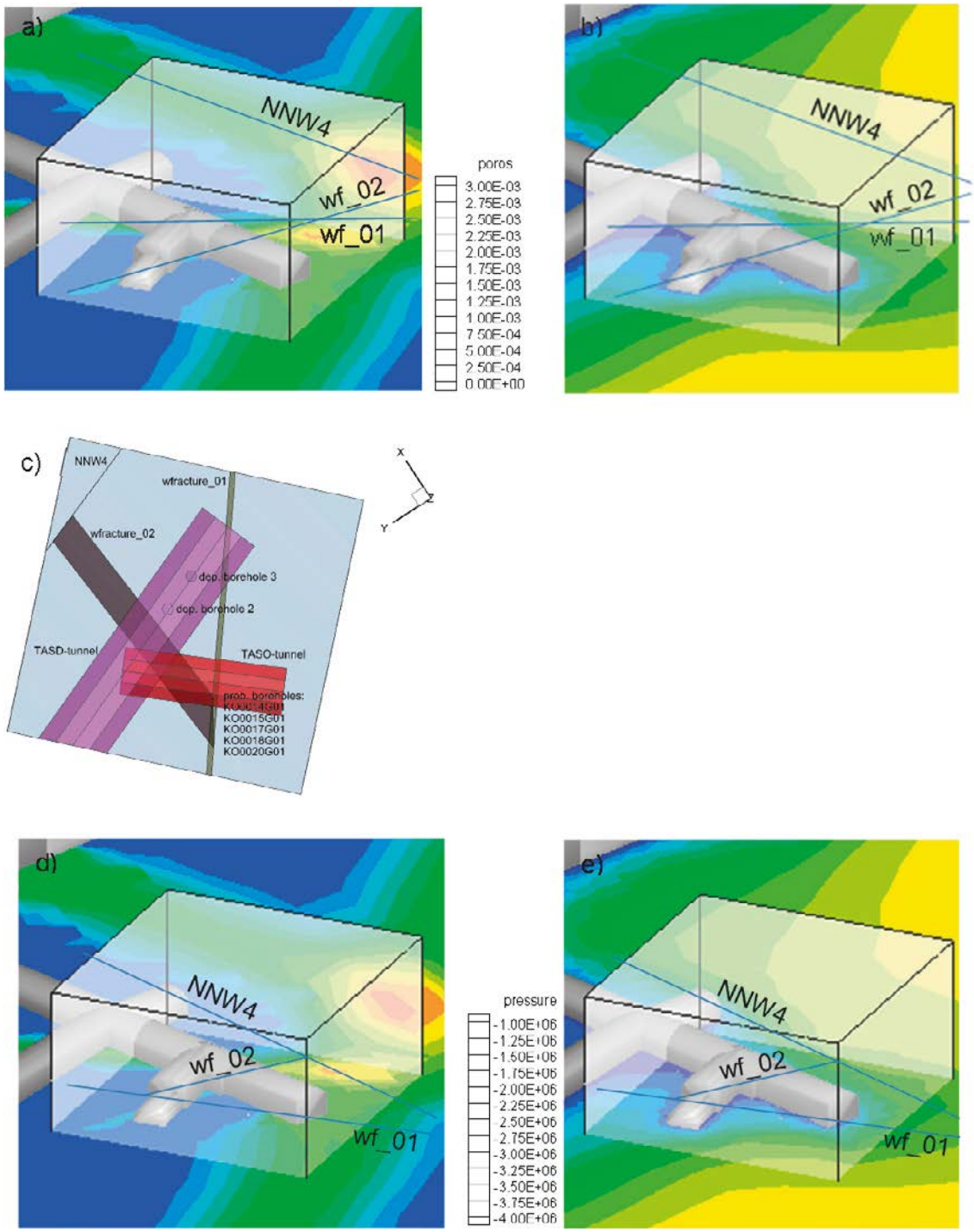

Figure 3-9. *Location of large deterministic fractures at the BRIE-site.*
a) Porosity distribution and referring fracture locations.*
b) Pressure distribution and fracture locations from a).*
c) Fracture locations in the BRIE-site model.
d) Porosity distribution and fracture locations after Vidstrand et al. (2017).*
e) Pressure distribution and fracture locations after Vidstrand et al. (2017).*

** Large-scale model; from Vidstrand et al. (2017).*

3.6 Conclusions and recommendations

According to the strategy outlined in Section 2.2.2 the first step of setting up a flow model has significantly progressed by including the effect of background fractures. This has been done by two measures. Background fractures considered to be opened by boreholes were included as discrete fractures embedded in an otherwise undisturbed matrix. An accordingly low permeability was therefore assigned to the matrix in a box-like zone of 1 m thickness around the boreholes. Beyond this box the background fractures were assumed to form an additional equivalent continuum adding to the hydraulic effect of the matrix. The stochastic element of a discrete network of background fractures gets lost with this conceptual simplification. What remains is the requirement that the fractures crossing boreholes need to be described.

Most useful is such an approach if the purpose of modelling is the interpretation of hydraulics in a well known fracture layout. In the light of the discussion in the previous section the value for predictive modelling is limited, though. The same applies to interpretive modelling with only partial knowledge about the domain in question.

For another reason, even the conceptually simplest problem of steady-state flow at the BRIE-site seems to be not a well posed one in Task 8c. Comparatively little is known for a major part of the model domain. Control data are essentially known in the framework of Task 8c for the immediate area of the BRIE-site. Restricting the attention to the BRIE-site improves therefore the situation a bit. But it is doubtful that a unique representation of the model domain can be found with more data exclusively from the BRIE-site.

Besides the problem with control data there is also a problem with scales. In the immediate vicinity of the probing boreholes background fractures contribute significantly to the flow system. On the one hand they are hardly large enough to be characterized discretely but on the other hand they are too sparsely distributed on the scale of the BRIE-site to allow forming a REV. Only geostatistical descriptions exist for these fractures. Basically this is emphasizes the earlier statement that in Task 8 deterministic answers are expected from a system that is known only in terms of geostatistics.

The need for understanding the flow model increases with the degree to which water uptake in the bentonite depends on quantification of the outflow from the rock. With regard to the bentonite-rock interaction the availability of groundwater for the bentonite re-saturation process is considered to be of major interest. For a reliable prediction the flow model should be set up with a clear view concerning the following two key questions: “Where does the water come from?” and “On which way does it get to the boreholes?”. However, based on the data from the task description there is no clear answer to these questions and the worth of just one flow model in a row of equally justified alternative models is limited with a view to quantitative predictions.

The problem of predictions for the concrete small-scale experiment appears to have in principle different requirements than those for a site-characterisation. Water conducting background fractures or sub-networks play apparently an important role for wetting of a specific borehole. But the stochastic nature of these fractures prevents a deterministic representation and the real flow system remains therefore unknown.

In contrast to the BRIE, a first site-characterisation questions the qualification of an ensemble of boreholes as a whole. The focus is shifted then from small-scale to large-scale domains. In this situation the stochastic description of the background fracture networks can answer the question about the qualification of a borehole field as a whole by means of statistics. While qualification cannot be predicted for a specific borehole the percentage of qualified boreholes in the ensemble can be determined. Assessment of a single borehole would still require individual inspection though.

4 Task 8d: Predictions for BRIE and Water uptake test

4.1 Objectives

The main objectives of Task 8d were more or less the same as of Task 8c with additional probing boreholes, widening of the test boreholes, emplacing the bentonite buffer, and additional data. They were again divided into two subtasks that firstly addressed flow only and then also the wetting of the bentonite:

- Task 8d1
  - Calculation of "inflows and inflow characteristics to two 76 mm diameter probing boreholes".
  - Calculation of "inflows and inflow characteristics to two 30 cm diameter open boreholes".
  - Comparison of "inflows calculated for probing boreholes with inflows calculated for enlarged 30 cm boreholes".
  - Provision of "boundary conditions and initial conditions to the field experiment on the emplaced bentonite packs within the two 30 cm boreholes".
- Task 8d2
  - Evaluation of "the resulting wetting of the bentonite installed in the borehole characteristics established in Task 8d1".
  - Evaluation of "effects of heterogeneous fracture flow on the wetting".
  - Evaluation of "effects of heterogeneous matrix properties on the wetting".
  - Provision of "a base case for comparison with earlier results based on less elaborated hydrogeological models".

The new and modified geometries of the geotechnical openings called for a revised model of the site. Focus concerning Task 8d1 lay on setting up a flow model representing the actual status at the BRIE-site so the test boreholes are considered only in their widened state in this report. With the advanced code VIPER the difference between wetting at a contact with a fracture and wetting at a bentonite-matrix contact was investigated addressing Task 8d2.

In the course of activities for Task 8d it was decided to add a benchmark for modelling a water uptake test performed at Clay Technology (Vidstrand et al. 2017). This test was set up in such a way that it represented re-saturation in a horizontal slice through the bentonite at mid-height of the test borehole. As the test setup was most similar to the re-saturation model for Task 8d this additional task was addressed as well.

4.2 Approach

4.2.1 Flow model

By and large the same approach for the flow model as for Tasks 8b and 8c was used. The model domain was not increased despite the doubts about appropriateness of the size – it implied a rather close vicinity of model boundary to the end of the TASO-tunnel (cp. Section 3.5.1) – to avoid the effort of deriving the new boundary conditions.

Sticking to modelling groundwater migration as single-phase flow it appears from different observations – see Appendix E for details – that a reduction of flow by a narrow zone of reduced permeability adjacent to the geotechnical openings, a so-called "skin", would be required for the flow model of the BRIE-site. The concept of a hydraulically rather tight box at the boreholes that was cut by assumed fractures as in Task 8c was therefore dropped. Instead, a skin zone around all geotechnical openings was adopted. Except for the three large fractures no smaller fractures were considered to cut through the skin. The effect of these small intersecting fractures was assumed to be averaged over the surface of the skin. While losing accuracy with respect to local flow features the approach allowed for a quick application to the complete ensemble of geotechnical openings.

While the physical reason for the observed considerable flow reductions related to the skin has not been determined yet there are two mechanisms thought to be responsible, degassing of dissolved gases where the water pressure drops below vapour pressure and mechanical effects from changes of the stress field in the rock. Impediment of flow by forming of gas bubbles can take place only in rather small flow channels where a high capillary pressure prevails. This would affect the matrix with its very small pores rather than the fractures where bubbles are likely to be flushed out right after forming. Increased stresses on the other hand should affect the transmissivity of fractures more than the permeability of the matrix.

The revised model was therefore designed to contain a low permeability skin around tunnels and boreholes. It also allowed for a reduction of permeability where the large deterministic fractures were located within this skin. As in Task 8c the effect of a network of small background fractures was reflected by an increase of the permeability of the otherwise undisturbed matrix.

4.2.2 Re-saturation model

Unrestricted water supply had been addressed for the bentonite in the re-saturation model for Task 8c. Complying with the conceptual re-saturation model a Dirichlet type boundary condition assigning maximum humidity to the inflow boundary is prescribed in this case. But the calculated flow rates at the BRIE site did not meet this assumption for the rock matrix. A new boundary condition restricting water uptake to a maximum inflow rate had therefore been formulated as described in Appendix F and implemented in the code. This allowed in principle to calculate water uptake of the buffer in the BRIE experiment at the observed large water-bearing fractures as well as over the areal matrix boundary.

For predictions of the water uptake in the BRIE test three cases were set up:

- Outflow concentrated to just one fracture of a width of 0.1 mm (case I).
- Outflow concentrated to a borehole section of one metre in height (case II).
- Outflow over the whole borehole surface according to the estimated outflow rate from the TASO tunnel (case (III).

To address uncertainties caused by inaccurately calculated flow rates from the flow model the prescribed inflow rates for cases I to III were increased and decreased by a factor of 5 leading to supplemental models. The calculated times until saturation was reached gave an idea about the sensitivity related to this type of uncertainty.

At Clay Technology a water uptake test supporting the BRIE had been performed whose results formed the basis for an additional benchmark within Task 8d. The conditions for this test were chosen to comply with a horizontal slice of bentonite in mid-height of the vertical cylindrical bentonite column. They matched the GRS re-saturation model for unrestricted water uptake so that a model very similar to the model for Task 8c could be used to simulate the test. As the results for Task 8c were produced without knowledge of the new benchmark they could be taken as a blind prediction.

4.3 Model setup

4.3.1 Coordinates

(See related Section 2.3.1 for Task 8b.)

4.3.2 Model domain

The flow model for Task 8d encompassed all 23 boreholes. Taking the skin effect into account the model contained the following structural elements:

- Matrix including background fractures.
- Tunnel skin.
- Borehole skin.

- Large fractures (wfracture_01, wfracture_02, NNW4).
  - wfracture_01 within tunnel skin
  - wfracture_01 within borehole skin of KO0011A01 and KO0011B01
  - wfracture_02 within tunnel skin

Shown in Figure 4-1 is a part of the model where the skin around the TASD-tunnel is partly removed and around the TASO-tunnel even totally omitted. Also not depicted are the borehole skins outside the tunnel skins.

According to Appendix E a thickness of 1 m was adopted for the skin around the tunnels. In the absence of direct evidence the skin around the boreholes is assumed to amount to a thickness of approximately one half of the borehole radius.

4.3.3 Drifts and boreholes

Additional to the five probing boreholes considered in Task 8c fourteen vertical and four horizontal observation boreholes had been drilled before the beginning of Task 8d. Locations of these boreholes are depicted in Figure 4-2 and Figure 4-3, respectively. The diameter of the test boreholes KO0017G01 and KO0018G01 had been increased to 30 cm. Implementation of the new boreholes into the model was made easier than for Task 8c as the location data for all boreholes was provided as an excel-file where the coordinates were given with a sufficient numerical accuracy.

4.3.4 Fractures

(See related Section 3.3.4 for Task 8c.)

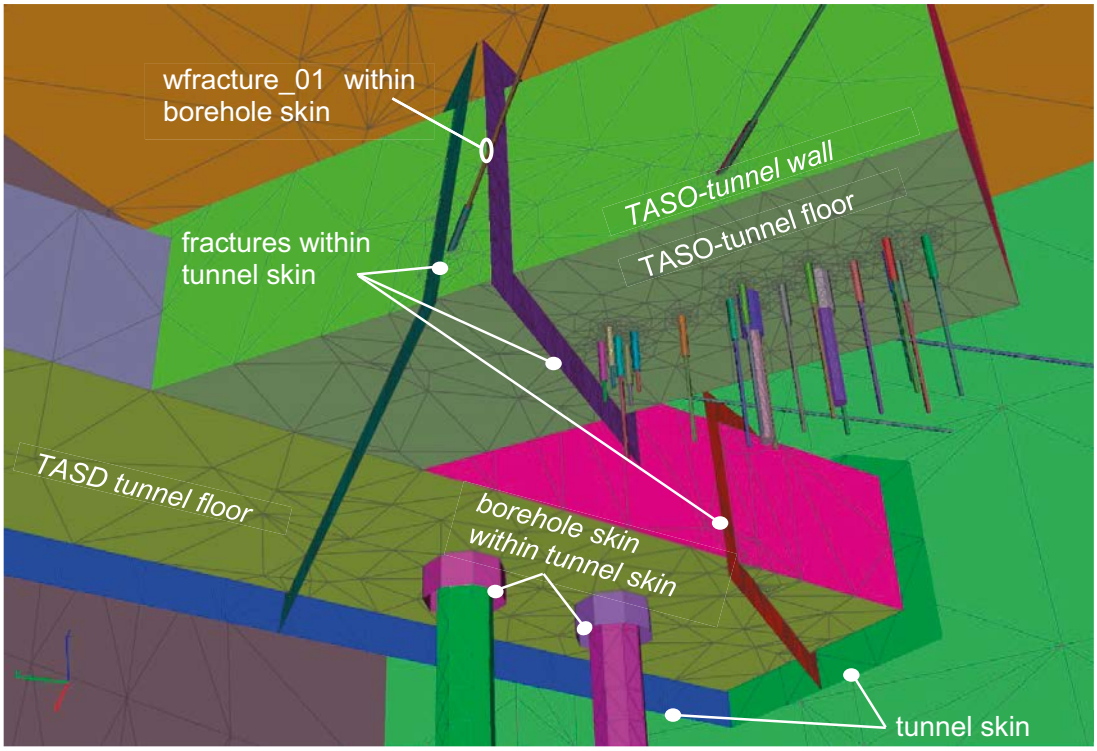

Figure 4-1. *Look from below at the BRIE-model for Task 8d.*

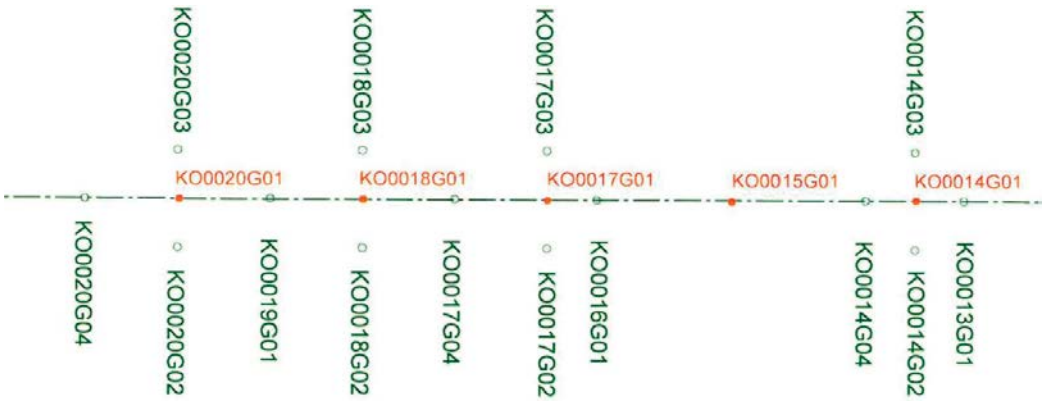

Figure 4-2. *Location of the vertical boreholes in the TASO-tunnel; from Vidstrand et al. (2017).*

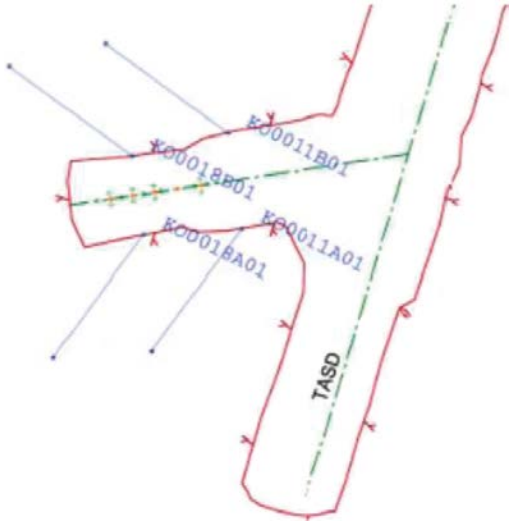

Figure 4-3. *Location of the horizontal boreholes in the TASO-tunnel; from Vidstrand et al. (2017).*

4.3.5 Hydraulic properties

New laboratory tests on de-stressed matrix core samples showed a range of permeability values between 6×10^{-21} m^2 and 9×10^{-20} m^2 (Vidstrand et al. 2017) which appeared to be very much in line with the data for Task 8c (cp. Section 3.3.5). However, as the calibration exercise for Task 8c had shown the effective permeability including the influence of the background fractures was apparently much higher. The value of 10^{-17} m^2 derived for Task 8c was also adopted for Task 8d.

Hydraulic tests in borehole KO0011A01 provided a somewhat reduced transmissivity value of $4 \times 10{-}16$ m^2/s for wfracture_01 in comparison to the value from Task 8c. Where the fractures lay within a skin zone fracture permeability was generally reduced by one order of magnitude in comparison to the measured data.

The permeability of the tunnel skin was assumed to be 10^{-18} m^2 that is one order of magnitude lower than the matrix permeability. For the assignment of permeability values for the borehole skins the boreholes were divided into two groups according to the preliminary outflow rates indicated in Figure 4-4. The skin permeability for all boreholes with an outflow rate above 0.1 ml/min was chosen to be 10^{-19} m^2 while a value of 10^{-20} m^2 was assigned to boreholes with an outflow rate below 0.1 ml/min. These values are generally lower than the permeability of the tunnel skin since it was expected that a zone of degassed bubbles would be more localised around a borehole than around the tunnel thereby impeding flow more effectively. The assignment of permeabilities to the structural elements of the model in the reference case is summarised in Table 4-1.

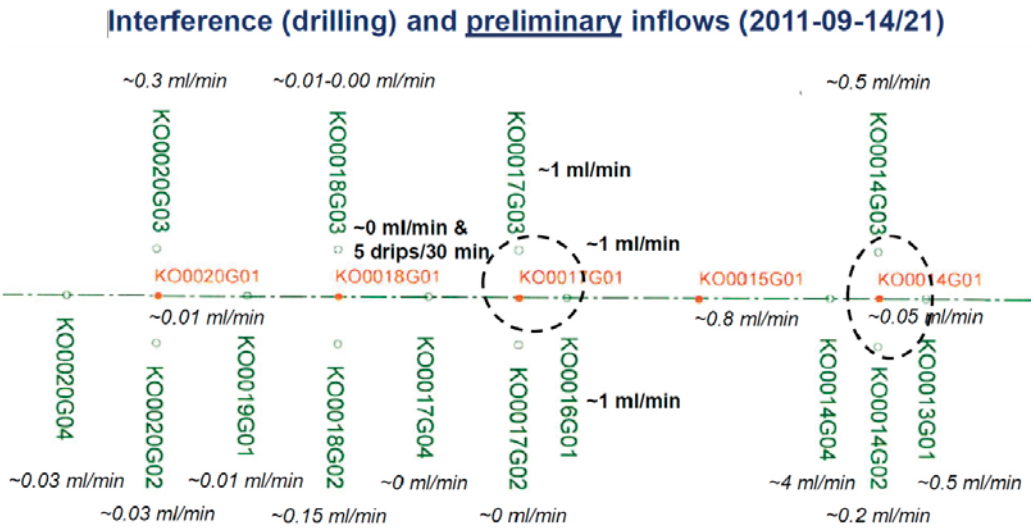

Figure 4-4. *Preliminary outflow data for the vertical boreholes; from Fransson et al. (2017).*

4.3.6 Hydraulic boundary conditions

(See related Section 3.3.6 for Task 8c.)

4.3.7 Effects from groundwater salinity

(See related Section 2.3.7 for Task 8b.)

Table 4-1. Assignment of permeabilities to hydraulic structures; reference case.

Structure	Permeability [m^2]
Matrix including background fractures	10^{-17}
wfracture_01, wfracture_02, NNW4	4×10^{-16}, 2×10^{-16}, 6.5×10^{-15}
Tunnel skin	10^{-18}
wfracture_01 within tunnel skin	4×10^{-17}
wfracture_01 within borehole skin	4×10^{-17}
wfracture_02 within tunnel skin	2×10^{-17}
Skin for boreholes KO0013G01 KO0014G02, KO0014G03, KO0014G04 KO0015G01,KO0016G01 KO0017G01, KO0017G03 KO0018G02, KO0020G03	10^{-19}
KO0014G01, KO0017G02, KO0017G04 KO0018G01, KO0018G03 KO0019G01 KO0020G01, KO0020G02, KO0020G04	10^{-20}

4.3.8 Calibration of the flow model

Calibration parameters

In order to fit the outflow rates of the model to the measurements, some of the quantities listed in Table 4-2 were varied. The table also provides indications for possible parameter ranges.

Table 4-2. Permeability values and possible ranges for the Task-8d model.

Hydraulic structure	permeability range
Matrix	10^{-17} m^2 ± one order of magnitude
Tunnel skin	Less than matrix permeability
Borehole skin	Less than matrix permeability
wfracture_01	4×10^{-16} m^2 ± one order of magnitude
wfracture_02	2×10^{-16} m^2 ± one order of magnitude
NNW4	6.5×10^{-15} m^2 ± one order of magnitude
wfracture_01 within tunnel skin	Between 1 and 1/100 of fracture permeability
wfracture_02 within tunnel skin	Between 1 and 1/100 of fracture permeability
wfracture_01 within borehole skin	Between 1 and 1/100 of fracture permeability

Control quantities and data for checking the model

There had been several campaigns to measure outflow into the boreholes:

- 2010 (campaign A):
  Short-term measurements after drilling the first five boreholes for all five boreholes.
- 2010 (campaign B):
  A 400 minute test of inflow into KO0017G01.
- 2011 (campaign C):
  Short-term measurements (15 min) after drilling 18 additional observation boreholes.
- 2012 (campaign D):
  Investigation of outflow distribution into KO0017G01 after
  - widening and deepening of KO0017G01,
  - widening of KO0018G01.

The task description concentrated on data for the first five probing boreholes which is summarized in Table 4-3. The data varied from campaign to campaign and thus seemed to indicate a certain change in the flow system. The pronounced short-term transient behavior of the outflow rates as depicted in Figure 4-5 for KO0017G01 and for KO0011A01 suggested that short-term tests overestimated the steady-state flow rate. The two columns furthest to the right in Table 4-3 contain the outflow values against which the flow model has been calibrated. They are actually based on some scientific guesswork because they are especially uncertain if one campaign provided no flux above the detection limit.

Table 4-3. Outflow rates at different times.

Borehole	Outflow in [ml/min] from campaign				Adopted	
	A	B	C	D	[ml/min]	[m^3/s]
KO0014G01	1.0	–	0.1	–	0.03	5.00×10^{-10}
KO0015G01	0	–	0.6	–	0.15	2.50×10^{-9}
KO0017G01	0.5	0.25	1.0	0.12–0.25	0.25	4.17×10^{-9}
KO0018G01	0	–	0	0.01–0.03	0.02	3.33×10^{-10}
KO0020G01	0	–	0.01	–	0.01	1.67×10^{-10}
KO0011A01*	–	–	0.1	–	0.10	1.67×10^{-9}

* Filed under campaign C because it was performed at the same time as the other tests of this campaign. In contrast to the other tests however this particular test lasted about 120 min.

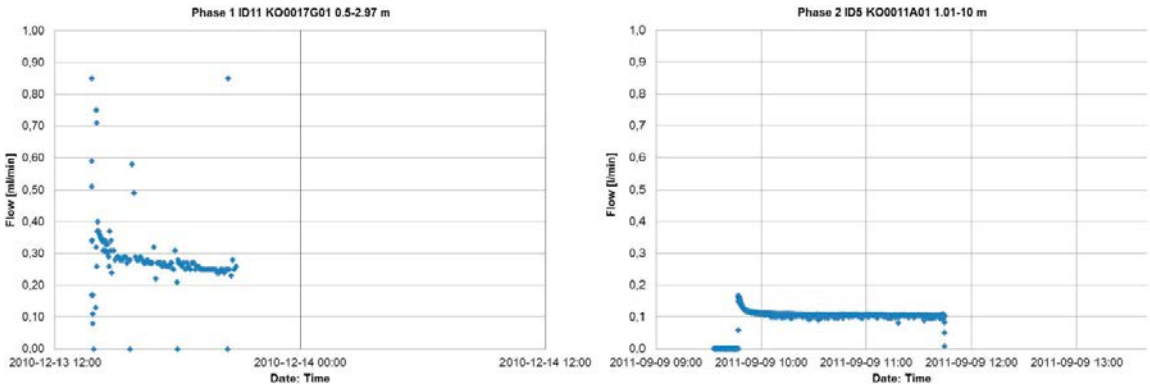

Figure 4-5. *Outflow rates for KO0017G01 and for KO0011A01; from Vidstrand et al. (2017).*

Note that the adopted flow rates were in contradiction to the trend of increasing pressure gradients towards the end of the TASO-tunnel. Since model geometry and boundary conditions are basically the same as for Task 8c the same contradiction was expected for the Task 8d model. However, the preliminary flow data for all vertical boreholes summarised in Figure 4-4 indicated that the flow rates can change from borehole to borehole by two orders of magnitude if an outflow rate could be measured at all (e.g. KO0014G01 and KO0014G04 or KO0017G01 and KO0017G02). A rather high inhomogeneity in the permeability appears to be introduced by water conducting background fractures. The adopted flow rates for calibration were therefore considered to be more a guideline than an absolute target.

New data from the test with sorbing mats (cf. Section 2.4.3) provided an estimation for the outflow into the TASO-tunnel of only 1.7 ml/s for Task 8d (Vidstrand et al. 2017). While it is not explicitly mentioned in the task description it is assumed from the data of this test (cp. Section 2.4.3, Figure 2-16) that this value does not account for outflow from the large deterministic fractures.

Water pressure in the packered-off boreholes cannot be simulated with the model described here. A qualitative assessment by looking at the calculated pressure field was performed though. Basis was the data summarized in Table 4-4. In the Task description it was asked to “use primarily KO0017G01 and boreholes in wall (11A01, 11B01, 18A01, 18B01)” as calibration targets.

Table 4-4. Pressure measured in the packered-off boreholes; after Vidstrand et al. (2017).

Borehole	Orientation	Section [m]	Pressure [bar]
KO0015G01	Vertical	2.1–3.03	5
KO0017G01	Vertical	2.11–2.97	5
KO0018G01	Vertical	1.42–3.06	4
KO0020G04	Vertical	2.0–3.5	10.5
KO0020G03	Vertical	2.0–3.5	9
KO0011A01	Horizontal	1.01–10	27
KO0011B01	Horizontal	1.24–10	3
KO0018A01	Horizontal	1.11–10	26
KO0018B01	Horizontal	1.28–10	21

Strategy

Modelling groundwater flow for Task 8d started out again with a reference case which was then supposed to be adjusted in order to match the calibration targets. As it turned out, though, the resulting match was not bad from the beginning on. The remaining discrepancies could not be resolved so that the reference case became the final flow model for Task 8d. For the reference case the following models were set up:

- Model A: All boreholes closed.
- Models B to G: Just one of the following boreholes open: KO0014G01, KO0015G01, KO0017G01, KO0018G01, KO0020G01, and KO0011A01.
- Model H: Only both test boreholes KO0017G01 and KO0018G01 open.

4.3.9 Re-saturation model for the BRIE and the water uptake test

Geometry

The re-saturation model for Task 8c (cp. Figure 3-4) had not accounted for the central tube of the test-pack for the BRIE (see Figure 4-6). Therefore the model geometry was slightly revised as depicted in Figure 4-7.

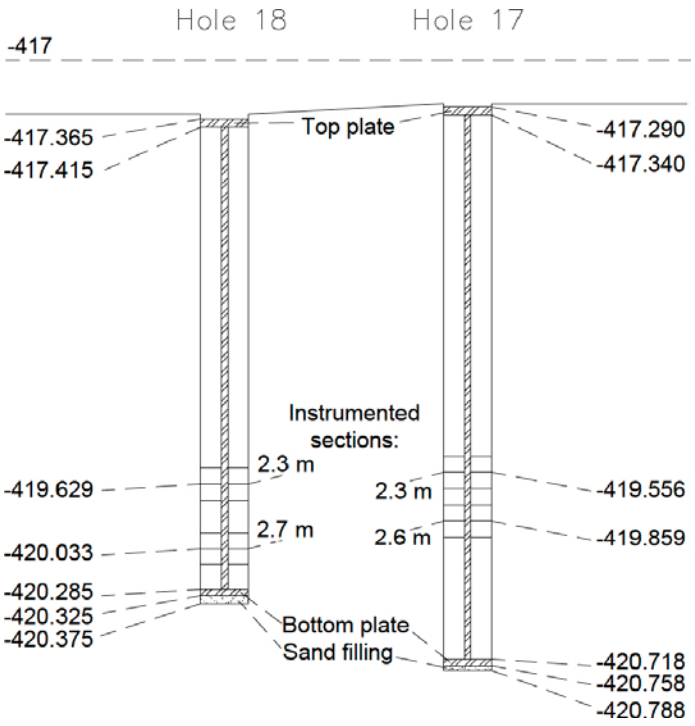

Figure 4-6. *Sketch of the bentonite installation packs; from Vidstrand et al. (2017).*

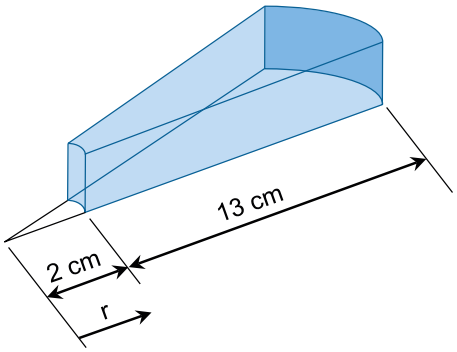

Figure 4-7. *Geometry of the re-saturation model.*

Bentonite

(See related subsection in section in 3.3.9 for Task 8c.)

Initial and boundary conditions

The water uptake test consisted of two identical test cells in which a cylindrical bentonite disk was saturated from the perimeter mimicking the situation of unrestricted water supply in the BRIE. In this case instantaneous full saturation at the bentonite-water contact and thus fully water saturated air at the model boundary as indicated in Figure 4-8 a) could safely be assumed.

The two tests were terminated at 107 and 203 days, respectively, to provide an idea of the development of the water content distribution within the samples. The re-saturation model for Task 8c (described in Section 0 and discussed in Section 3.4.2) could be looked upon as a blind prediction for the water uptake test based on a slightly different geometry because the central hole in the bentonite blocks had not been considered yet in Task 8c. The geometry was corrected to match the shape depicted in Figure 4-7 a) and the resulting model was calibrated by adapting the interlayer tortuosity.

In case of the BRIE outflow from the test boreholes KO0017G01 and KO0018G01 outflow rates had been measured. Additionally, there was the estimate for flow through the tunnel surface. Here the new boundary condition for the re-saturation model could be used where a maximum inflow rate is prescribed as indicated in Figure 4-8 b).

For the purpose of predicting the water uptake in the BRIE test three cases were set up:

- In case of KO0017G01 outflow is concentrated to just one fracture of a width of 0.1 mm (case I).
- In case of KO0018G01 outflow is concentrated to a borehole section of one metre in height (cp. Vidstrand et al. 2017) (case II).
- For the remaining parts of KO0017G01 and KO0018G01 an inflow rate according to the estimated outflow rate from the TASO tunnel is assumed (case III).

Measured or estimated outflow from the rock as well as the ensuing inflow values to be used as boundary conditions for the re-saturation model are summarized in Table 4-5.

Table 4-5. Inflow data as boundary condition for the re-saturation model.

Case	Location	Flow rate [m^3/s]	Related area [m^2]	Flux density [$m^3/(m^2\ s)$]	Model input value [$kg/(m^2\ s)$]
I	Fracture in KO0017G01	4.17E−09 (measured)	9.43E−05	4.42E−05	4.42E−02
II	Inflow area in KO0018G01	3.33E−10 (measured)	0.943	3.53E−10	3.53E−07
III	Tunnel surface	1.67E−06 (estimated)	460.0	3.63E−09	3.63E−06

The data from Table 4-5 shows that inflow from the tunnel surface was by a factor of ten larger than areal inflow into the borehole KO0018G01. Apparently there was a certain amount of fractures contributing to the outflow from the tunnel while the borehole was more or less fractureless. Case III had therefore been dropped.

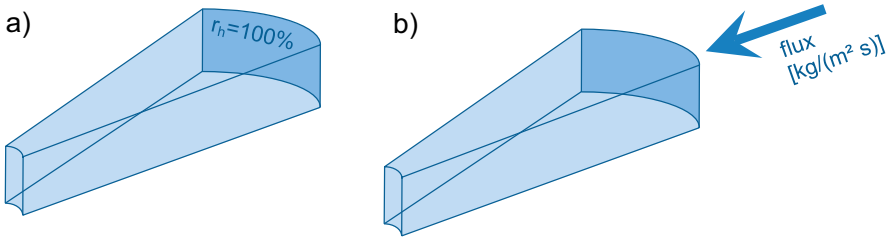

Figure 4-8. *Boundary conditions for the re-saturation model; a) for the water uptake test, b) for the BRIE test.*

The derived outflow value of 4.42×10^{-2} kg/(m^2 s) for case I exceeds the maximum inflow density of 2.2×10^{-4} kg/(m^2 s) calculated for the bentonite at free access to water in Task 8c (cp. Figure 3-7) by two orders of magnitude. Case I thus represents the situation of free access to water while water supply is restricted in case II.

If predictions of re-saturation times were based on simulated flow data, deviations between measured flow rates and calculated flow rates can represent a source of considerable uncertainty. This uncertainty was also investigated by re-running the model for case II with inflow rates increased and decreased by a factor of 5.

An initial water content of 10 % was assumed as prescribed in the task description for the bentonite in the BRIE as well as in the water uptake test (Vidstrand et al. 2017).

4.4 Results

4.4.1 Flow model

General observations

The trend of decreasing pressure from the model boundary towards the geotechnical openings is not surprisingly also found in the flow model for Task 8d as shown in the two cross-sections in Figure 4-9. In graph a) the traces of wfracture_01 and wfracture_02 are noticeable. Graph b) demonstrates the effect of the skin zone around the TASO-tunnel if compared to the analogous cross-section in Figure 3-6 a). Clearly recognizable is the shift of the high pressure zone towards the geotechnical openings that occurs because in comparison to a model without skin the pressure gradient within the skin increases while it decreases outside the skin.

The influence of the skin around the boreholes on the pressure field is rather little, though, as Figure 4-10 shows. Plot a) depicts the dynamic pressure when all boreholes are closed while plot b) shows the pressure field if only KO0017G01 is opened. The most prominent difference between plots a) and b) is the very low pressure zone tightly enveloping the borehole. Otherwise the differences appear to be marginal even if shown in a different scale as in plots c) and d).

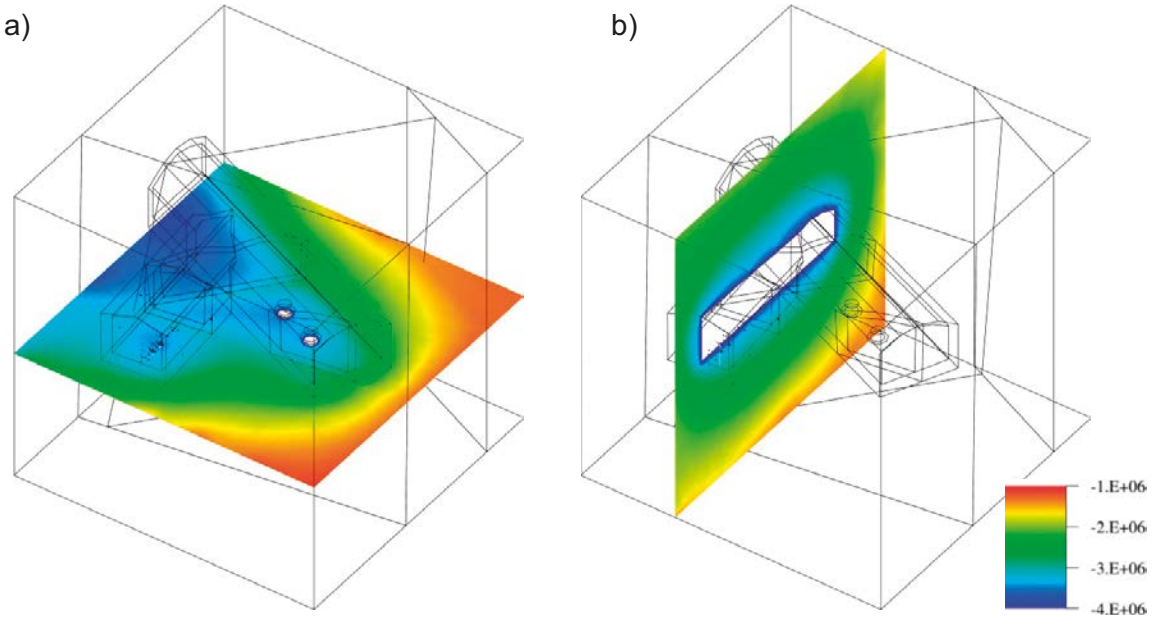

Figure 4-9. *Pressure distribution in a horizontal cross-section 1 m below tunnel floor; a) horizontal cross-section 1 m below tunnel floor, b) vertical cross-section through some of the boreholes*

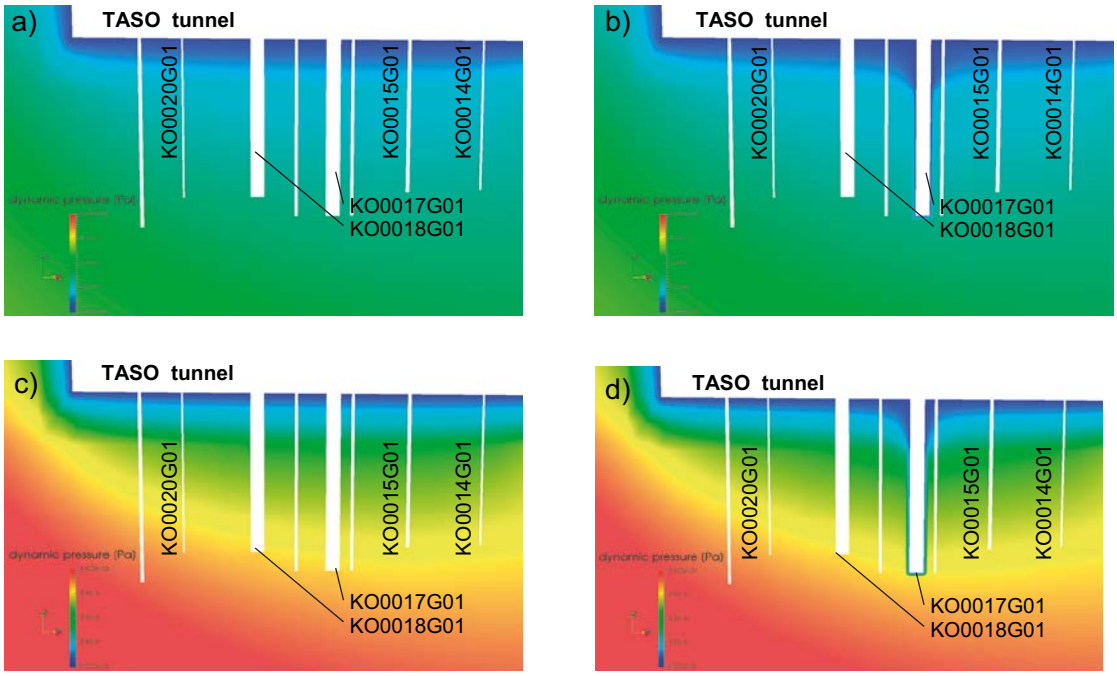

Figure 4-10. *Pressure in a vertical cross-section through some of the boreholes; a) all boreholes closed, b) only KO0017G01 open, c) and d) like a) and b) with different scales.*

Plots c) and d) in Figure 4-10 show clearly, that the vertical pressure gradient from the tunnel floor into the rock increases along the TASO-tunnel towards the tunnel face. Since the boreholes have roughly the same length they reach therefore deeper into the field of increasing pressure the closer they are located to the tunnel face. The model thus predicts a tendency of higher outflow rates from open boreholes and higher pressure in closed boreholes towards the end of the tunnel.

The composite view of the pressure field and the resulting flow in Figure 4-11 shows nicely the water-drawing effect of borehole KO0017G01 in the TASO-tunnel and of the boreholes for the TBT and the CRT in the TASD-tunnel. Additionally, water flow from the fractures into the matrix in the range of the tunnel system can be observed. Outside this range the effect of the fractures appears to be very limited.

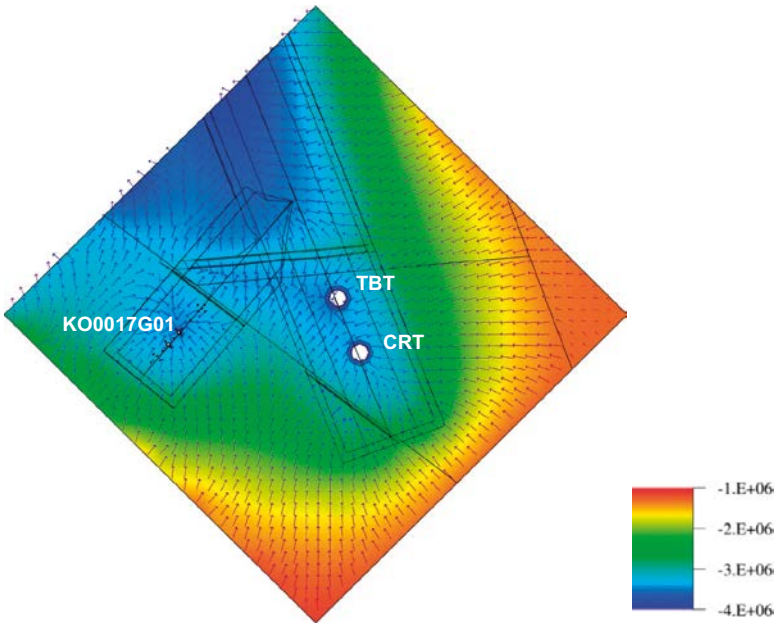

Figure 4-11. *Velocity and pressure in a horizontal cross-section 1 m below tunnel floor.*

Introducing a low permeable skin around an open structure like a tunnel or a borehole means a higher resistance to outflow into the referring structure. Water migrating towards this structure could therefore be diverted along hydraulically easier ways to nearby boreholes and fractures. The hydraulic effect of introducing a skin at a structure on other the structures depends on permeability and structure geometry. It has been tentatively tested with the model by switching skin zones on and off. The results are graphically summarized in Table 4-6. While the most system responses are as expected it is noteworthy that the effect of any skin is hardly observable in the fractures because of the rather high flow rates.

Table 4-6. Effect of permeability reduction on outflow.

Outflow via	Tunnel surface	Fractures	Boreholes
Perm. reduction in the			
tunnel skin	↘	–	↗
fractures in tunnel skin	↗	↘	↗
borehole skins	↘	–	↗

Reference case / final model for Task 8d

The calculated flow rates from models A to H are compiled in Table 4-7. Outflow into the boreholes was generally rather too high than too low in the model. In contrast outflow into the TASO-tunnel was too low. Any decrease of flow in the matrix that would have adjusted flow into the boreholes would also have decreased flow into the tunnel. As the outflow value for the tunnel was an estimate and the flow regimes in the borehole field was highly inhomogeneous no sense was seen in further adjustments of the permeabilities. The reference model thus represents already the final flow model for Task 8d.

Table 4-7. Comparison of outflow rates for the reference case; values in [m^3/s].

	Boreholes						
	KO14	**KO15**	**KO17**	**KO18**	**KO20**	**KO11**	**TASO-tunnel**
Measured	5.00E−10	2.50E−09	4.17E−09	3.33E−10	1.67E−10	1.67E−09	1.67E−06
Model A							5.47E−07
Model B	1.59E−09						5.46E−07
Model C		2.15E−09					5.46E−07
Model D			3.99E−09				5.45E−07
Model E				2.73E−09			5.45E−07
Model F					1.70E−09		5.46E−07
Model G						4.32E−08	5.42E−07
Model H			2.62E−09	2.62E−09			5.43E−07

Value lower than 0.2 times the measurement.
Value higher than 5 times the measurement.

Outflow from the tunnel surface was generally one third of the estimated value and can thus be considered to have been matched. Hardly any influence of open boreholes on the outflow from the tunnel surface can be noticed.

In model H both test boreholes were opened. A comparison of the outflow rates with those of models D and E shows that the flow rate is only moderately affected by opening a neighbouring borehole.

The calculated outflow for boreholes KO0014G01, KO0015G01, and KO0017G01 is matching the measured values. But it is too high for the two last vertical boreholes toward the end of the TASO-tunnel (KO0018G01 and KO0020G01). Increase of outflow toward the end of the TASO-tunnel is

consistent with the pressure distribution in Figure 4-10 around the TASO-tunnel as discussed in the previous subsection. Since the measured outflow in these two boreholes actually decreases towards the end of the tunnel, flow must be strongly influenced by local inhomogeneities caused by fractures.

The calculated high outflow rate from the horizontal borehole KO0011A01 is also too high, obviously a consequence of the immediate connection of the borehole with wfracture_01. While Figure 4-12 shows that a slight shift in the location of wfracture_01 would avoid a direct contact with KO0011A01 the task description states expressively that hydraulic tests had been performed in the fracture from this borehole. The reason for this massive discrepancy is therefore unclear which is quite unsatisfactory in the light of the comparatively well matched other data.

The model without any open borehole formed the basis for the comparison of measured and calculated hydraulic pressure. For this comparison it was assumed that the highest pressure found in the packered test interval (cp. Table 4-4) would reflect the measured pressure. The data were retrieved with the help of a visualization tool from a view as depicted in Figure 4-13 and are compiled in Table 4-8.

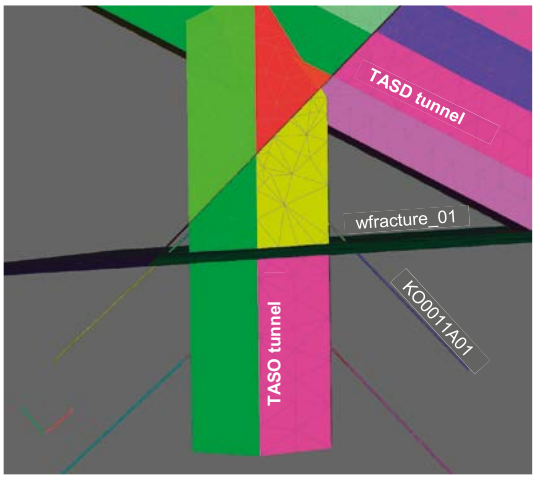

Figure 4-12. *View on the BRIE-model from above.*

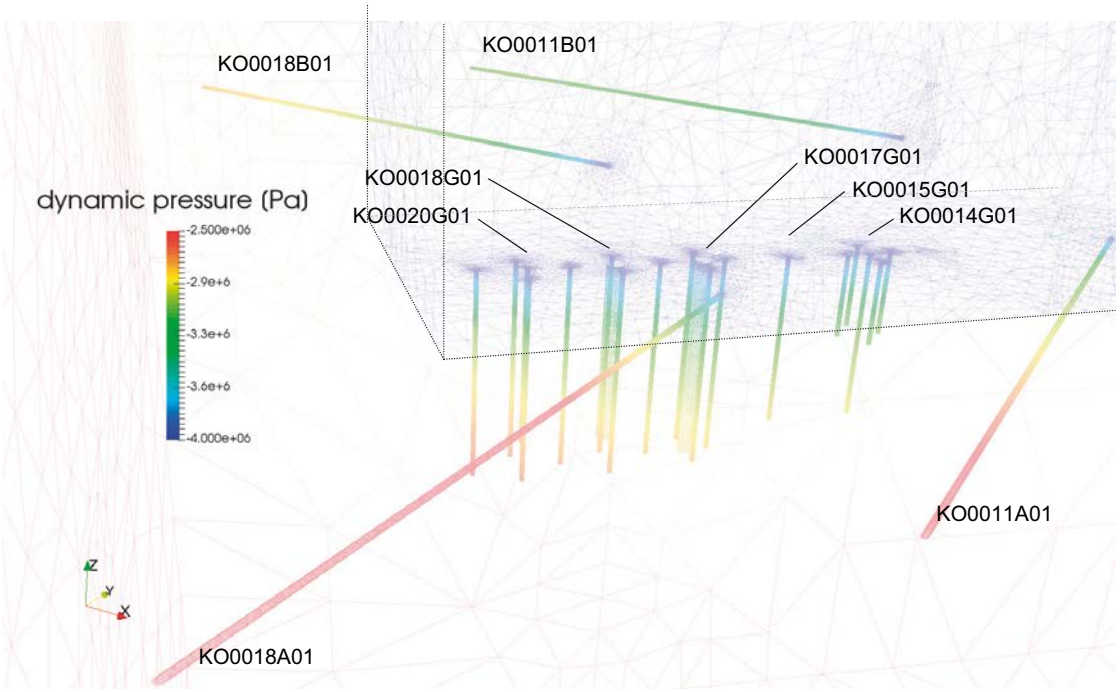

Figure 4-13. *Pressure at the surface of the boreholes.*

Table 4-8. Measured and calculated hydraulic pressure in the boreholes.

Borehole	Orientation	Pressure [bar] Measured	Calculated
KO0015G01	Vertical	5	11.2
KO0017G01	Vertical	5	11.6
KO0018G01	Vertical	4	12
KO0020G04	Vertical	10.5	14.5
KO0020G03	Vertical	9	13
KO0011A01	Horizontal	27	17
KO0011B01	Horizontal	3	9
KO0018A01	Horizontal	26	24
KO0018B01	Horizontal	21	13

Value higher than 2 times the measurement.

The calculated pressure in the vertical boreholes is generally higher than the measured pressures while the pressure in the horizontal boreholes is underestimated by the model except for KO0011B01. However, in all cases the calculated value is not off by more than a factor of 3.

By and large the pressure in the horizontal boreholes is higher than in the vertical boreholes as these boreholes reach deeper into the areas where high pressures prevail. The value of 3 bar for KO0011B01, however, appears to be strange in in the light of the 21 to 27 bar for the other horizontal boreholes. It strongly suggests a wrong assumption concerning the size of wfracture_02. As the model layout depicted in Figure 4-14 indicates, KO0011B01 is almost parallel to wfracture_02. If the fracture was not ending right at wfracture_01 but would extend a few metres beyond this intersection, KO0011B01 would be very closely aligned to wfracture_02 over the whole length. Since wfracture_02 is hydraulically highly conductive the pressure in the vicinity of this fracture would be quite low which would account for a rather low pressure in the packered borehole KO0011B01. Unfortunately, this was realized only after the model had already been set up so there was no possibility to check this hypothesis with the help of model variations.

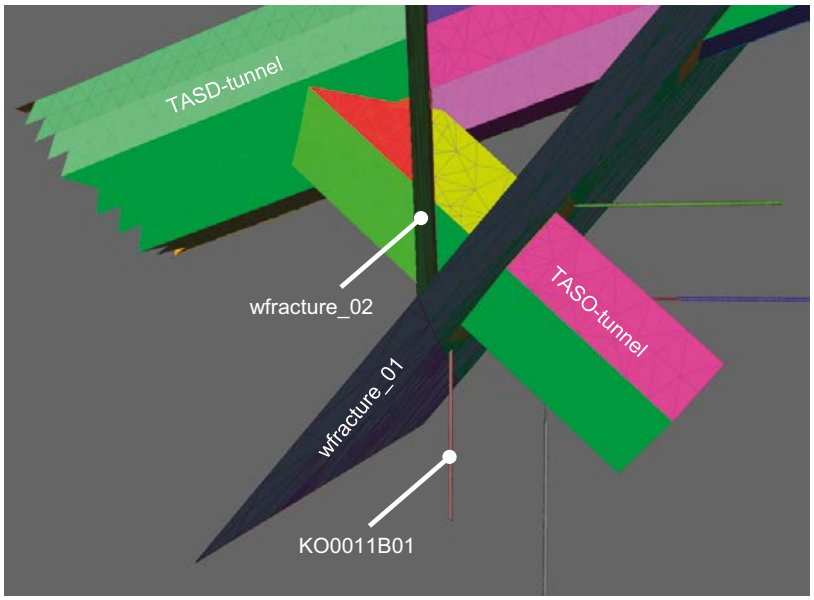

Figure 4-14. *Look from above at wfracture_02 and borehole KO0011B01.*

4.4.2 Re-saturation model for the BRIE test

The inflow data for cases I and II – large inflow concentrated in a fracture and low inflow distributed over a borehole surface related to a borehole section of 1 m length – were discussed in Section 4.3.9. The results from the re-saturation model for these two cases are given in terms of

- the development of the water content distributions in case of
  - free access to water (case I; see Figure 4-15 a)), and
  - restricted water supply (case II; see Figure 4-15 b)),
- the total water flow at the inflow boundary over time (see Figure 4-16), and
- the total water mass in the bentonite over time (see Figure 4-17).

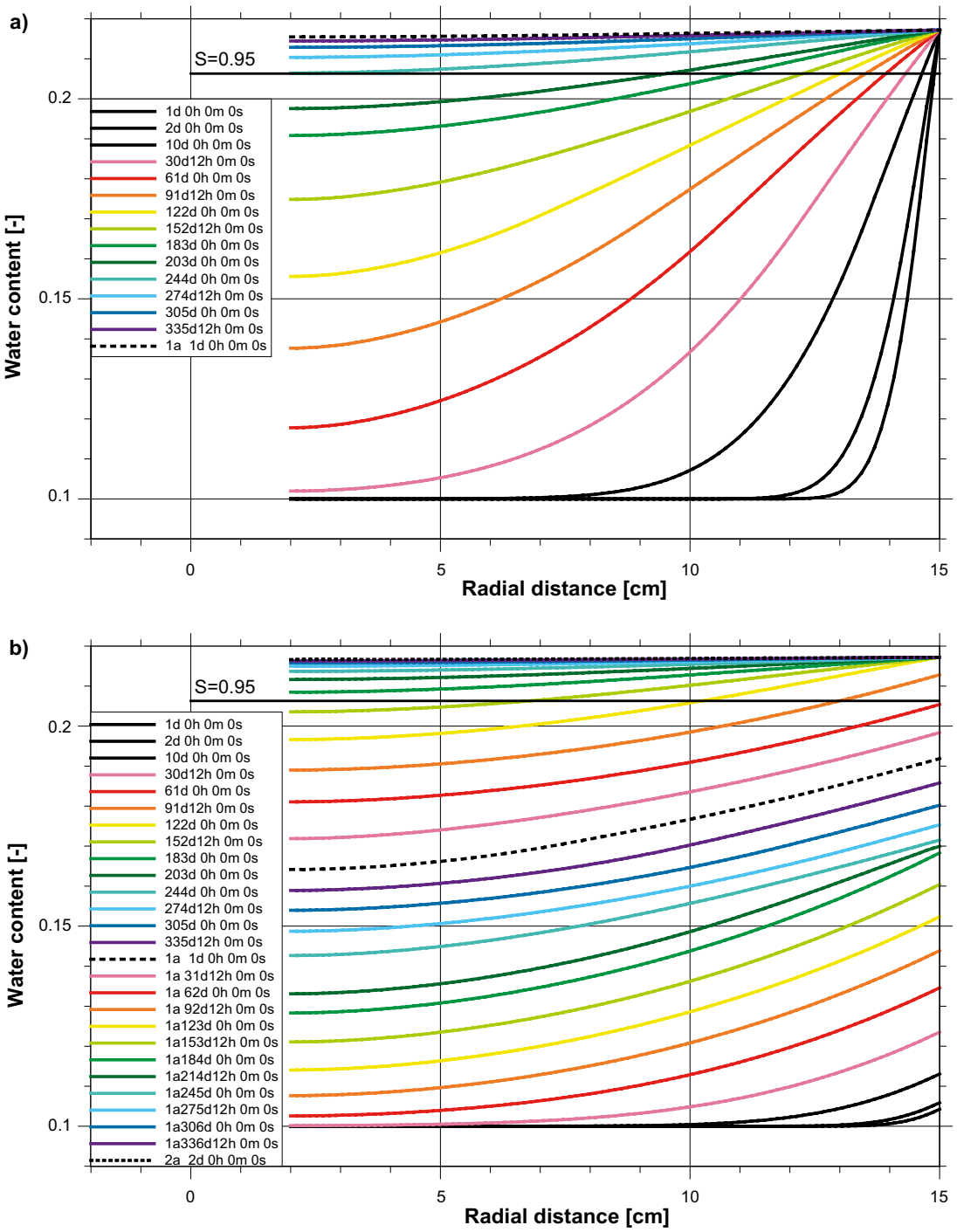

Figure 4-15. *Development of the water content distributions; a) case I: dynamics at unrestricted water supply, b) case II: dynamics at restricted water supply*

Full saturation can mathematically never be reached in the model since water flow in the bentonite depends ultimately on the gradient of the water content. Full saturation is therefore defined as the situation when at least 95 % saturation prevail in the whole domain. According to Figure 4-15 the bentonite is therefore called saturated after about 232 days in case I and after about 515 days in case II. Since the localized inflow is described in case I without considering 3d-effects, the value of 232 days represents only a lower limit for the true re-saturation time.

The dynamics of water uptake is rather different in cases I and II. In case of free access to water, inflow is very high in the beginning but subsequently decreasing rapidly. In case II it is constant at the rather low prescribed maximum inflow rate (outflow from the rock at atmospheric pressure) for quite some time before the phase of decrease commences also in case II. The uptake dynamics for cases I and II can be compared in Figure 4-16.

However, the total amount of water present in the bentonite in case I is never exceeding 160 % of the water in case II. The uptake rate in case I goes below the rate in case II at about 160 days. The difference in total mass of water in the bentonite decreases again after that time which can be seen in Figure 4-17.

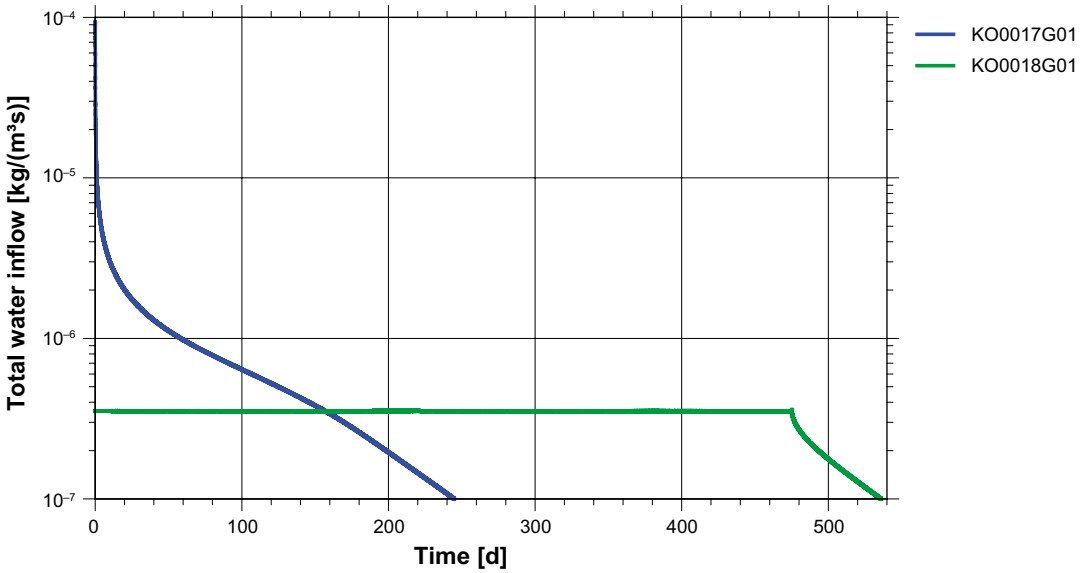

Figure 4-16. *Total water flow at the inflow boundary.*

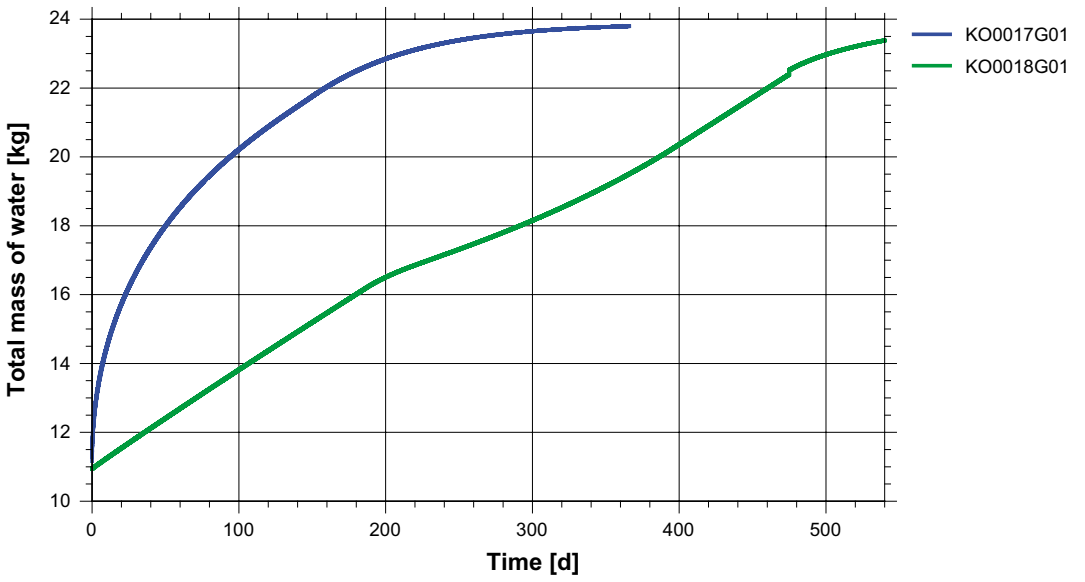

Figure 4-17. *Total mass of water in the bentonite.*

Note that the slightly changed trend in the water content distribution between 203 and 244 days in Figure 4-15 b) is a consequence of the increased water mobility in the interlamellar space that comes after completing the second hydrate layer (Kröhn 2011). Hydration in a third layer begins above a water content of about 17 %.

In case I with unrestricted access of the bentonite to water, the uptake dynamics are controlled by the re-saturation behaviour of the bentonite. Outflow rates from the rock are only relevant inasmuch they decide about the applicability of case I or case II. Inaccurately calculated flow rates would thus affect the re-saturation time only if the uncertainties would allow for a possible outflow rate below this threshold value. This, however, is not the case at the BRIE where outflow from the water-bearing fractures exceeds the threshold by several orders of magnitude (cp. Section 4.3.9).

In contrast even small differences in the outflow rate can be significant in case II as tentative calculations had shown. For a deeper insight into the relation between maximum outflow rate from the rock and re-saturation time, the prescribed inflow rates were modified stepwise by a factor of 5. The ensuing re-saturation times are summarised in Table 4-9 and some of the related inflow rates are depicted in Figure 4-18.

Maximum outflow rate from the rock and re-saturation time are apparently non-linearly related. By restricting the maximum outflow from the rock to 1/100 of the initial inflow rate in case of free access to water, the re-saturation time increases only by 9 % (case I and case II, inflow multiplied by 5). Restricting inflow further by an additional factor of 5 increases re-saturation time already by 131 % (case I and case II, reference value), and with the next reduction step re-saturation time amounts even to 800 % (case I and case II, reference value divided by 5). The relationship between outflow rate and re-saturation time seems to converge to a linear relation with decreasing outflow, though.

Table 4-9. Times required to reach full saturation in the re-saturation model.

Case	Inflow rate as measured	Time until full saturation [d]	Ratio to case I	Ratio to previous case
I	(Reference)	232	1	–
II	Multiplied by 5	254	1.09	1.09
	(Reference)	535	2.31	2.03
	Divided by 5	2087	9.00	3.90
	Divided by 25	10540	45.43	5.05
	Divided by 125	55354	238.60	5.25

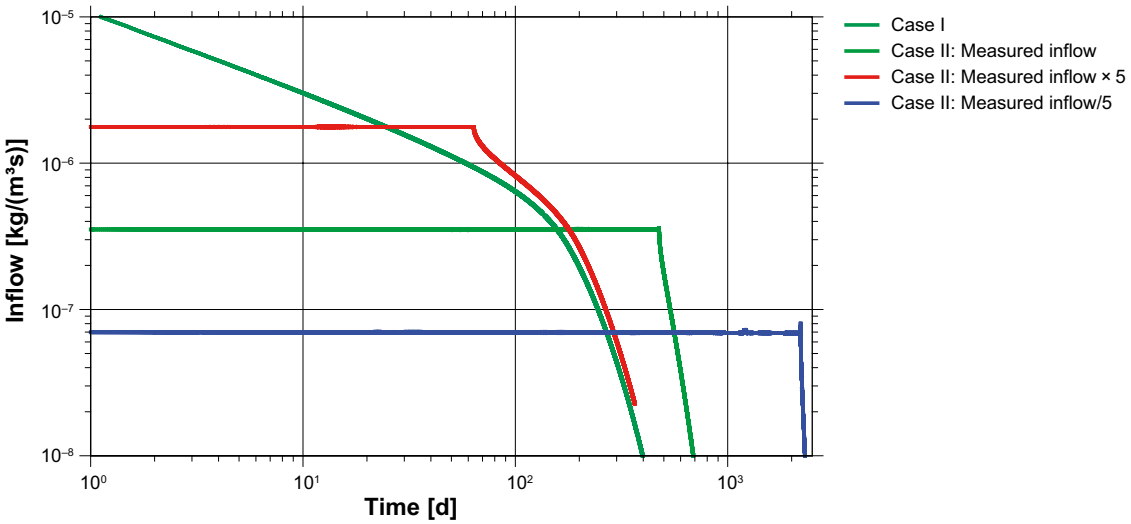

Figure 4-18. *Calculated inflow rates for varied maximum inflow rates.*

The reason for this non-linear relation appears to be the consequence of the complex interplay between three processes and effects:

- The prescribed flow rate at the inflow boundary.
- The re-distribution of water inside the bentonite.
- The possible change from restricted to unrestricted water supply when the prescribed maximum outflow rate from the rock exceeds the demand of the bentonite for water during the uptake. This implies a switch from Neumann boundary conditions as initially in case II to Dirichlet boundary conditions as in case I at all times.

The lower the inflow, the lower are the gradients of water content and relative humidity at the inflow boundary. Water migration into the bentonite is thus slowing down with a decreasing inflow rate so that the water content profiles in the bentonite flatten. This can lead to the situation where Neumann boundary conditions prevail until full saturation. The effect can be seen in Figure 4-19. The water content profiles for the different cases listed in Table 4-9 are plotted here at the time of reaching full saturation (as defined at the beginning of this section). The switch of boundary conditions has happened in the reference model for case II before reaching full saturation as the maximum water content at the right hand side lies at a saturation of 1. Reducing the inflow rate by a factor of 5, though, slows re-saturation down and prevents the model from switching the boundary conditions thus keeping the water content at the inflow boundary below a value of 1.

Without looking deeper into this matter, it can generally be concluded that the higher the outflow from the rock, the less sensitive is the re-saturation time to variations of the inflow.

4.4.3 Water uptake test

While the water content distributions calculated in Task 8c matched the measured distributions in the water uptake test qualitatively quite well already the simulated uptake was a bit too fast. But after adapting the model geometry and correcting the interlayer tortuosity (one of the very few parameters allowing model calibration to a certain extent) from 0.75 to 0.28 the model results matched the measurements well as shown in Figure 4-20.

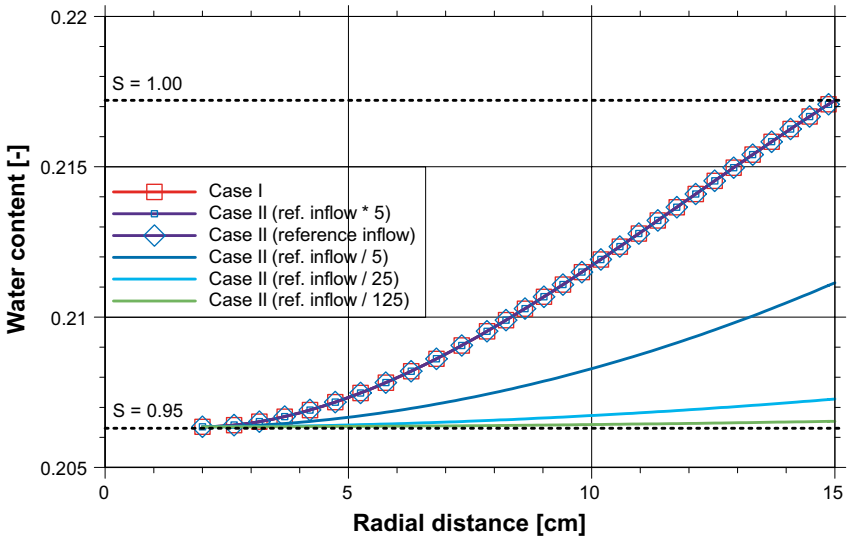

Figure 4-19. *Water content profile at reaching 95 % saturation at the driest location.*

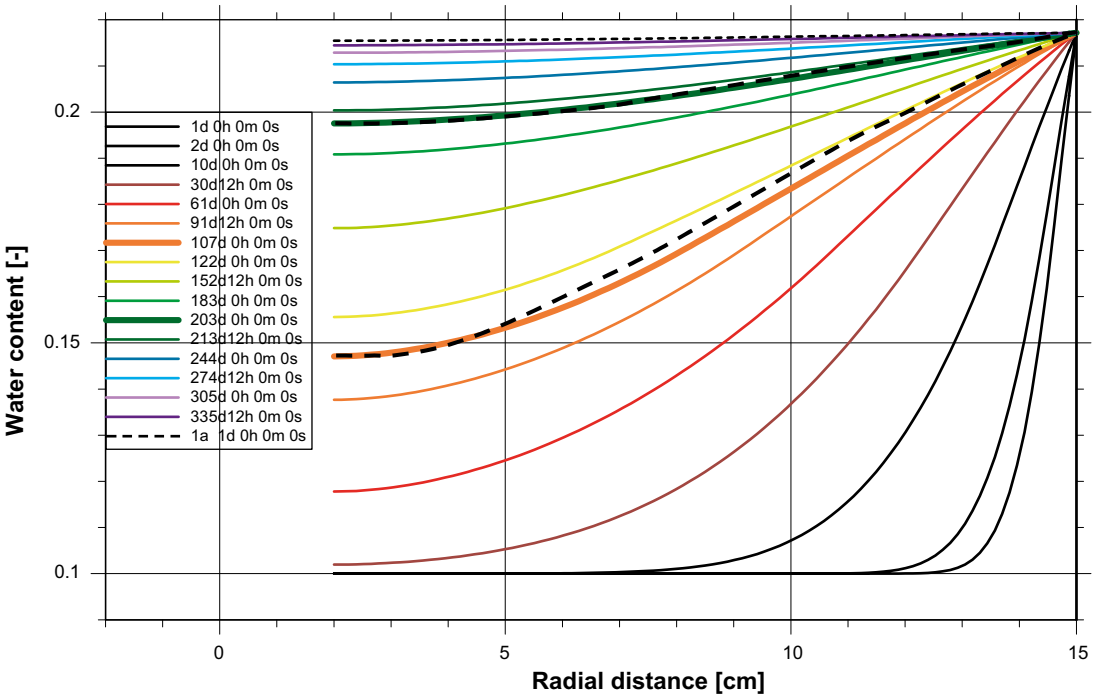

Figure 4-20. *Prediction of the water content evolution in the water uptake test; measured curves in black dashed lines.*

4.5 Discussion and conclusions

The following items had changed in the flow model from Task 8c to Task 8d:

- Additional probing boreholes had been drilled.
- There were more outflow and pressure measurements available.
- Conceptionally, the direct modelling of assumed fractures to account for the locally varying outflow from borehole to borehole had been dropped in favour of a low permeable skin at tunnel and borehole walls which was believed to be a more general approach.

Pressure data from the horizontal borehole KO0011B01 suggested a larger extension of wfracture_02 than prescribed in the task description. Unfortunately, this had been realised too late to be taken into account for the model.

The set of permeabilities for the reference case provided already a match with the measured and estimated outflow rates that could only marginally be improved by further calibration. The assumptions that led to the reference/final model were that

- the effective permeability of the matrix of 10^{-17} m^2 exceeds the value for the undisturbed matrix by about three orders of magnitude as in Task 8c, and is possibly caused by a well-connected network of smaller fractures,
- the skin permeability around the tunnels is one order of magnitude lower than the effective matrix permeability,
- the skin permeability around the boreholes is even two orders of magnitude lower to account for a more concentrated impediment by gas bubbles due to stronger converging streamlines,
- the permeability of fractures within a skin is one order of magnitude lower than fracture permeability outside the skin, and
- just one permeability per borehole skin was adopted.

That the flow field resulting from the first try could not be substantially improved is certainly no prove for a correct representation of reality by the model. But it provides the warm feeling that a good approximation within the limits of the model concept has been found.

There were of course some shortcomings. The outflow from KO0018G01 and KO0020G01 was too high by a factor of about 10. However the inconsistent trend of increasing pressure in the model and the measured decreasing outflow towards the end of the TASO-tunnel indicates an influence of background fractures that could not be captured by a deterministic model.

Even higher is the difference between measured and calculated outflow from the horizontal borehole KO0011A which had been drilled through wfracture_01 according to the task description. Decreasing the fracture permeability within the borehole skin did not help sufficiently because of the little dimension of this zone. The discrepancy could have been fixed alternatively by shifting the position of wfracture_01 by a little bit more than just a metre to avoid a crossing of fracture and borehole. But the task description indicates that wfracture_01 is indeed crossing KO0011A. This contradiction could not be resolved.

Modelling bentonite re-saturation for the BRIE confirmed the conclusion from Task 8c that re-saturation would be prolonged because of large areas of restricted access to water in comparison to the unrestricted access at the high and concentrated outflow from fractures. However, the differences in re-saturation time are not nearly as big as the differences of the outflow rates suggest.

The sensitivity of the re-saturation model against variations of the outflow rate from the rock has therefore been looked at more closely. The non-linearity of the relation between outflow rate and re-saturation time is significant. It leads generally to water uptake dynamics that are increasingly sensitive to variations of the outflow rate with decreasing outflow rates.

In case of local concentrated outflow as from a fracture the re-saturation model provides only a lower limit for the time until full saturation since modelling was restricted to an axisymmetric geometry. Full 3d-modelling would have been required for a precise prediction. As it is a re-saturation time of no less than 232 days and up to 515 days is expected.

Modelling the water uptake test proved to be successful. Only a comparatively little change in the parameter set resulted in a very good match of the model results with the measured data.

5 Task 8f: Checking predictive results against post-test data

5.1 Objectives

Task 8f had not been part of the original Task description. It had been felt valuable within the TF GWFTS, though, to check the predictive results especially of Task 8d against the post-test data that would soon be available. In a provisional Task definition it was then expressed that

- "Task 8f has not as Task 8c and 8d been divided into two parts; Task 8f only considers the bentonite wetting part."
- "The main objective of Task 8f is to evaluate the resulting wetting of the bentonite installed in the two boreholes."
- The modelling teams should have the opportunity "to re-evaluate their initial hypotheses and address sensitivities concerning conceptual issues, …"

This section is thus concerned with increasing model consistency by comparing results from the previous section to sensor and post-test data.

5.2 Approach

In the BRIE transient water uptake had been monitored by means of relative humidity sensors. So-called "wet" and "dry" sections in the test boreholes KO0017G01 and KO0018G01 had been identified. Wet sections were the ones where water producing fractures with the high outflow rates had been found. Applicability of a re-saturation model with unrestricted water supply for the bentonite was assumed here. Dry sections in contrast should represent restricted water supply at a minimum outflow rate from the rock.

In the following, thought is given basically to data that became available after dismantling the stack of bentonite blocks, called "parcels" in Fransson et al. (2017) in the two test boreholes. This includes the transient relative humidity data acquired during the test and extensive post-test data for the water content distribution in the bentonite parcels. There was an abundance of data but for an application of the VIPER, only data could be used where water uptake could be essentially interpreted by either a 1d-linear or 2d-axisymmetric model.

According to the calculations for Task 8d, water uptake under unrestricted availability of water for the bentonite was expected in the vicinity of the wetting fractures in the wet sections of the test boreholes. The first step was therefore a reconstruction of the wetting fractures in the wet sections of the test boreholes. By identifying the direction from which the water had entered the bentonite, location and direction for a 1d-model domain could be defined and a sequence of related sensor responses could be deduced.

Then a section was sought with as little water uptake as possible. The underlying assumption was here that such a section would represent water coming exclusively from the matrix and thus represent the case of restricted availability of water.

However, it was suggested that the sensor data from the chosen dry section might have been compromised by the wet section located only 30 cm lower in the parcel (Fransson et al. 2017). A third model was therefore set up to check this assumption. As it turned out it was not possible to discriminate in the dry section between water uptake from the matrix and vertical water migration based on the humidity sensor data.

In the hope to arrive still at some conclusions about re-saturation from the matrix, the post-test water content data were analysed in order to find a dry cross-section that was unaffected by vertical water migration. While such a section could be found the related water content profile raised new questions.

5.3 Model setup

5.3.1 Reconstruction of the test set-up

Since the sensors were installed for technical reasons at the interfaces of two prefabricated blocks the relative humidity measurements were influenced by the moisture development in both of these two blocks. Figure 5-1 shows a schematic view of the instrumentation as well as photographs from the realized installation.

In order to identify the sensor data that should compare best with a 1-D re-saturation model for unrestricted water supply, the strike lines of the fractures on the borehole surface at the instrumented wet sections were reconstructed. For this purpose the orientation of the fractures was calculated using information about dip and dip direction of the main fractures from Fransson et al. (2017) (cp. Figure 5-2). These data are compiled in Table 5-1. The strike would be the angle of the dip direction minus 90°. The shift of the strike lines from the instrument level to the top level of the upper block and the bottom level of the lower block is then easily calculated.

Table 5-1. Data for reconstructing the orientation of the main fractures.

Hole	Dip	Dip direction	Strike	Shift
17	66°	196°	106°	4.45 cm
18	53°	302°*	212°	7.53 cm

* Corrected value after correlation with wetting pattern of the retrieved bentonite parcel.

What remains is to pinpoint the location of the strike lines in relation to the instrumentation. The ones at instrument level can easily be constructed making use of the information "… that the pore pressure sensor came as close as possible to the fracture of interest in each bore hole." (Fransson et al. 2017). It would thus have to be assumed that the strike lines at instrumentation level would be very close to the position of the pore pressure sensors. However, at KO0018G01 an additional strike angle of the main fracture of 10° had been found after dismantling.

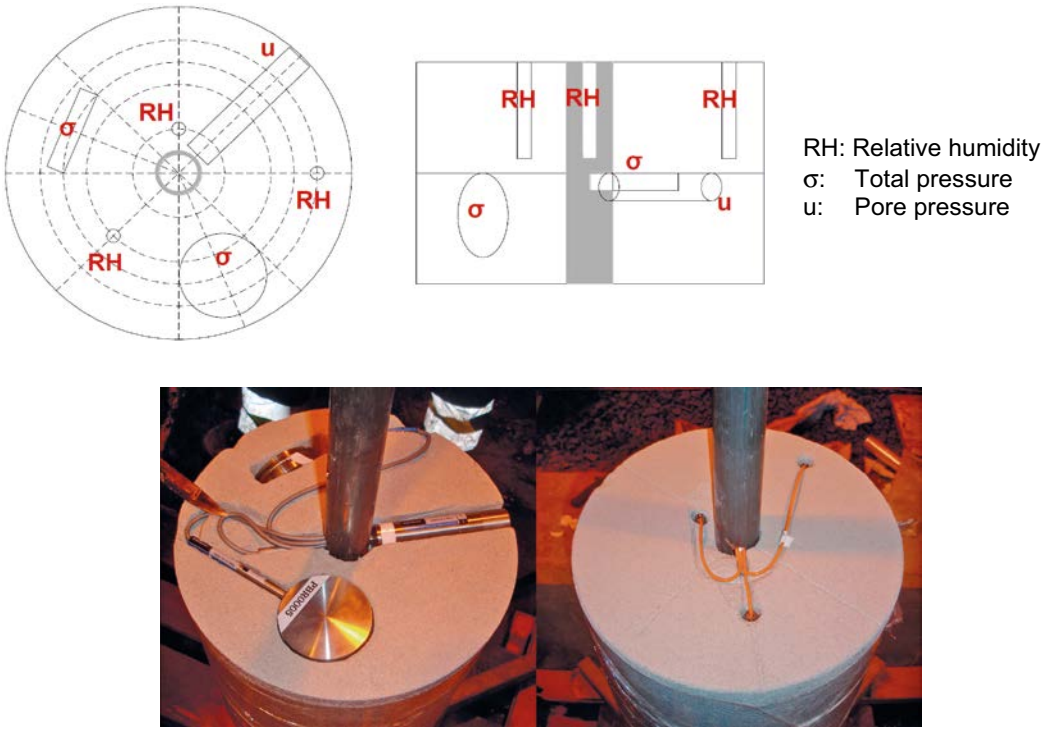

Figure 5-1. *Position of the sensors between two bentonite blocks (Fransson et al. 2017).*

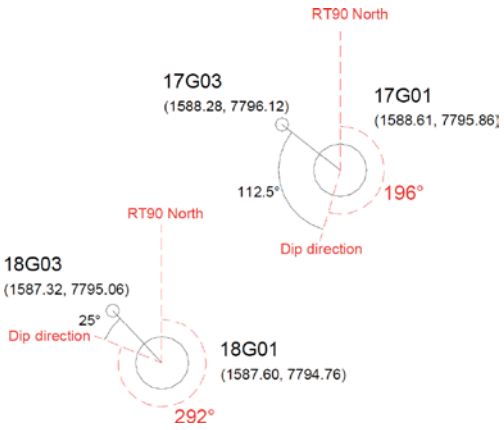

Figure 5-2. *Dip direction of the main fractures in the test boreholes; from Fransson et al. (2017).*

Later in the report it is stated "… that none of the (pore pressure) sensors were located close to a water bearing fracture." (Fransson et al. 2017). This implies a certain shift of the strike line in an unknown direction. As the relation of fractures and sensors in space is only sought in principle this last uncertainty will be ignored further on. The position of the relative humidity and pore pressure sensors in the dry and in the wet sections of boreholes KO0017G01 and KO0018G01 as well as the position of the reconstructed fracture strike lines are indicated in Figure 5-3. A 3d-reconstruction for the wet sections in KO0017G01 and KO0018G01 as well as the expected general water uptake dynamics is given in Figure 5-4.

Having established the complex three-dimensional relation between the sensor position and the fracture trace on the borehole wall the question which data set is most compatible with the model for unrestricted water uptake in Task 8d can be addressed. Ideal would have been an axisymmetric wetting from the borehole wall which is certainly not the case in the wet sections of the BRIE. The next best approximation is that of a vertical fracture being close to the outermost sensor (which would rather call for a model with a constant cross-section). This is also not found at the BRIE. However, with a dip of 66° the fracture in the wet section of KO0017G01 appears to be slightly better suited than the fracture with a dip of 53° in KO0018G01.

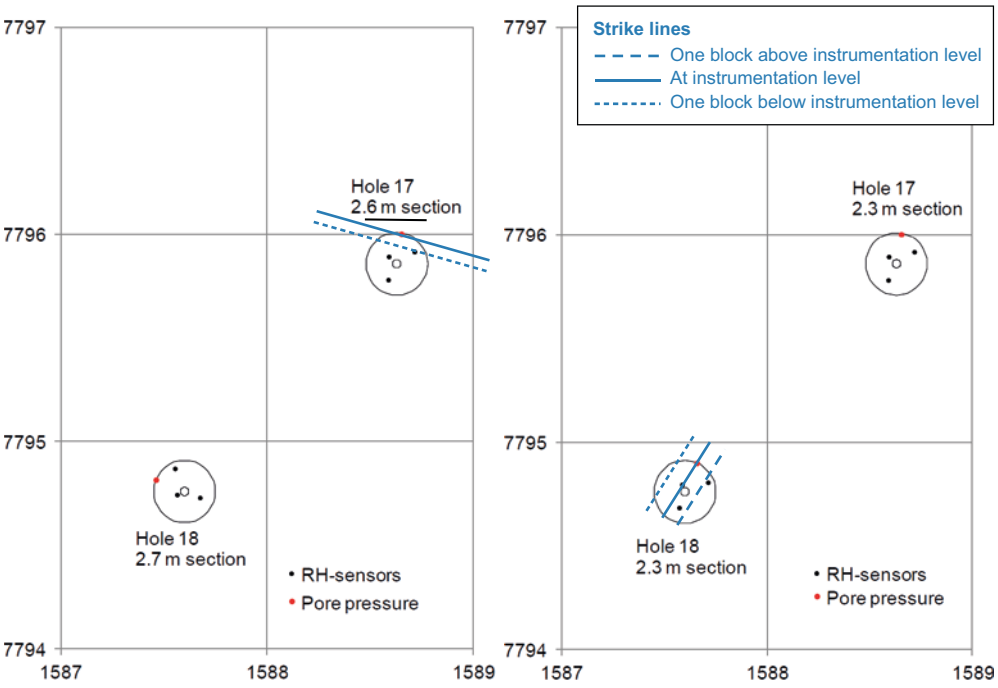

Figure 5-3. *Position of the relative humidity sensors in the dry and in the wet sections; modified from Fransson et al. (2017).*

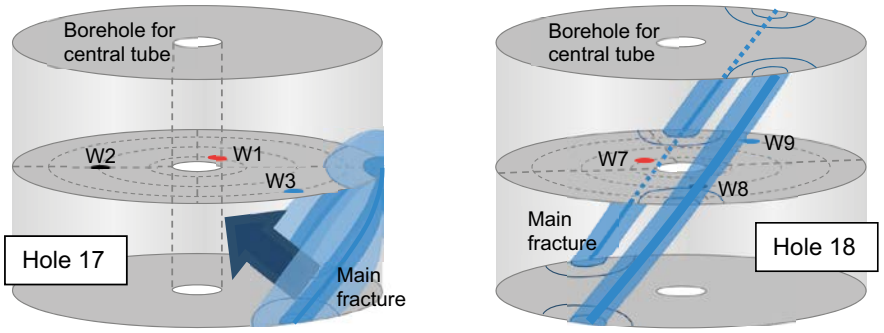

Figure 5-4. *3-D reconstruction of wetting from the fractures at the wet sections.*

5.3.2 Sensor data for KO0017G01

Position of the sensors in the instrumentation levels as well as the position of the instrumentation levels in the parcels for the wet as well as for the dry section in hole KO0017G01 are depicted in Figure 5-5. Also plotted in this figure are the measured relative humidity data for each sensor. The test ran for 420 days after which the sensors were disconnected.

General evolution

In the beginning most sensors show a similar behaviour passing through the following phases:

- Initial relative humidity of 58 % to 60 % (all sensors).
- Almost instantaneous increase to 95 % to 99 % right at the beginning of the test.
- Subsequent fast decrease to a first minimum between 64 % and 72 % in a matter of 1.5 days up to 4 days.
- Then increase by 2 % to 4 % to a second maximum at 67 % to 76 % in 4 to 16 days.

There are only two exceptions:

- Sensor W1 is not showing the almost instantaneous increase but instead a steady increase to what is the second maximum for the other sensors.
- Sensor W3 is not showing the second maximum but increasing steadily after the first minimum.

Characteristic differences for wet and dry section appear only after the second maximum. In the wet section

- there is a second minimum after 28 days at 67 % (W1) and after 70 days at 66 % (W2),
- beyond which all sensors show an increase for the rest of the test ending at 92 %, 79 %, and 100 % (sensors W1 to W3).

In the dry section

- a very shallow minimum is reached after about 150 days at about 65 %,
- the measured maximum difference in humidity for all three sensors does not exceed 1 % between 40 days and 270 days,
- something lets the humidity rise comparatively strongly at the inner sensors W4 and W5 at about day 270. However, this unknown process keeps up only for a few days thus leading to an increase of only less than 1 %,
- afterwards all three sensors show more or less the same increase which is now more or less linear and noticeably higher than before day 270 as indicated by the three straight lines in Figure 5-6,
- values at end of test lie between 66.7 % and 68.2 %.

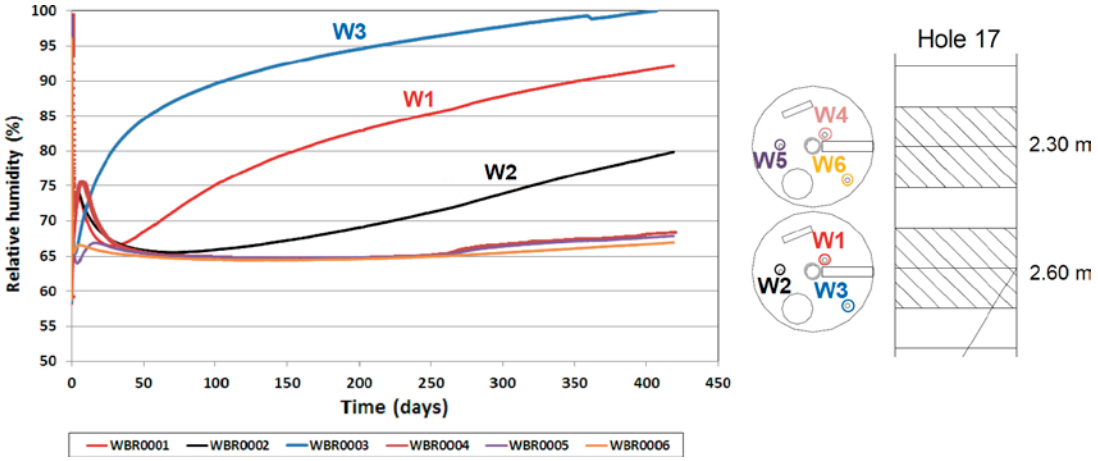

Figure 5-5. *Relative humidity in borehole KO0017G01; modified from Fransson et al. (2017).*

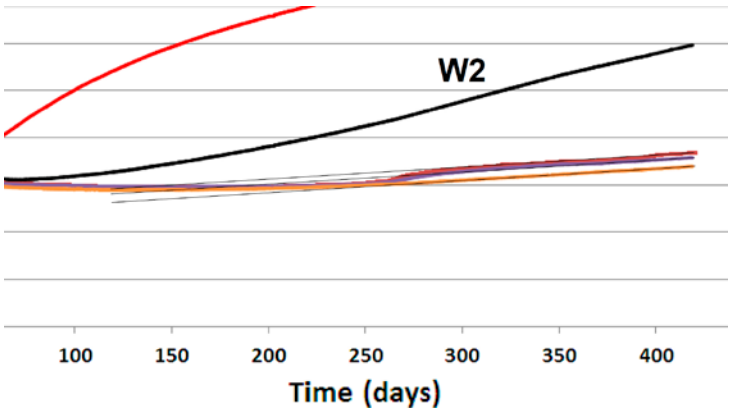

Figure 5-6. *Close-up of Figure 5-5 including three straight superimpose lines; modified from Fransson et al. (2017).*

Interpretation

The very fast first peak in four sensors in combination with the fact that the humidity which amounted initially to 59 % never fell below approx. 65 % afterwards, seems to indicate a short-term flooding that has affected a high percentage of the interface area between the two blocks containing the sensors. Under the assumption that this interface had a rather little aperture, swelling would have quickly sealed it off from further water uptake. The water already taken up would then migrate perpendicular to the now closed interface into the blocks letting the humidity drop quite fast again.

The planned flooding of the outer gap of 1 mm between bentonite blocks and borehole wall must have led to a fast initial wetting of the outer region of the bentonite blocks. The mean increase of the water content after complete redistribution can be calculated with the help of the following equations:

$$V_b = (r_0^2 - r_i^2)\pi = 684.90 \text{ cm}^3/\text{cm} \quad (5\text{-}1)$$

V_b: volume of the bentonite per centimetre parcel height [cm^3/cm]
r_o: outer radius of the bentonite toroidal blocks [cm]; r_o = 14.9 cm
r_i: inner radius of the bentonite toroidal blocks [cm]; r_i = 2.0 cm

$$V_g = (r_b^2 - r_o^2)\pi = 9.39 \text{ cm}^3/\text{cm} \quad (5\text{-}2)$$

V_g: volume of the outer gap per centimetre parcel height [cm^3/cm]
r_b: radius of the borehole wall [cm]; r_o = 15.0 cm

$m_s = \rho_d V_b = 1\,068.44$ g/cm (5-3)

m_s: mass of solids in the bentonite per centimetre parcel height [g/cm]
ρ_d: dry density of the bentonite [g/cm^3]; $\rho_d = 1.56$ g/cm^3

$\Delta m_w = \rho_w V_g = 9.39$ g/cm (5-4)

Δm_w: mass of water in the outer gap per centimetre parcel height [g/cm]
ρ_w: density of free water [g/cm^3]; $\rho_d = 1.0$ g/cm^3

$$\Delta w = \frac{\Delta m_w}{m_s} = 0.0088 \quad (5\text{-}5)$$

Δw = Mean excess water content from water in the outer gap [-]

Full re-distribution of the up taken water from the gap would lead to an average increase of the water content of 0.88 %. The overall impact of flooding of the gap would thus be hardly noticeable in the long run. The minimum at 65 % humidity indicates therefore a yet incomplete re-distribution in combination with additional water uptake from a different source.

The unplanned flooding of the central tube is assumed to have begun with the test and lasted about three days during which an unknown amount of water entered the bentonite from the axis side of the blocks. In a comparable one-dimensional uptake experiment about 6 cm^3 of Äspö-solution had been taken up during three days over an area of 19.63 cm^2 (Kröhn 2004). The area related to the inner radius of the bentonite toroidal block amounts to 12.57 cm^2/cm. The ratio of inflow areas eventually provides an estimate of the amount of 3.84 cm^3/cm of water entering from the central borehole. The evenly distributed increase of the water content after a completed re-redistribution amounts to about $\Delta w = 1.2$ %.

After the first three days water in the dry section is exclusively taken up from the rock. But the water content in the bentonite is of course still additionally influenced by the re-distribution processes from the planned and the unplanned temporary water uptake described above. The time during which significant water migration occurs due to this re-distribution can be estimated from the humidity evolution in the dry section. After about 50 days, a high degree of uniformity in the water content over the whole cross-section of the bentonite had been apparently reached indicating an end of significant re-distribution. Later on, the three breakthrough curves can hardly be discriminated.

No good reason could be found to explain the fact that the humidity decreases continuously if little towards days 130 to 160 in the whole dry cross-section. The underlying process, though, seems to become less and less effective and vanishing completely at day 270 when the increase of the humidity becomes almost linear. This almost linear increase indicates either little inflow from the matrix (cp. Section 4.4.2) or water migration in the vertical direction of the parcel as suspected in Fransson et al. (2017). One way or the other, water re-distribution appears to be much faster than water uptake from the matrix. The reason of the sudden increase of relative humidity at sensors W4 and W5 around day 270 remains to be unclear, though.

Comparison of data and expectations; conclusions for model set-up

The general water uptake dynamics in the wet section were expected to be controlled by the water bearing fracture. According to the 3d-reconstruction in the left plot in Figure 5-4 the sensors should have responded in the sequence W3, W1, and W2 which they did as shown in Figure 5-5. A simplification to a 1d-model with a constant cross-section appears therefore not entirely unreasonable.

Apart from the effect of the flooding events the water content appears to increase very slowly in the dry section (see Figure 5-5). This is consistent with the idea of slow water uptake from the undisturbed matrix. In the absence of irregular pattern across the cross-section an axisymmetric 2d-model appears to be appropriate to simulate the water uptake from the matrix.

5.3.3 Sensor data for KO0018G01

Analogously to the procedure for KO0017G01 a data analysis for KO0018G01 begins with Figure 5-7 showing sensor layout, position of instrumented cross-sections in the parcel and the data for the relative humidity. The test ran for 516 days until disconnection of the sensors.

General evolution

At the beginning of the test all sensors show a relative humidity between 57 % and 59 %. There is an immediate response to the flooding of the outer gap in this borehole also. But it appears that the reaction resulted only in a small peak of a few percent. Moreover, it is not clear from data and available graphics whether all sensors show this behaviour.

All following minima and maxima amount only to a few percent until day 37. This date marks the beginning of a flooding in the central borehole that went unobserved until day 46. At 37 days some sensors (W8, W10, W11, and W12) showed a very short increase of the relative humidity between a few percent and 95 %, similar to the signals from the intentional flooding of the outer gap in KO0017G01. A much smoother peak can be seen later at sensors W7, W8, W10, and W11 between day 48 and day 58. No impact at all was registered by sensor W9 who shows a continuous rising during the whole period.

Eventually all sensor signals in KO0018G01 show a significant increase after about 120 days ending at 81 %, 77 %, and 93 % in the wet section (W7, W8, and W9) and 78 %, 73 %, and 87 % (W10, W11, and W12) in the dry section.

Interpretation

Again there are two types of responses of the humidity sensors to flooding, a very short one related to high temporary increases of humidity and a comparatively slow one related to small up to medium sized maxima. In the first case little open gaps between the blocks are suspected to form very short-lived flow paths for the water that are closing quickly due to swelling, followed by a subsequent also fast water re-distribution. By comparison the re-distribution from flooding at the inner parcel surface takes noticeably more time in KO0018G01 than in KO0017G01.

The effect of redistribution appears to be over after 150 days latest. That the increase in water content in the dry section at sensors W11 and W12 compares rather well with the signals from W7 to W9 in the wet section indicates that the dry section is actually not that dry. The same can also be concluded from a comparison of data from sensor W11 in Figure 5-7 with sensors W4 to W6 from the dry section in KO0017G01 (cp. Figure 5-6).

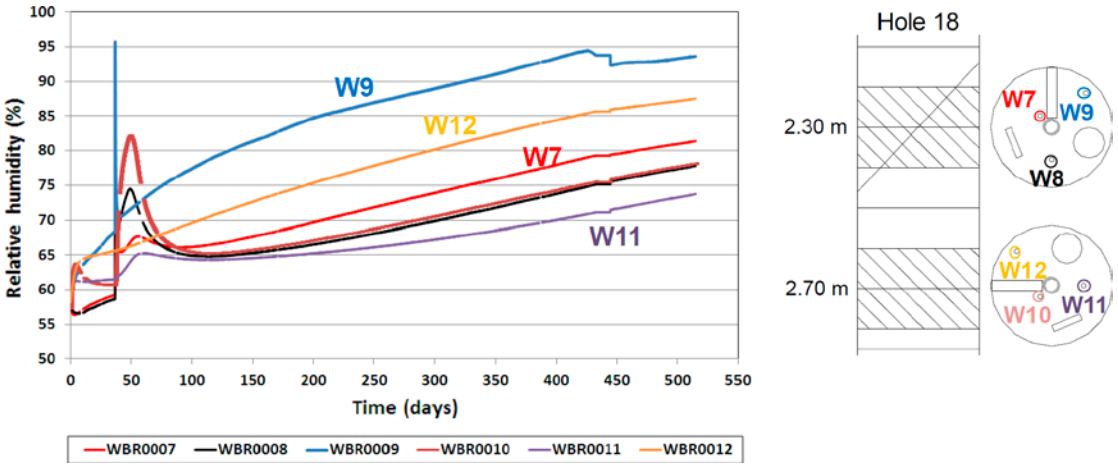

Figure 5-7. *Measured relative humidity in borehole KO0018G01; from Fransson et al. (2017).*

Comparison of data and expectations; conclusions for model set-up

In case of the wet section of KO0018G01 wetting is not straightforward. The 3d-reconstruction in the right plot in Figure 5-4 indicates that the humidity signals should have been detected in the sequence W8, W9, and then W7 while W8 would be shortly followed by W9. The data in Figure 5-7, however, show an entirely different sequence, W9, W7, and then W8. Apparently there are additional significant sources for the re-saturation in this section. This makes the wet section of KO0018G01 unsuitable for modelling with a 1d-code.

Also in the dry section there is significant wetting presumably from unchartered fractures. The sequence in which the sensors detect increasing humidity, W12, W10, and W11, suggests a wetting front beginning in the top left quadrant in the cross-section depicted in Figure 5-7. Since the wetting is already very advanced in comparison to the wetting in the dry section of KO0017G01, water from the matrix appears to be of secondary relevance to the overall wetting in the dry section. Therefore, also this section is not considered for subsequent modelling.

5.3.4 Data for the suspected vertical water migration

It has been speculated that a fast uptake in the wet section of KO0017G01 might have been the source for wetting the dry section as schematically shown in Figure 5-8: "The very slow increase of RH in the *Dry section* (see data for W4 –W6 in Figure 6-14) appeared to be caused by moisture transfer from the main fracture of interest in the Wet section." (Fransson et al. 2017). This would mean moisture transfer in axial direction must be taken into account .

This suspicion was substantiated by the results of the extensive post-test investigations concerning the water content distribution at the end of test. The results are depicted in Figure 5-9 as vertical cross-sections in five radial directions (0°, 72°, 44°, 216°, and 288°), the horizontal axis marking the distance from the borehole axis and the vertical axis indicating the height above the bottom. A clear vertical gradient from the wet to the dry section can be observed.

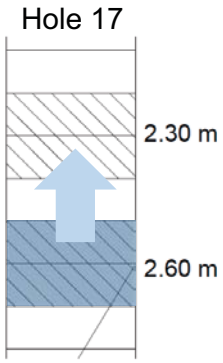

Figure 5-8. *Suspected water migration path in KO0017G01; modified from Fransson et al. (2017).*

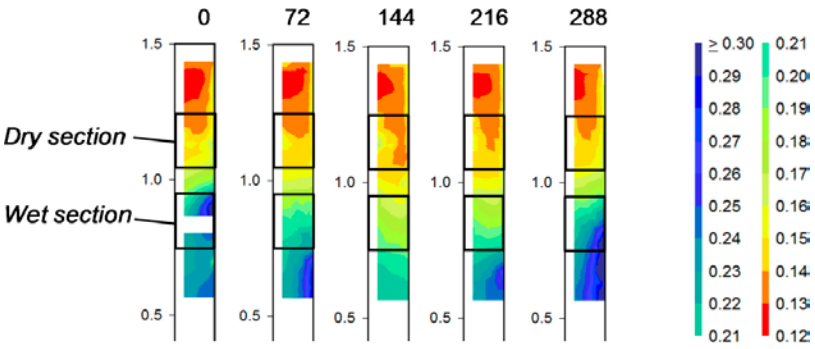

Figure 5-9. *Measured post-test water content in borehole KO0017G01; from Fransson et al. (2017).*

5.3.5 Post-test water content data for a dry cross-section

In order to identify a cross-section that had not been influenced by vertically migrating water the whole set of water content data from Fransson et al. (2017) (depicted in Figure 5-10) was looked at. The plots confirm the conclusion from the transient humidity data that the bentonite in KO0018G01 is all over influenced by outflow from fractures. An even higher water saturation can be seen in the lowest metre of KO0017G01. However, very low water contents can be observed at the level of 1.40 m in KO0017G01. Above and below that level the water content increases only slowly. Data from this level were therefore processed further.

The water content at level 1.40 m is shown in a close-up in Figure 5-11. It is marked there by a thin line. The water content along this line was extracted and plotted as single points in Figure 5-12 instead of a continuous function. The measured water content is more or less constant at about 13 % between the inner boundary and a distance of 11 to 12 cm from the axis. But beyond that distance a clear increasing trend can be observed reaching almost 16 % at the outer boundary. This feature appears to be axially symmetric.

Another of the laboratory tests accompanying the BRIE was the so-called “Test 3”. It was designed to investigate the dynamics of re-saturation after flooding the 1 mm outer gap. The water content profiles measured after 107 days are depicted in Figure 5-13. They look very similar to the profiles from the post-test data including the increase toward the outer boundary. This increase thus appears to be persistent over time.

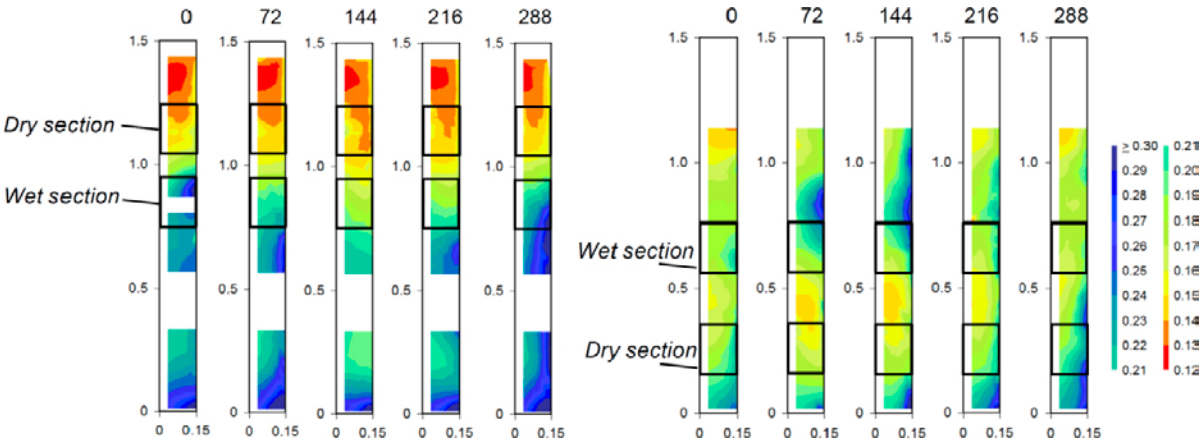

Figure 5-10. *Post-test water content in holes 17 (left) and hole 18 (right); from Fransson et al. (2017).*

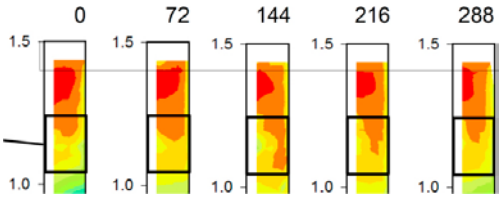

Figure 5-11. *Post-test water content data for hole 17 at 1.40 m above the bottom; from Fransson et al. (2017).*

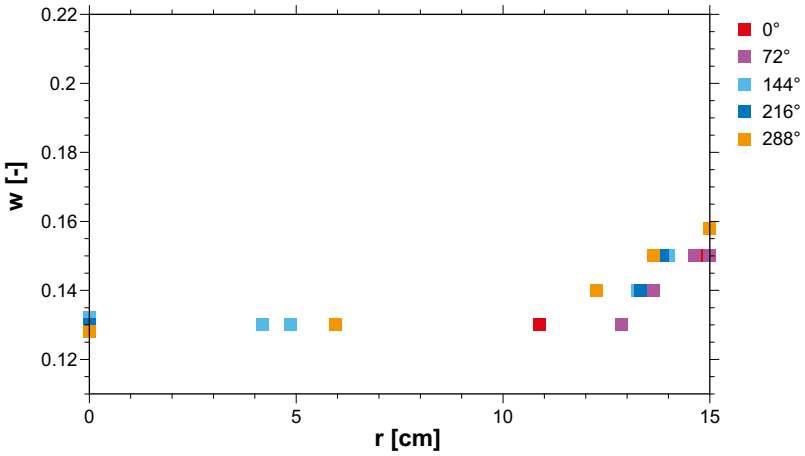

Figure 5-12. *Profiles of content in the alternative dry section after ~ 430 days.*

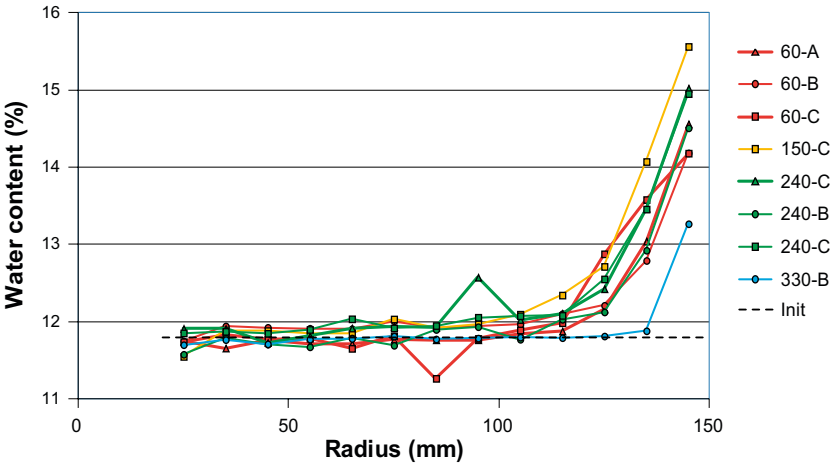

Figure 5-13. *Profiles of water content in Test 3 after 107 days; from Fransson et al. (2017).*

5.3.6 Model for the wet section of KO0017G01

The domain for modelling unrestricted water uptake in the wet section of KO0017G01 was bar-shaped meaning that it had a constant cross-section as depicted in Figure 5-14. It covered the distance of 13 cm between the inner and the outer gap.

The adsorption isotherm found to be characteristic for MX-80 bentonite in the Canister Retrieval Test (Kröhn 2011) as well as in the accompanying water uptake test (cp. Section 4.3.9) was adopted for the re-saturation simulation. According to the Task Description (Vidstrand et al. 2017) the bentonite had a dry density of 1 560 kg/m^3 and an initial humidity of 59 %. The same characteristic parameters were also used for the following models. Note that calculating the water content based on the isotherm and a humidity of 59 % leads to an initial water content of 12.8 % instead of the suggested 11.6 % in the Task Description. Either the initial water content or the initial relative humidity had therefore to be modified.

Full water saturation at all times was assumed for the model boundary at r = 15 cm and full water saturation for the first three days at r = 2 cm. The temperature was assumed in this model as well as in all other models for the BRIE to be constant at 14 °C.

5.3.7 Model for the dry section of KO0017G01

The model for restricted inflow from the matrix in the dry section of KO0017G01 was 2d-axisymmetric thus representing a horizontal disk in the bentonite parcel as shown in Figure 5-15. Full water saturation was prescribed for the boundary at r = 2 cm for the first three days. Afterwards, this boundary was treated as a no-flow boundary. The outer gap at r = 15 cm was supposed to provide a constant inflow rate that was to be determined yet by back analysis of the resulting water content profiles.

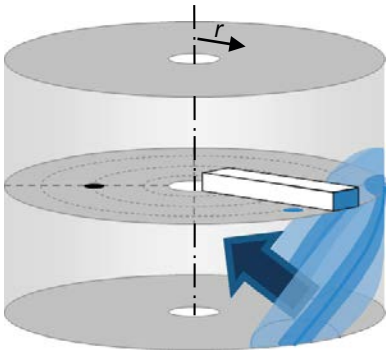

Figure 5-14. *Model domain for water uptake from the fracture in the wet section.*

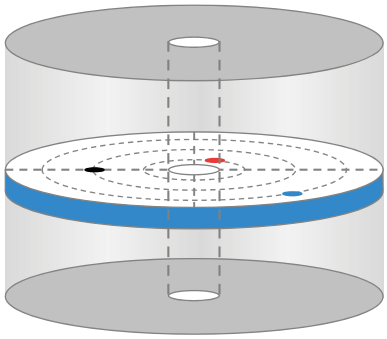

Figure 5-15. *Model domain for water uptake from the matrix in the dry section.*

5.3.8 Model for vertical water migration

The assumption of upward flow from the wet section was investigated with the help of a vertical bar-shaped model. The model boundaries were placed at z = 0.90 m and at z = 1.30 m. Full water saturation was assumed at 0.90 m above bottom while the boundary at 1.30 m above bottom was closed for flow. Breakthrough curves were obtained for z = 1.20 m which was the height of the sensors. The model domain is sketched in Figure 5-16.

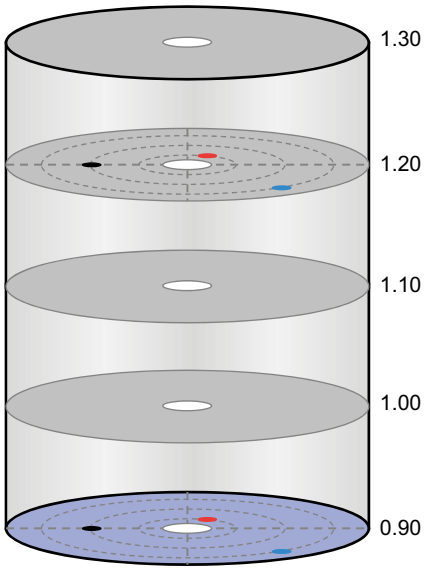

Figure 5-16. *Model domain for vertical water migration towards the dry section.*

5.3.9 Models for the alternative dry cross-section

Four 2d axisymmetric models were set up to investigate the radial water content distribution in the alternative dry cross-section at z = 1.40 m in hole KO0017G01. In the first model, called "**basic model**" further on, the boundary at the outer gap was assumed to be a no-flow boundary. The planned flooding of the outer gap was accounted for by a zone of 97 % water saturation. Its thickness was calculated under the simplifying assumption that the water from the gap would fill up the available pore space at the outer boundary which leads to a thickness of 5.2 mm. At the inner gap full water saturation was prescribed for the first three days. Afterwards, this boundary was also treated as a no-flow boundary. The boundary condition for the inner gap was used for all four models.

As an alternative, **temporary inflow from the outer slot** was considered essentially to check the initial conditions chosen in the basic model. In this case the initial water content was constant. Full water saturation was prescribed for 1 day at the outer gap. After this period the boundary condition was switched to no-flow.

The effect of **vapour flow from the matrix** was investigated in the third model. This was a variant of the basic model where 100 % relative humidity was assigned to the outer boundary but where the water content was allowed to rise from the initial value over time.

Finally, the calculated increase of the water content due to the unintentional flooding was checked with the fourth model. Here, **zero mass flux** at the outer gap was prescribed. An according evenly increase of 1.18 % of the water content has been determined in Subsection 5.3.1.

5.4 Results

5.4.1 Model for the wet section of KO0017G01

Considering the simplicity of the model in the face of the potential complexity of the fracture network at the BRIE, the fit of the model results to the data from sensor W3 shown in Figure 5-17 is satisfying. The model assumption that the main fracture provides more water than the bentonite can consume is thereby confirmed. Other fractures are suspected, though, to have had significant influence on the the data from W1 and W2. No reasonable fit for the data from these sensors could be found with this model, a task for which a more detailed 3d-model is probably required.

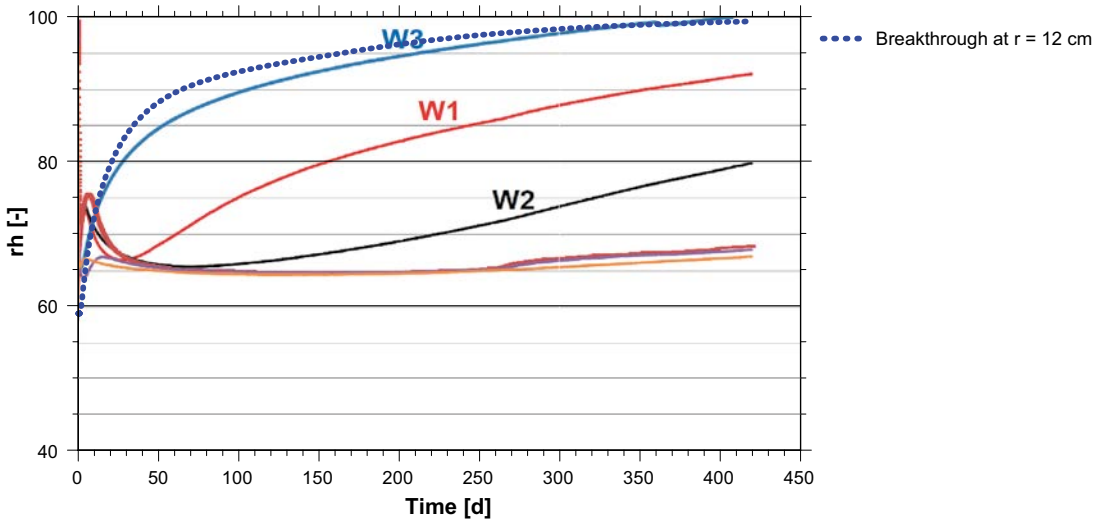

Figure 5-17. *Measured and simulated relative humidity in the wet section of hole 17; adapted from Fransson et al. (2017).*

5.4.2 Model for the dry section of KO0017G01

The outflow rate from the undisturbed matrix which was input for the model was varied in such a way that

- "…after the flooding events, no sensor showed values below a level of 64 %." (Fransson et al. 2017) and that
- the temporal gradient of the relative humidity after 270 days fits the data as this increase appears to be the least distorted indication of the inflow rate.

By trial and error it was found that an outflow rate from the matrix of 3×10^{-8} kg/(m^2 s) can lead to the rather good fit of calculated and measured relative humidity in the dry section of KO0017G01 shown in Figure 5-18. Hole KO0018G01 had been considered to be a rather dry hole in the description for Task 8d and the related mean outflow rate was determined to be approximately 3.5×10^{-7} kg/(m^2 s) (see case II in Table 4-5). The back calculated outflow rate from the matrix is more than an order of magnitude lower than that, confirming the notion that the dry section in KO0017G01 was comparatively free of water-producing fractures.

5.4.3 Model for vertical water migration

Axial water movement from the wet section in KO0017G01 to the dry section was simulated in the model for vertical water migration. The comparison of model results and measurements is shown in Figure 5-19. This model reproduces the slow sensor reactions in dry section as well as the previous model with little inflow from the matrix. In the end, the modelling of the dry section does therefore not provide conclusive evidence to decide whether the wetting of the dry section is caused by water from the wet section below or by water from the matrix.

5.4.4 Models for the alternative dry cross-section

In a final attempt to identify decisive data for checking of the re-saturation model for restricted water supply, an alternative dry section had been sought and eventually found at 1.40 m in KO0017G01. The **basic model** yields the profiles shown in Figure 5-20. The initial water content distribution is plotted here as well as the end-of-test distribution. The profile at 3 days is plotted since the unintentional wetting from the inner boundary at r = 2 cm stops at that time. This curve indicates therefore the maximum water uptake at the inner boundary and gives at the same time some insight into the dynamics of moisture re-distribution. Note that in principle the same dynamics apply also for the outer boundary (r = 15 cm). The profile at 107 days is plotted for comparison with the end-of-test data from the laboratory test "Test 3" (see Figure 5-13).

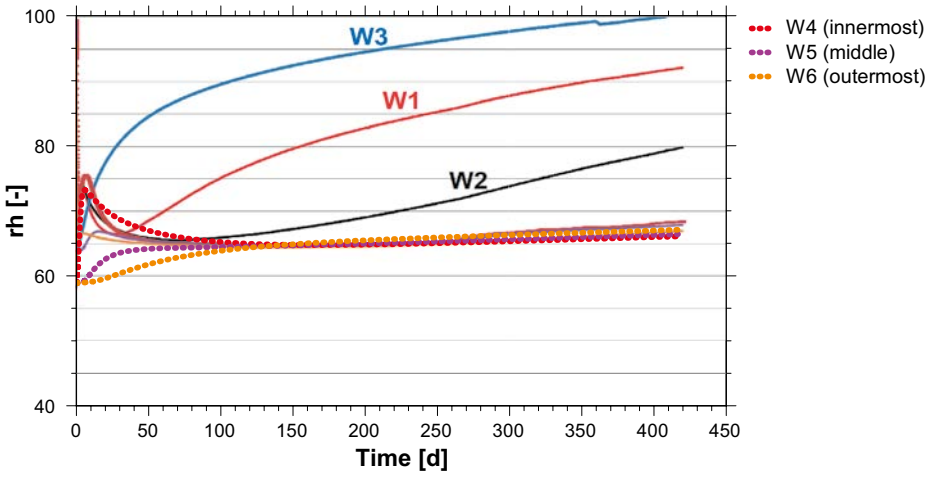

Figure 5-18. *Results for relative humidity in the dry section, inflow from the matrix; adapted from Fransson et al. (2017).*

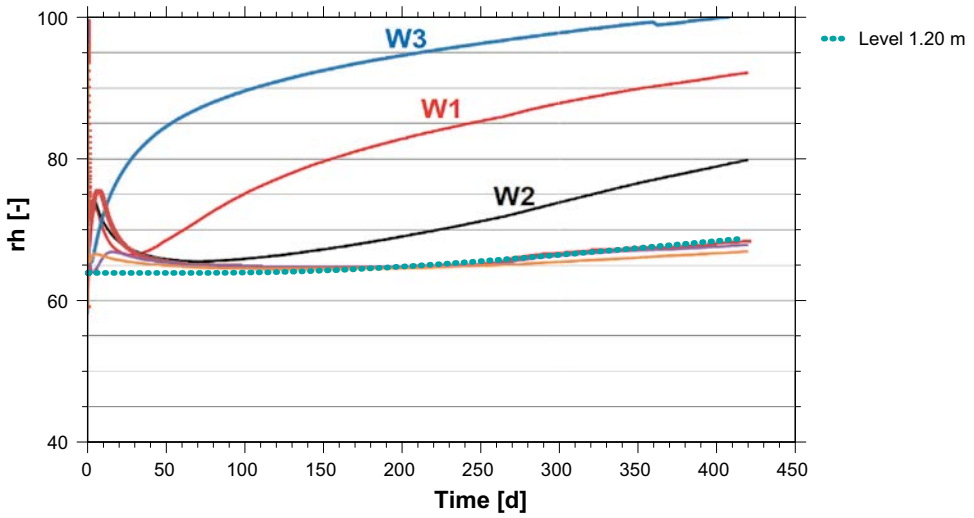

Figure 5-19. *Results for relative humidity in the dry section, vertical water migration; adapted from Fransson et al. (2017).*

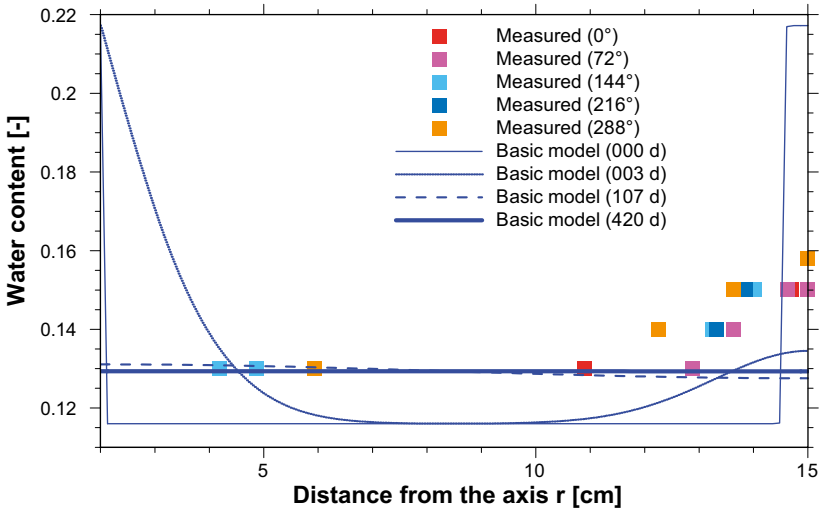

Figure 5-20. *Water content at 1.40 m; basic model.*

Redistribution of water from the outer boundary is quite advanced in only three days. The peak value of 21.7 % has already dropped down to 13.5 % during this time and the resulting distribution reaches already about 4 cm into the bentonite. The distribution starting from the inner boundary reaches even 6 cm into the bentonite. However, after 107 days the water content is almost evenly distributed over the cross-section and is constant for all practical purposes after 420 days. Where the measured water content is constant it is very well matched by the model results thus explaining the increased water content in this cross-section exclusively by the two flooding events. The measured increase at the outer boundary is not even remotely met by the model, though.

Similar re-saturation dynamics can be observed in Figure 5-21 depicting the results from the model with **temporary inflow from the outer slot** and in Figure 5-22 showing results of the model with **vapour flow from the matrix**. The humidity curves are basically the same for all three models with some minor differences in the curve for three days confirming by and large the assumed initial conditions at the outer rim in the basic model. Note that water content profiles very similar to those in Figure 5-22 were received when a mass inflow of 2×10^{-8} kg/(m^2 s) was prescribed at the outer rim instead of vapour flow.

Finally, the model with **zero mass flux at the outer gap** resulted in an evenly distributed increase of water content of almost exactly 1 % (see Figure 5-23) which is in good agreement with the estimated value of 1.2 % (cp. Section 5.3.2).

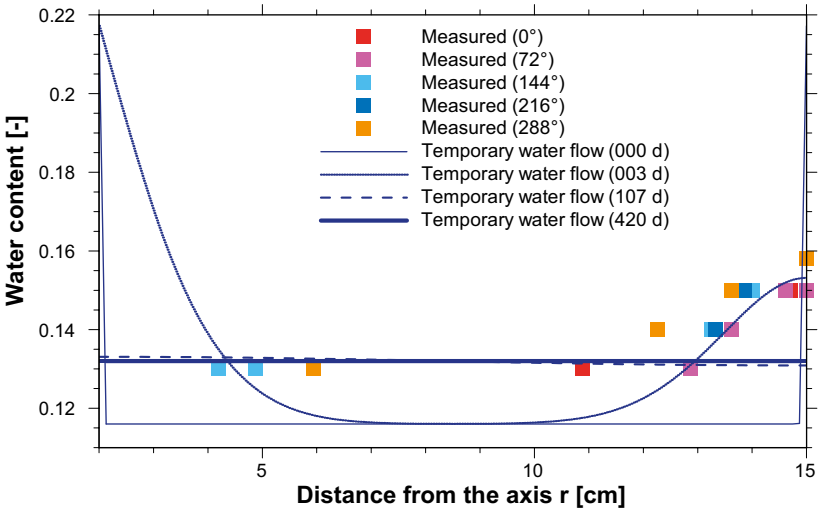

Figure 5-21. *Water content at 1.40 m; temporary inflow from the outer slot.*

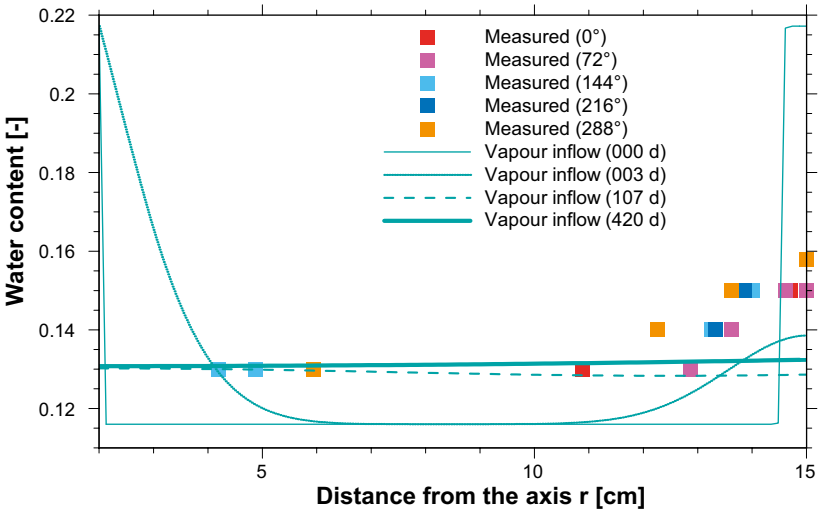

Figure 5-22. *Water content at 1.40 m; vapour flow from the matrix.*

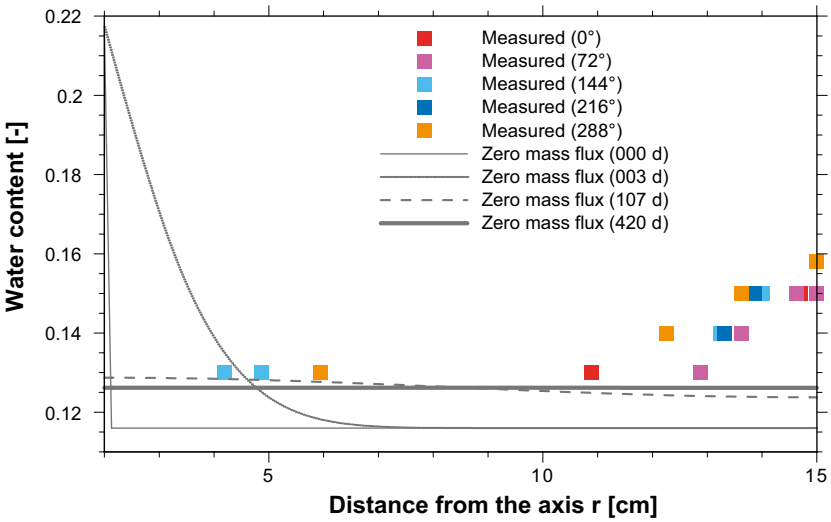

Figure 5-23. *Water content at 1.40 m prescribed constant flow from the matrix.*

5.4.5 Comparison of blind predictions with calibrated model

Unrestricted water supply (from a fracture)

The time until full re-saturation, defined as a degree of saturation above 95 % in the whole cross-section, has been predicted during Task 8d with an axisymmetric model. A period of 232 days had been found (cp. Section 4.4.2). For modelling the uptake in the wet section of KO0017G01 in Task 8f the material parameters were not changed. The only modifications applied concerned the initial and boundary conditions. In contrast to the predictive calculations, the unintentional wetting over three days at the inner boundary was included. Also the initial water content of 11.6 % was adopted. The saturation process is depicted in Figure 5-24 in terms of the increasing water content. The saturation of 95 % was reached after about 215 days. This result was to be expected because the bentonite in the model for Task 8f has less capacity to take up water than the model for Task 8d due to the increased initial water content and considering the effect of the unintentional flooding.

The end-of-test data for the water content (cf. Figure 5-10) suggest that re-saturation in the wet sections was not complete even after 420 to 520 days. The prediction of 215 days therefore seriously undervalued the real re-saturation time for the BRIE. It has to be mentioned again, though, that code VIPER does not allow for 3D-calculations. Using an axisymmetric model domain does not reflect the localized inflow from fractures and does not acknowledge spreading of water in the vertical direction. The predicted re-saturation time can therefor only be a generous lower bound for the actual value.

Restricted water supply (from the matrix)

The blind prediction of 515 days or 1.41 years until full saturation in case of restricted water inflow from the matrix was based on a constant outflow rate from the matrix of 3.53×10^{-7} kg/(m^2 s) (see Table 4-5 in Section 4.3.9). The material parameters for the bentonite were the same as for the model for unrestricted water supply.

In the model for Task 8f the effect of the unintentional flooding as well as the higher water content of 11.6 % were considered. Calibration of flow in the dry section of KO0017G01 indicated a maximum inflow rate of 3×10^{-8} kg/(m^2 s) (cp. Section 5.4.2) which is about one order of magnitude lower than in the predictive model. The water uptake dynamics in this case are shown in Figure 5-25. They indicate an uptake time of about 11.3 years. An even longer time would have resulted if the original initial and boundary condition would have been used thus confirming the observation in Section 4.4.2 that the re-saturation time increases non-linearly with a decrease of the prescribed inflow rate.

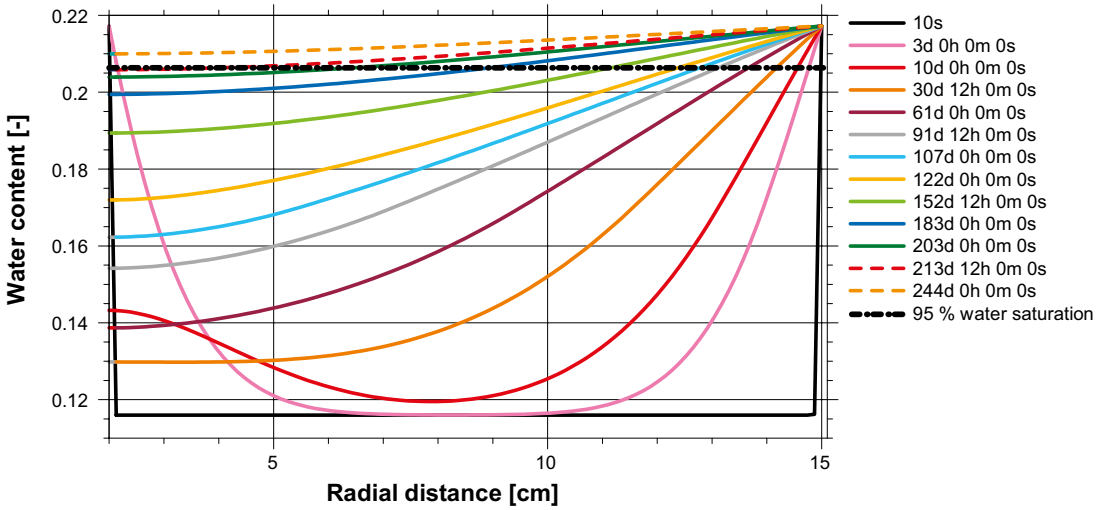

Figure 5-24. *Water content evolution in the axisymmetric model for the wet section.*

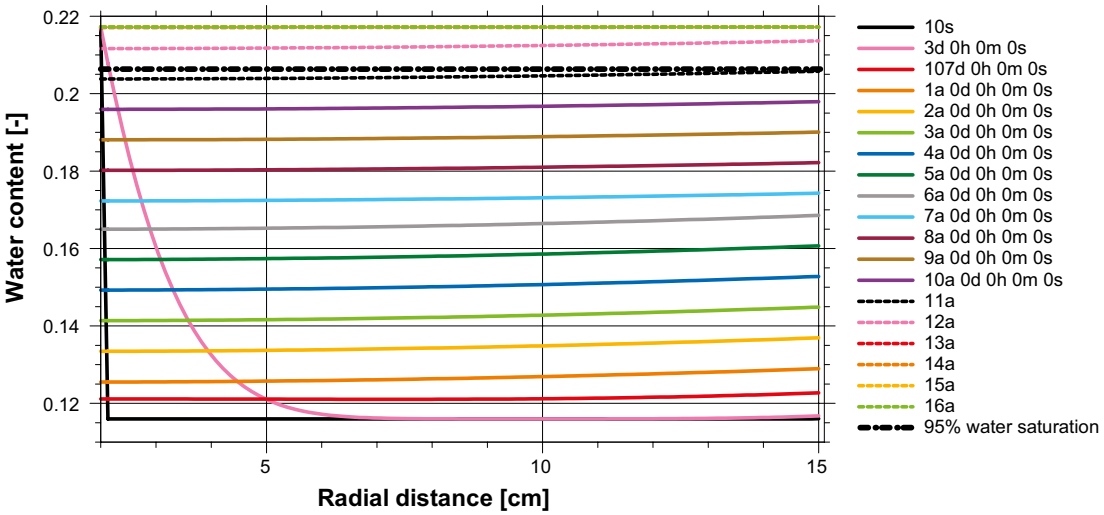

Figure 5-25. *Predicted water content evolution until full saturation in the dry section.*

5.5 Discussion

Analysis of the sensor and the post-test data has shown that borehole KO0017G01 provides the best data base for the simplified re-saturation models discussed here. Simulating water uptake in the wet section with a model for unrestricted water supply proved to be successful as far as wetting in the vicinity of a fracture was concerned. The model failed when looking further away from the water producing fracture. However, this can easily be attributed to the basically 1d-geometry of the model which is certainly not appropriate in the light of water migration in all three dimensions. Reproducing the transient humidity curve from sensor W3 justifies the assumption of unrestricted water supply from the water-bearing fracture.

Back calculating the outflow rate from the matrix based on sensor data from the dry section yielded the reasonable outflow rate of 3×10^{-8} kg/(m^2 s) seemingly confirming the notion that the dry section in KO0017G01 was comparatively free of water-producing fractures. However, flow from the wet section also explains sensor data. It is therefore impossible to discriminate inflow from the matrix and water migration from the wet section on the basis of data from the dry section.

To determine the outflow rate from the matrix an alternate dry section was sought on the basis of the post-test data. It was found at 1.40 m in KO0017G01. The effect of the two flooding events appears to be caught nicely by all models for this alternate dry section. However, the basic model without water inflow (other than from flooding) gives essentially the same system response as the model where vapour flow is allowed to enter the bentonite. The same applies to a model with a constant inflow rate of 2×10^{-8} kg/(m^2 s). Note that this rate is in good agreement with the back calculated value of 3×10^{-8} kg/(m^2 s) for the original dry section. It thus seems to pose an upper bound for the outflow rate from the matrix.

Anyway, water flow from the matrix appears to be rather low and the BRIE did not nearly take enough time to show a significant re-saturation by water from the matrix. It was thus speculated in Fransson et al. (2017) that a major drawdown of the groundwater around the boreholes might have decreased water outflow to this extent. On the other hand, very recently a mathematical model for the pressure decrease at the test boreholes including the effect of background fractures has been put up (Fransson et al. 2017). Using Äspö-specific data for the fracture network indicated that significant pressure drawdown should not have reached deeper than very few decimeters into the rock. Whether the naturally low matrix permeability or this drawdown is applicable could not be decided. The data from BRIE do thus not suffice to characterize outflow from the undisturbed matrix.

A second remaining question concerns the persistently increased the water content towards the outer rim. None of the models was able to reproduce this feature even remotely using reasonable parameters. Redistribution by the established mechanisms was much too fast to allow for the initially increased water content to remain over the 107 days of Test 3 or even over the 420 days in the BRIE. It has been

speculated if this could be the result of the hysteresis of the adsorption isotherm / retention curve. It will require some deep insight, though to explain why this effect should occur at the side of the intentional flooding but not at the side of the unintentional flooding.

A final point in the matter of the persistently increased water content concerns the rather spectacular and surprisingly clear pattern of water conducting fractures on the surface of the parcels – informally called "bentographs" – after retrieval from the bore holes (see Figure 5-26). The mere existence of these clearly limited footprints of fractures appears also to be curious in the light of the present understanding of wetting and moisture re-distribution. In case of a fracture producing only little water, moisture re-distribution should prevent a build-up of significant water content as in the models for the alternative dry section. But the bentograph shows flow even from fractures that had not been identified as water producing during the intensive characterisation of the borehole before the test. On the other hand, in case of a strongly water producing fracture a considerable spreading of water perpendicular to the opening of the fracture and along the bentonite-rock interface would be expected. This feature can also not be observed in Figure 5-26. Since it could be shown that the shades of grey relate to the local water content this is highly surprising.

Essentially two changes affected the models for the prediction of the re-saturation time as the properties of the bentonite were not modified:

- Updated initial and boundary conditions accounting for
  - the intentional flooding of the outer gap,
  - the unintentional flooding from the parcel axis,
  - an increased initial water content/relative humidity.
- A calibrated inflow rate in the dry section(s) assumed to represent outflow from the matrix.

Figure 5-26. *"Bentograph" of the parcel from KO0018G01; from Fransson et al. (2017).*

The calculated uptake time did not decrease considerably in case of the model with unrestricted access to water – from 232 days to 215 days. Note (again) that these values represent only lower bounds due to the geometrical simplification of the model domain. The calibrated outflow rate from the matrix in contrast proved to be about one order of magnitude lower than in the blind prediction leading to a substantial increase – from 1.41 years to 11.3 years.

5.6 Conclusions and recommendations

In the course of Task 8 it has been vividly discussed whether the fractures or the matrix control the re-saturation of the buffer. At the BRIE the significantly water bearing fractures can be associated with locally unrestricted water supply for the bentonite while water from the matrix comes at rather limited rates. Re-saturation from a fracture affects only a limited volume in the beginning, then covers the whole cross-section and eventually keeps spreading vertically. By comparison, re-saturation from the matrix takes much more time. In fact, the outflow rates from the matrix were so low that the re-distribution process was faster than the wetting process from the rock. The water content profiles therefore tended to be quite flat after the effect of the flooding events had subsided. With respect to re-saturation, the buffer as a whole can thus be structured into three zone types whose size change with time:

- Zone F: zones affected by significantly water-bearing fractures (unrestricted water supply).
- Zone M: zones affected by the matrix (restricted water supply).
- Zone U: yet unaffected zones.

A simplifying sketch of this concept is given in Figure 5-27.

According to this conceptual view Zones F and M grow at the expense of Zone U. However, Zones M grow slower than Zones F and they get under the influence of Zones F in case of overlapping. In the end the re-saturation time is controlled by the flow rates from fractures and from the matrix as well as by the fracture intensity and the buffer thickness. In case of the BRIE the highest uncertainty is introduced by the outflow rate from the matrix. About the reason for the very low outflow rate from the matrix it is speculated in Fransson et al. (2017) that it might either be the result of the naturally low matrix permeability or be caused by a pressure drawdown with subsequent degassing of the groundwater. The BRIE was not designed to address this question leaving identification of the relevant flow process to future investigations.

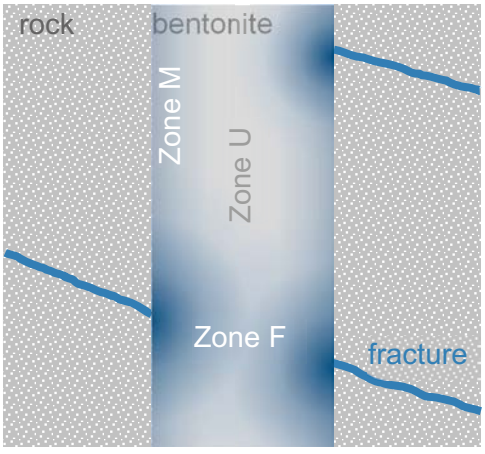

Figure 5-27. *Principal water uptake dynamics in a buffer.*

However, considering that vertical water migration from the wet into the dry section has possibly obscured inflow from the matrix indicates that the process of re-saturation was dominated by the contribution from the fractures during the lifetime of the BRIE. Predictions about the hypothetical further development of the water content distribution in the parcels appear to be a rather delicate, though due to the remaining conceptual uncertainty.

Possible fields of further investigations concern therefore

- a better understanding of the flow processes in the matrix close to a borehole/tunnel wall,
- a quick and reliable method to locate water-bearing fractures and to determine their outflow rate, and
- the reason for the slightly increased water content that was found exclusively at the outer rim.

6 Summary and conclusions

6.1 Summary

The problem of predicting water uptake of a bentonite buffer in the granitic host rock at the BRIE-site in the Hard Rock Laboratory Äspö has been approached by decoupling the aspects of groundwater flow and bentonite re-saturation. Groundwater flow was simplified to a steady-state single-phase flow as only a rather narrow unsaturated zone at the tunnel and borehole walls was expected.

Large fractures were incorporated as deterministic features in the model from the beginning on. The approach for the smaller and only statistically known background fractures in contrast changed with increasing conceptual understanding. For Task 8b they were simply neglected. In Task 8c they were considered by a homogeneous permeability that was added to the undisturbed matrix except for a box-like zone around the five probing boreholes. Here, some discrete artificial fractures were introduced to connect the boreholes across this zone of undisturbed matrix with the part of the matrix that included the effect of the background fractures. While this concept appeared to work for Task 8c it would not have been viable for Task 8d anymore because new estimations for the outflow from the tunnel surface provided a value that was lower by a factor of ten. Recognizing then that

- two-phase flow effects by means of degassing, and
- influence of mechanical stresses on fracture permeability

would affect not only the immediate borehole area but all tunnels and boreholes, the box-like zone and the artificial fractures were dropped in favour of a narrow zone of low permeability – a so-called skin – around the geotechnical openings.

Generally it was looked to it that geometry and boundary conditions in the model were used as close as possible to the task description. Modelling was performed with the code d^3f. The resulting flow model showed that even despite proximity of large water bearing fracture outflow into tunnel and boreholes is more or less unaffected by these large fractures. Only direct contact has influence on outflow.

Calibrating to measured outflow rates yielded a surprisingly high effective matrix permeability that exceeded the permeability of the undisturbed matrix by three orders of magnitude. On the scale of the boreholes high inhomogeneities in the flow field were deduced form the measured outflow into the boreholes. Outflow rates varied from borehole to borehole up to two orders of magnitude (where outflow could be measured at all) despite the fact that the boreholes were located at a distance of only 1.5 m from each other. The reason for this phenomenon is believed to be background fractures whose locations and sizes were unknown. This introduced a considerable uncertainty in the deterministically calculated model response. It also questions some of the tasks as deterministic answers were asked to a problem that was posed to a great extent in terms of geostatistics.

Another uncertainty for the calibration process was the fact that most data to check the behavior of the flow model were strongly concentrated to the BRIE-site. Virtually no data outside the TASO-tunnel was available rendering a check of the hydrogeologic system over a large part of the model impossible. The calculated outflow rates from the rock that form the basis of the re-saturation calculations are thus subject to uncertainties on model scale.

Outflow data from the rock was then assigned to the inflow boundary of a re-saturation model for the bentonite. The seemingly contradicting conditions for the groundwater flow model at the borehole walls, meaning open borehole for calculating flow and installed bentonite for calculating re-saturation, are easily reconciled considering the processes acting at the bentonite-rock contact. In case of lower outflow from the rock than demand from the bentonite, water is sucked by the bentonite from the rock as it comes thereby reflecting the conditions of the open borehole. In the opposite case water flow across the bentonite-rock contact is controlled by the demand of the bentonite while the hydraulic pressure in the rock increases without noticeable consequences for the re-saturation process essentially decoupling re-saturation from flow from the rock.

Only three processes are considered in the re-saturation model: vapour diffusion in the pore space, diffusion of water in the interlamellar space and an instantaneous exchange of water between these

two spaces controlled by an adsorption isotherm. For the boundary full vapour saturation of the pore air and the referring maximum water content in the interlayer were initially provided in the model. In the course of working on Task 8 also a Neumann type boundary condition prescribing a maximum outflow rate from the rock into the bentonite was developed and implemented. This conceptual model was realized in the code VIPER. As the code is still experimental to demonstrate the validity of this conceptual model it is restricted to one-dimensional and axisymmetric geometries.

Water uptake rates for a bentonite with free access to water were calculated and compared with the outflow measurements at the BRIE-site showing clearly that a considerable part of the buffer material would re-saturate under restricted access to water. This led to a certain leveling of the water content distribution and to longer re-saturation times.

Since the initially high uptake rate at free access to water drops fairly quickly, the differences in re-saturation time to cases with restricted water uptake were not nearly as big as the differences of the prescribed maximum inflow rates suggested. These differences increase non-linearly, though with the ratio of maximum inflow at unrestricted water supply to the (restricted) maximum outflow from the rock. The sensitivity of the re-saturation model to variations of the steady-state outflow from the rock increases therefore significantly with a decreasing level of this outflow.

Modelling the water uptake test proved to be successful as only a comparatively little change in the parameter set resulted in a very good match of the model results with the measured data. The parameters used for VIPER were therefore expected to be also well fitting for modelling bentonite re-saturation in the BRIE.

6.2 Conclusions

Calibrating the flow model has shown that there is a considerable contribution of background fractures to the effective matrix permeability as it has been increased by three orders of magnitude in comparison to the permeability values for the undisturbed matrix. However, the measured outflow rates cannot all be captured by the model indicating significant inhomogeneities on the scale of the borehole field.

Variations of the permeability in the strongly water producing large fractures had only little effect on outflow into the boreholes. Outflow thus appears to be controlled by the effective matrix permeability and local inhomogeneities but not by the highly conductive fractures except when directly crossed.

Deterministic prediction of an inflow rate or even an inflow distribution into a borehole is impossible because of the stochastic nature of those background fractures that cannot be detected.

Comparing measured outflow rates from the BRIE-site and calculated inflow rates into the bentonite showed that the bentonite in the BRIE will encounter locally free access to water as well as restricted access at the matrix and at very small fractures.

Restricting water inflow into the bentonite leads to non-linear model responses in terms of water content distributions and re-saturation times. Estimation of uncertainties ensuing from variations of the restricted inflow depends therefore strongly on the reference inflow value.

The buffer material appears to be well characterized as the results of the water uptake test could be reproduced after a minor adjustment of the parameter set that was used for the uptake model of the bentonite in the BRIE.

6.3 Evaluation

Modelling groundwater flow at the BRIE-site increased the understanding of a flow system in granitic rock considerably. The calibration process was here most enlightening. It gave strong indications of the nature of the only statistically known background fractures. It also appeared to confirm the existence of a low permeability skin around the geotechnical openings.

Working on Task 8 revealed a deficiency in VIPER concerning boundary conditions that had gone unnoticed up to then. VIPER was therefore advanced accordingly and thus covers a wider range of applications.

The model for the blind prediction of water uptake under unrestricted access to water was also used to interpret the results of the additional water uptake test. Success by a very good match after only a little parameter adjustment demonstrated that the envisaged buffer material had been well characterized in the framework of the VIPER-model. This inspires also confidence in the predictive models for the BRIE.

6.4 Open issues

Due to the geometric restrictions in VIPER it was not possible to investigate the effect of local outflow from fractures with sufficient confidence. A full 3d-model for bentonite re-saturation is required to answer the questions addressed in Task 8 in more detail. It remains open how the re-saturation is changed by localised water input. Also unclear is the influence of tilting the fracture plane in the model against the borehole axis. And of course there was no way to predict the uptake dynamics for the complete borehole.

A bit disturbing remains the possibility of changing flow conditions during the lifetime of the BRIE. Changes in the flow field had been observed raising the question about reasons, mechanisms and possible extent to which they can affect the initially observed flow rates. This may become highly relevant for the building phase of a repository in granitic rock.

In general, a better understanding of the flow processes in the matrix close to a borehole/tunnel wall is required. Application of a skin with a reduced permeability is no substitute for understanding the processes occurring on the micro-scale and questions strongly the predictive capability of such a model.

Another open question concerns the slightly increased water content that was found exclusively at the outer rim in the BRIE as well as in Test 3. This observation indicates a possible gap in understanding water migration in the bentonite under alternating adsorption and desorption conditions.

6.5 Comments and recommendations

With respect to modelling groundwater flow it appears that very little can be done about the inherent problem of a large amount of fractures being only known in terms of statistics. Where it comes to investigating a concrete site as the TASO-tunnel it can only be hoped for as much information as possible. As flow models usually handle pressures and flows these quantities should be known at many and distributed locations. Since most data for the BRIE model was concentrated around the borehole field the influence of model parts beyond the TASO-tunnel could not be evaluated within the limits of the available resources.

On the scale of the BRIE the stochastic nature of the fracture network prevented deterministic predictions and interpretations to a comparatively high extent. Evaluation of the qualification of an ensemble of boreholes on the scale of a repository might make efficient use of stochastic fracture network models, though. Here, not a specific borehole is questioned but a percentage of qualified boreholes is sought. This percentage can be determined by Monte Carlo methods in a straightforward manner. However, after setting up a repository there is no way around individual inspections of each individual borehole.

What might make sense here is a meaningful catalogue of possible outflow situations that forms the basis for a series of re-saturation simulations. This could help to decide if an individual borehole would meet the safety requirements for the buffer.

Several open issues were pointed out in the previous section. They concern understanding of flow in the rock as well as of migration in the bentonite. Since reliability of model predictions depends on a thorough understanding of the processes involved it is highly advisable to address these open issues in future investigation programs.

Acknowledgements

This report summarises work for the BMWi between 2010 and 2016 under contracts no. 02 E 10336 (E-DuR), 02 E 10548 (WiGru-6), 02 E 10558 (A-DuR), 02 E 11102 (WiGru-7), and 02 E 11213 (QUADER). Funding of this work is gratefully acknowledged.

Working on Task 8 would not have been possible without numerous discussions within the Task Forces on Groundwater Flow and Solute of Transport as well as the Task Force on Engineered Barrier Systems. All questions and requests for data have been answered with a delightful professional swiftness that helped many times. Thank you to everybody in these groups.

Many thanks are also due to the developers of d^3f at the University of Frankfurt, especially Dr. Dmitrij Logashenko and Sebastian Reiter without whose help the groundwater flow models would neither have been set up nor would have worked. Also many thanks go to Anke Schneider and Anne Gehrke from GRS who gave a lot of practical help and advice concerning the handling of d^3f.

Thank you to you all.

References

SKB's (Svensk Kärnbränslehantering AB) publications can be found at www.skb.com/publications.

Brooks R H, Corey A T, 1964. Hydraulic properties of porous media. Fort Collins: Colorado State University. (Hydrology Papers 3)

Bruus H, 2008. Theoretical microfluidics. Oxford: Oxford University Press.

Börgesson L, Hernelind J, 1999. Coupled thermo-hydro-mechanical calculations of the water saturation phase of a KBS-3 deposition hole. Influence of hydraulic rock properties on the water saturation phase. SKB TR-99-41, Svensk Kärnbränslehantering AB.

Dershowitz W, Winberg A, Hermanson J, Byegård J, Tullborg E-L, Andersson P, Mazurek M, 2003. Äspö Hard Rock Laboratory. Äspö Task Force on modelling of groundwater flow and transport solutes. Task 6c. A semi-sythetic model of block scale conductive structures at the Äspö HRL. SKB IPR-03-13, Svensk Kärnbränslehantering AB.

Dueck A, 2004. Hydro-mechanical properties of a water unsaturated sodium bentonite: laboratory study and theoretical interpretation. PhD thesis. Lund University, Sweden.

Dueck A, Börgesson L, 2007. Model suggested for an important part of the hydro-mechanical behaviour of a water unsaturated bentonite. Engineering Geology 92, 160–169.

Finsterle S, Pruess K, 1995. Solving the estimation-identification problem in two-phase flow modeling. Water Resources Research 31, 913–924.

Fransson Å, Åkesson M, Andersson L, 2017. Bentonite Rock Interaction Experiment. Characterization of rock and installation, hydration and dismantling of bentonite parcels. SKB R-14-11, Svensk Kärnbränslehantering AB.

Grillo A, Logashenko D, Stichel S, Wittum G, 2010. Simulation of density-driven flow in fractured porous media. Advances in Water Resources 33, 1494–1507.

Guo R, Dixon D, 2006. The isothermal test: description and material parameters for use by the Engineered Barriers Systems Taskforce. Technical memorandum. 06819(UF)-03700.3 SKB-T05, Ontario Power Generation, Canada.

Helmig R, 1997. Multiphase flow and transport processes in the subsurface: a contribution to the modeling of hydrosystems. Berlin: Springer.

Kahr G, Kraehenbuehl F, Müller-Vonmoos M, Stoeckli H F, 1986. Wasseraufnahme und Wasserbewegung in hochverdichtetem Bentonit. Nagra Technischer Bericht NTB 86-14, Nagra, Switzerland. (In German.)

Kröhn K-P, 2004. Modelling the re-saturation of bentonite in final repositories in crystalline rock. Final report. GRS-199, Gesellschaft für Anlagenund Reaktorsicherheit (GRS) mbH, Braunschweig, Germany.

Kröhn K-P, 2011. Code VIPER – Theory and current status. Status report, FKZ 02 E 10548 (BMWi). GRS-269, Gesellschaft für Anlagen- und Reaktorsicherheit (GRS) mbH, Köln, Germany.

Kröhn K-P, 2012. Qualifying a computer program for simulating fracture flow. Computing and Visualization in Science 15, 29–37.

Kröhn K-P, 2016. Bentonite re-saturation: different conceptual models – similar mathematical descriptions. In Norris S, Bruno J, Van Geet M, Verhoef E (eds). Radioactive waste confinement: clays in natural and engineered barriers. London: Geological Society. (Special publication 443), 269–280.

Kröhn K-P, 2017. Bentonite re-saturation: different conceptual models – similar mathematical descriptions. London: Geological Society. (Special publication 443), 269–279.

Kröhn K-P, Stührenberg D, Herklotz M, Heemann U, Lerch C, Xie M, 2009. Restporosität und -permeabilität von kompaktierendem Salzgrus-Versatz; Projekt REPOPERM – Phase 1. GRS-254, Gesellschaft für Anlagenund Reaktorsicherheit (GRS) mbH, Braunschweig, Germany. (In German.)

Kull H, Miehe R, 1995. Der Einfluss der Stollen-Ventilation auf die hydraulischen Fliessverhältnisse im ausbruchsnahen Gebirgsbereich (Kristallin) : Felslabor Grimsel. Nagra NTB 94-04, Nagra, Switzerland. (In German.)

Kull H (ed), Helmig R, Jacobs H, Jockwer N, Kröhn K-P, Zimmer U, 2002. Two-phase-flow experiment in the fractured crystalline rock of the Äspö Hard Rock Laboratory. Final report. GRS-183, Gesellschaft für Anlagen- und Reaktorsicherheit (GRS) mbH, Germany.

Lenhard R J, Parker J C, Mishra S, 1989. On the correspondence between Brooks-Corey and Van Genuchten models. Journal of Irrigation and Drainage Engineering 115. doi:10.1061/(ASCE)0733-9437(1989)115:4(744)

Leverett M C, 1941. Capillary behavior in porous solids; Petroleum Transactions of the AIME 142, 152–169.

Olsson O (ed), Black J, Gale J, Barton N, Birgersson L, Cosma C, Dershowitz B, Doe T, Herbert A, Holmes D, Laaksoharju M, Long J, Neretnieks I, 1992. Site Characterisation and Validation – Final Report. Stripa Project Technical Report TR 92-22, Svensk Kärnbränslehantering AB.

Pusch R, Kasbohm J, 2001. Can the water content of highly compacted bentonite be increased by applying a high water pressure? SKB TR-01-33, Svensk Kärnbränslehantering AB.

Reiter S, Logashenko D, Grillo A, Wittum G, 2012. Preparation of grids for simulations of groundwater flow in fractured porous media. Computing and Visualization in Science 15, 209–225.

Reiter S, Logashenko D, Stichel S, Wittum G, Grillo A, 2014. Models and simulations of variable-density flow in fractured porous media. International Journal of Computational Science and Engineering 9, 416–432.

Schneider A (ed), 2012. Enhancement of d^3f und r^3t (E-DuR). Final report. GRS-292, Gesellschaft für Anlagen- und Reaktorsicherheit (GRS) mbH, Germany.

Staub I, Fredriksson A, Outters N, 2002. Strategy for a Rock Mechanics Site Descriptive Model. Development and testing of the theoretical approach. SKB R-02-02, Svensk Kärnbränslehantering AB.

Stichel S, Logashenko D, Grillo A, Reiter S, Lampe M, Wittum G, 2012. Numerical methods for flow in fractured porous media. In Delgado J (ed). Heat and mass transfer in porous media. Berlin, Heidelberg: Springer. (Advanced Structured Materials 13), 83–113.

Thomas H R, Cleall P J, Chandler N, Dixon D, Mitchell H P, 2003. Water infilration into a large-scale in-situ experiment in an underground research laboratory. Géotechnique 53, 207–224.

van Genuchten M T, 1980. A closed-form equation for predicting the hydraulic conductivity of unsaturated soils. Soil Science Society of America Journal 44, 892–898.

Vidstrand P, Åkesson M, Fransson Å, Stigsson M, 2017. SKB Task Forces EBS and GWFTS. Modelling the interaction between engineered and natural barriers. A compilation of Task 8 descriptions. SKB P-16-05, Svensk Kärnbränslehantering AB.

Vilks P, 2007. Forsmark site investigation. Rock matrix permeability measurements on core samples from borehole KFM01D. SKB P-07-162, Svensk Kärnbränslehantering AB.

Wass E, Nyberg G, 2009. Äspö Hard Rock Laboratory. Hydro Monitoring Program. Report for 2008. SKB IPR-09-11, Svensk Kärnbränslehantering AB.

Wikipedia, n d1. Stereografische Projektion. Available at: https://de.wikipedia.org/wiki/Stereografische_Projektion (In German).

Wikipedia, n d2. Directional statistics. Available at: https://en.wikipedia.org/wiki/Directional_statistics

Wikipedia, n d3. Von Mises–Fisher distribution. Available at: https://en.wikipedia.org/wiki/Von_Mises%E2%80%93Fisher_distribution

List of figures

List of tables

Appendix A

Fracture permeability

A1 Transmissivity

While flow resistance in the undisturbed matrix is usually described in terms of hydraulic conductivity or permeability it is given in terms of transmissivity if related to fracture flow. At Äspö, the transmissivity T is believed to be depending on fracture size by a power law:

$$T = a\,L^{b} \tag{A-1}$$

T: transmissivity [m^2/s]

L: fracture size [m]

a, b: constants

In the framework of Task 6c fractures were considered down to a size of 1 m or down to a transmissivity of 10^{-9} m^2 providing the values of $a = 5 \times 10^{-10}$ and $b = 1.386$ (Dershowitz et al. 2003). Approach and parameters are roughly confirmed by the transmissivity-fracture size plot given in Vidstrand et al. (2017) (see Figure A-1).

However, Figure A-1 includes also fracture sizes lower than 1 m which are showing a different trend. This trend is found to be represented by the values of $a = 5 \times 10^{-10}$ and $b = 3.1$.

The data from which Equation (A-1) is derived shows a significant scatter. Therefore Equation (A-1) is modified in Dershowitz et al. (2003) to

$$T = a\,L^{(b+cr)} \tag{A-2}$$

r: stochastic variable [-]

c: constant [-], $c = 0.3$

introducing an additional stochastic process to capture this scatter. The stochastic variable r is a uniform (−0.5 , +0.5) pseudo-random deviate. Note that the fracture length L is calculated as the trace in the horizontal plane. In the framework of Task 6c a mean transmissivity of $10^{-8.95}$ m^2/s for the background fractures with a standard deviation of $10^{0.93}$ was derived from this procedure (Dershowitz et al. 2003).

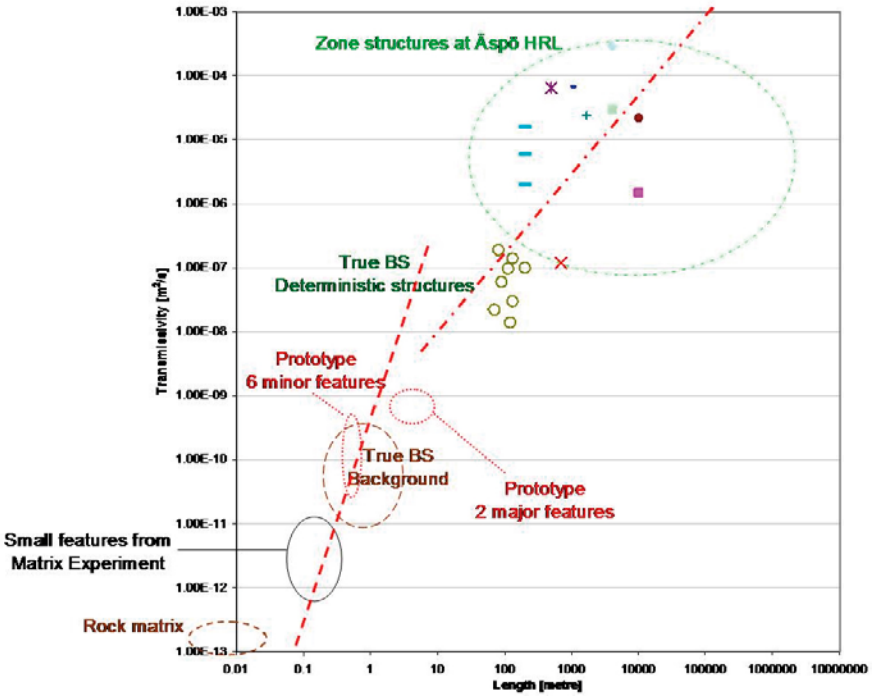

Figure A-1. *Transmissivity to size data from Äspö HRL; from Vidstrand et al. (2017).*

A2 Fracture aperture

Fracture aperture is the key property to derive fracture permeability. For Task 6c hydraulic aperture and transport relevant aperture were distinguished. According to Dershowitz et al. (2003) hydraulic aperture can be calculated by another power law:

$$e_h = a_h \, T^{b_h} \tag{A-3}$$

e_h = hydraulic aperture [m]
a_h, b_h = constants [-], $a_h = 0{,}5$, $b_h = 0{,}5$.

The transport relevant aperture is reduced by a factor of 8 in comparison to the hydraulic aperture.

$$e_t = a_t \, e_h \tag{A-4}$$

e_t = transport relevant aperture [m]
a_t = constant [-], $a_t = 0.125$.

Note that the approaches (A-3) and (A-4) may not be valid for fracture sizes below 1 m.

In Vidstrand et al. (2017) a power law for maximum aperture in the form

$$e = a_{ap} L^{b_{ap}} \tag{A-5}$$

e = aperture [m]
a_{ap}, b_{ap} = constants [-]

is suggested without quantifying the parameters a_{ap} and b_{ap}. Combining (A-1) and (A-3), however, yields the values $a_{ap} = 2.5 \times 10^{-10}$ and $b_{ap} = 0.648$ for $L > 1$ m or $b_{ap} = 1.55$ for $L < 1$ m.

A3 Permeability

With a given aperture there are two ways to derive permeability: firstly, the well-known relation (e.g. Bruus 2008)

$$k = \frac{e^2}{12} \tag{A-6}$$

k = permeability [m^2]

can be applied directly. Secondly, the transmissivity can be divided by the aperture to get a conductivity[8] and then further transformed into permeability. Combining for instance (A-1) and (A-3) to this effect, hydraulic conductivity could be calculated as

$$K = \frac{1}{a_h \left[\left(a \, L^b \right) \right]^{(b_h - 1)}} \tag{A-7}$$

K = hydraulic conductivity [m/s]

leading then to the expression

$$k = \frac{\eta}{\rho g} \frac{1}{a_h \left[\left(a \, L^b \right) \right]^{(b_h - 1)}} \tag{A-8}$$

Which of the several approaches for aperture and fracture permeability represents the actual situation best is hard to decide. As a basis for comparison fracture size is chosen to be the independent variable. Already the relations – (A-1) and (A-3); (A-1), (A-3), and (A-4); (A-5) – between fracture size and aperture show big differences as visualised in Figure A-2.

[8] This procedure is equivalent to ignoring a possible contribution to flow from the matrix.

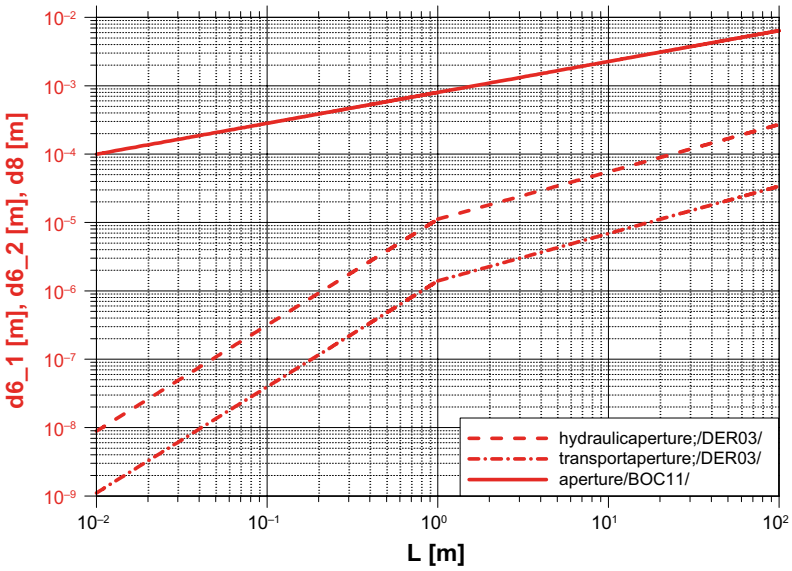

Figure A-2. *Aperture as a function of fracture size; data taken from Dershowitz et al. (2003) and Vidstrand et al. (2017).*

Appendix B

Basics for a statistical discrete fracture network

B1 Describing the orientation of fractures

In the following it is assumed that fractures are strictly planar structures.

The orientation of planes in space can be described by a vector that is normal to the plane. If no other information is to be conveyed with this vector like the position of the fracture the normal vectors of all fractures of a network can be arranged to start at one single point e. g. the origin of a coordinate system.

If these normal vectors are additionally normalized to unit length then the arrow heads end all on a hypothetical sphere with a radius of "1". The orientation of the fractures is thus also represented by dots on the sphere whose position can then be described by longitude and latitude, the North Pole being assigned to the top of the sphere.

A description of fracture orientation does not require to distinguish between the two sides of a fracture. It is therefore sufficient and advantageous for the purpose at hand to demand that the normal vector should either be horizontal or pointing upward. In this case the northern hemisphere including the equator contains all information about orientation of the fractures.

Visualized are the dots on the sphere by means of stereographic projection which is a mapping procedure to project the sphere onto a plane. Figure B-1 depicts the principle of the mapping. The plane is here a tangent to the north pole of the sphere. Centre S of the projection is located at the South Pole. A point A on the sphere is then projected onto the plane by a beam originating from S. Figure B-2 shows as an example the projected surface of earth's northern hemisphere. Map center is at 0° E, 90° N (North Pole). The marked circle covers the northern hemisphere, the white-shaded areas are on the southern hemisphere.

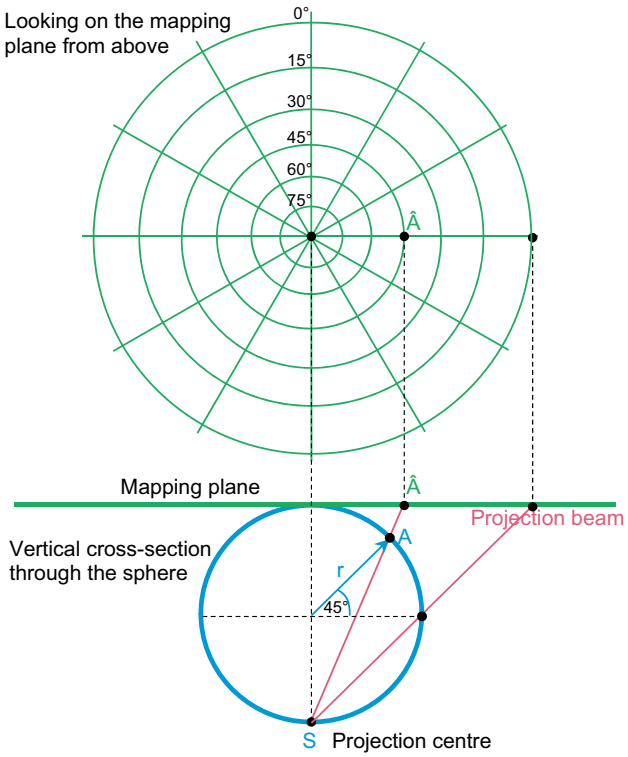

Figure B-1. *Principle sketch of a stereographic projection; after Wikipedia (n d1).*

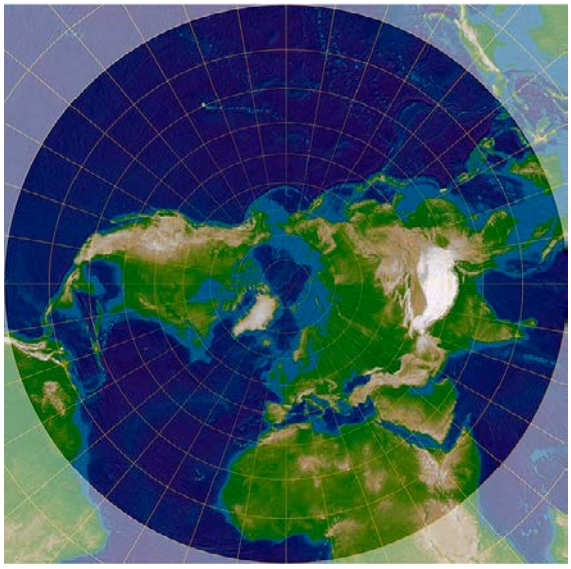

Figure B-2. *Example for a polar stereographic projection; from Wikipedia (n d1).*

B2 Directional statistics

"Directional statistics is the subdiscipline of statistics that deals with directions (unit vectors in R^n), axes (lines through the origin in R^n) or rotations in R^n" (Wikipedia n d2). "In directional statistics, the von Mises–Fisher distribution is a probability distribution on the (p-1)-dimensional sphere in R^p… The probability density function of the von Mises-Fisher distribution for the random *p*-dimensional unit vector **x** is given by" (Wikipedia n d3):

$$f_p(\mathbf{x};\boldsymbol{\mu},\kappa) = C_p(\kappa)\, e^{\kappa \boldsymbol{\mu}^{\mathrm{T}}\mathbf{x}} \tag{B-1}$$

f_p = probability density function

x = random unit vector

μ = unit vector of mean direction

κ = concentration parameter (kappa > = 0)

C_p = normalization constant.

In case of p = 3 the Mises–Fisher distribution is also simply called Fisher distribution for which the normalization constant reads

$$C_3 = \frac{\kappa}{4\pi \sinh \kappa} \tag{B-2}$$

These equations apply for polar coordinates only. A uniform distribution is described by a concentration parameter of $\kappa = 0$. An example of the effect of an increasing concentration for p = 3 is depicted in Figure B-3. Points from three Fisher distributions with different concentrations are sampled and displayed on a sphere (blue: $\kappa = 1$, green: $\kappa = 10$, red: $\kappa = 100$). The mean directions μ are also depicted by arrows.

B3 Directions

To describe a direction say of a straight line in space most intuitively an Euclidian vector can be used. An equivalent description involves a set of two angles known among geologists as "trend" and "plunge". While plunge is simply the angle between the line and a horizontal plane the explanation for trend requires a virtual vertical plane that contains the line. Trend is then the angle between the northern direction and the intersection line between the vertical and a horizontal plane. The main principal is illustrated in Figure B-4.

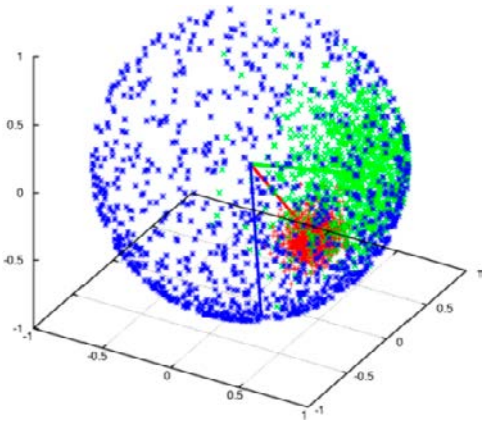

Figure B-3. *Probability density as a function of κ; from Wikipedia (n d3).*

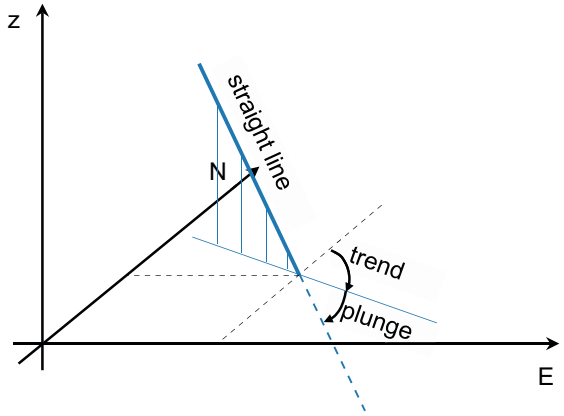

Figure B-4. *Concept of describing directions using trend and plunge.*

This concept can also be used to characterize the orientation of a planar structure in space. If the straight line coincides with the steepest gradient of the plain the concept of "dip and strike" applies where the dip angle would be the plunge and the dip direction – being orthogonal to the strike angle – the trend.

B4 Intensity

As a measure for the "density of fractures" in fractured rock the so-called "intensity" has been extensively used for modelling fracture networks at Äspö. The intensity is defined as the total area of fractures per cubic metre and denominated by the symbol P_{32}. Apparently, the index "32" indicates a two-dimensional quantity in a three-dimensional space. There are also other forms of intensity, namely the intensity P_{21} which can be used to calibrate a discrete fracture network (DFN) since P_{32} cannot be measured directly. In a geotechnical opening like a drift P_{21} can be calculated as the total length of fracture traces on the drift surface divided by the surface area. In a similar way the intensity can be measured as the amount of fractures along a scanline or a borehole (Staub et al. 2002). Both intensities P_{21} and P_{10} are linearly related to P_{32}:

$$P_{32} = C_{21} \cdot P_{21} \quad \text{and} \qquad \text{(B-3)}$$

$$P_{32} = C_{10} \cdot P_{10}$$

P = intensity; P_{32} [m^2/m^3], P_{21} [m/m^2], P_{10} [1/m]
C = constant; C_{21} [m/m], C_{10} [m^2/m^2]

The proportionality factors C_{21} and C_{10}, however, are not clearly defined because they depend on the properties of the fracture network namely orientation and the fracture size distribution as well as the orientation of the geotechnical openings. Calibration of a DFN means therefore

- estimating a value for P_{32},
- generating a DFN,
- checking the measured values for P_{21} and/or P_{10}, and
- correcting the estimated value for P_{32} accordingly.

Theoretically, all fracture sizes can be included in the process of generating a DFN from which an intensity value is subsequently derived. Practically, however, there are limits on both ends. There is a lower limit to the fracture size below which the fracture is either insignificant with respect to flow (Dershowitz et al. 2003) or below which it simply has not been detected (Vidstrand et al. 2017). A sensible upper limit would be a multiple of the maximum size of the domain in question.

Appendix C

Influence of CEs on breakthrough times

C1 Introduction

Unsaturated flow of water through a piece of granite from Äspö has been modelled with a view to the breakthrough time at the dry end of the sample. The water is assumed to be driven only by capillary forces through the initially dry rock. This physical problem allows several simplifications of a full set of two-phase flow equations that lead eventually to a saturation-based form of the Richards equation.

Modelling this water uptake requires knowledge about the hydraulic properties of the rock. While porosity and absolute permeability are rather well known there are considerable uncertainties concerning the constitutive equations (CE), namely the relative permeability-saturation relation (RPS) and the capillary pressure-saturation relation (CPS or retention curve). Presently, there is very little known about these relations from measurements at Äspö so formulations from other sites – Grimsel in Switzerland and the URL in Canada – were taken as a first approximation.

To investigate the impact of these uncertainties on the breakthrough time six series of models were investigated where the models vary according to different aspects of the uncertainties. The investigation was based on a 4 cm piece of rock that was discretized with 100 elements. Modelling took place with the ad-hoc Finite Element code UNSAT for simulating one-dimensional unsaturated flow.

Note that the investigations described in the following had been performed when measurements to determine the CEs for the BRIE-site had just begun. Therefore only tentative equations could be used.

C2 A simplified balance equation for unsaturated flow

The general form of the balance equations for multi-phase flow in the domain G is given by Helmig (1997) as

$$\int_G \left[\frac{\partial(\Phi\, S_\alpha\, \rho_\alpha)}{\partial t} + \Delta\left(\rho_\alpha \mathbf{v}_f\right) - \rho_\alpha q_\alpha \right] dG = 0 \qquad \text{(C-1)}$$

ρ_α = density of the α-phase [kg/m^3]
S_α = saturation of the α-phase [-]
Φ = porosity [-]
$\mathbf{v}_f$ = vector of the filter velocity for the α-phase [m/s]
q_α = sink/source of the α-phase [kg/(kg s)]
t = time [s]

In differential form (C-1) becomes

$$\Phi\rho_\alpha \frac{\partial S_\alpha}{\partial t} + \rho_\alpha S_\alpha \frac{\partial \Phi}{\partial t} + \Phi S_\alpha \frac{\partial \rho_\alpha}{\partial t} + \nabla \cdot \left\{\rho_\alpha \mathbf{v}_f\right\} - \rho_\alpha q_\alpha = 0 \qquad \text{(C-2)}$$

Assuming the extended Darcy's law to be valid

$$\mathbf{v}_f = k_{r\alpha} \frac{\mathbf{k}}{\mu_\alpha} \left[\nabla p_\alpha - \rho_\alpha \mathbf{g}\right] \qquad \text{(C-3)}$$

$k_{r\alpha}$ = relative permeability of the α-phase [-]
μ_α = viscosity of the α-phase [Pa s]
p_α = pressure of the α-phase [Pa]
$\mathbf{k}$ = tensor of the absolute permeability [m^2]
$\mathbf{g}$ = vector of the gravitational acceleration [m/s^2]

Equation (C-2) can be written as

$$\Phi\rho_\alpha \frac{\partial S_\alpha}{\partial t} + \rho_\alpha S_\alpha \frac{\partial \Phi}{\partial t} + \Phi S_\alpha \frac{\partial \rho_\alpha}{\partial t} - \nabla \cdot \left\{ \rho_\alpha \left(k_{r\alpha} \frac{\mathbf{k}}{\mu_\alpha} [\nabla p_\alpha - \rho_\alpha \mathbf{g}] \right) \right\} - \rho_\alpha q_\alpha = 0 \qquad \text{(C-4)}$$

Neglecting gas flow allows restricting to the water phase. It means also that the gas pressure is constant throughout the considered domain. Instead of index α for an arbitrary α-phase the index w can be used. Dropping also

- density changing effects like compressibility and thermal expansion,
- the influence of gravity,
- matrix deformation (thus assuming constant porosity), and
- water sinks and sources

transforms (C-4) into

$$\Phi \frac{\partial S_w}{\partial t} - \nabla \cdot \left(k_w \frac{\mathbf{k}}{\mu_w} \nabla p_w \right) = 0 \qquad \text{(C-5)}$$

Water pressure can be expressed by gas pressure and capillary pressure as

$$p_w = p_g - p_c \qquad \text{(C-6)}$$

p_g = gas pressure [Pa]
p_c = capillary pressure [Pa]

Note that capillary pressure is thereby defined to be a positive quantity. Since gas pressure was already assumed to be constant it follows from (C-6) that

$$\nabla p_w = -\nabla p_c \qquad \text{(C-7)}$$

Introducing a capillary pressure-saturation relation $p_c(S_w)$ allows to write (C-5) as

$$\Phi \frac{\partial S_w}{\partial t} + \nabla \cdot \left(\frac{k_{rw}}{\mu_w} \mathbf{k} \cdot \frac{\partial p_c}{\partial S_w} \nabla S_w \right) = 0 \qquad \text{(C-8)}$$

Rearranging (C-8) shows then that the balance equation for multiphase-flow has been reduced to a form that formally resembles Fick's second law with a saturation-dependent "diffusion coefficient" $\hat{D}$:

$$\frac{\partial S_w}{\partial t} + \nabla \cdot \left(\hat{\mathbf{D}} \cdot \nabla S_w \right) = 0 \text{ with } \hat{\mathbf{D}}(S_w) = \frac{k_{rw}(S_w)}{\mu_w} \frac{\mathbf{k}}{\Phi} \cdot \frac{\partial \{p_c(S_w)\}}{\partial S_w} \qquad \text{(C-9)}$$

$\hat{\mathbf{D}}$ = tensorial "diffusion coefficient" [m^2/s]

In the following (C-9) will be investigated in its one-dimensional form

$$\frac{\partial S_w}{\partial t} + \frac{\partial}{\partial x} \left(\hat{D} \frac{\partial S_w}{\partial x} \right) = 0 \text{ with } \hat{D} = \frac{k}{\mu_w \Phi} \cdot k_{rw} \frac{\partial p_c}{\partial S_w} \qquad \text{(C-10)}$$

The dependency of $\hat{D}$ on saturation is introduced by the relative permeability k_{rw} and by the derivative of the capillary pressure with respect to saturation $\partial p_c / \partial S_w$. The product of both terms is defined for the sake of simplicity as

$$r = k_{rw} \frac{\partial p_c}{\partial S_w} \qquad \text{(C-11)}$$

r = product of k_{rw} and $\partial p_c / \partial S_w$ [Pa]

leading to the final form of the balance equation for unsaturated flow:

$$\frac{\partial S_w}{\partial t} + \frac{\partial}{\partial x}\left(\frac{k}{\mu\, \Phi} r(S_w) \frac{\partial S_w}{\partial x} \right) = 0 \qquad \text{(C-12)}$$

C3 Specifying the saturation-dependent term *r*

The term *r* in (C-11) depends on the Relative-Permeability-Saturation relation (RPS) and the Capillary-Pressure-Saturation relation (CPS). Interestingly enough, the two most prominent approaches for these relations provided by Brooks and Corey (1964) and van Genuchten (1980) were both developed to predict the RPS from a measured CPR using general theorems that were based on a capillary bundle model. They both provide therefore a related set of equations where all parameters used for the RPS can also be found in the CPS. Nevertheless examples can be found also in the literature where models were based on independent formulations for the RPS and the CPS (e.g. Börgesson and Hernelind 1999).

The approach of van Genuchten (1980) for the RPS and the CPS reads

$$k_{rw}^{VG} = \sqrt{S_e}\left[1 - \left(1 - S_e^{\frac{1}{m}} \right)^m \right]^2 \qquad \text{(C-13)}$$

k_{rw}^{VG} = relative permeability after van Genuchten (1980) [-]
S_e = effective saturation [-], c.f. (C-16)
m = parameter [-]

and

$$p_c^{VG} = p_{c\,0}\left[(S_e)^{-\frac{1}{m}} - 1 \right]^{\frac{1}{n}} \qquad \text{(C-14)}$$

p_c^{VG} = capillary pressure after van Genuchten (1980) [Pa]
p_{c0} = scaling parameter; related to the air entry pressure [Pa]
n = parameter [-][9], c.f. (C-15)

with

$$n = -\frac{1}{m-1} \qquad \text{(C-15)}$$

and

$$S_e = \frac{S_w - S_{wr}}{S_{ws} - S_{wr}} \qquad \text{(C-16)}$$

S_{ws} = degree of saturation at saturation of the wetting phase [-]
S_{wr} = residual saturation [-]

resulting in

$$\frac{dp_c^{VG}}{dS_w} = -\frac{p_{c\,0}}{m\, n}\left[(S_w)^{-\frac{1}{m}} - 1 \right]^{\left(\frac{1}{n}-1\right)} (S_w)^{-\left(1+\frac{1}{m}\right)} \qquad \text{(C-17)}$$

The product r^{VG} thus amounts to

$$r^{VG} = -\frac{p_{c\,0}}{m\, n}\left[(S_w)^{-\frac{1}{m}} - 1 \right]^{\left(\frac{1}{n}-1\right)} \left[1 - \left(1 - S_w^{\frac{1}{m}} \right)^m \right]^2 (S_w)^{-\left(\frac{1}{2}+\frac{1}{m}\right)} \qquad \text{(C-18)}$$

r^{VG} = product of k_{rw}^{VG} and $\partial p_c^{VG}/\partial S_w$ after van Genuchten (1980) [Pa]

[9] The parameter n is proportional to the range of pore sizes constituting the pore space van Genuchten (1980).

Starting with the approach of Brooks and Corey (1964) the RPS and the CPS are given by

$$p_c^{BC} = p_e \cdot S^{-\frac{1}{\lambda}} \quad \text{(C-19)}$$

$$k_{rw}^{BC} = S^{\frac{2+3\lambda}{\lambda}} \quad \text{(C-20)}$$

p_c^{BC} = capillary pressure after Brooks and Corey (1964) [Pa]
pe = air entry pressure [Pa]
λ = pore size distribution index [-][10]
k_{rw}^{BC} = relative permeability after [-]

From this follow the derivative of the capillary pressure and term as

$$\frac{dp_c^{BC}}{dS} = -\frac{1}{\lambda} p_e \cdot S^{-\frac{1+\lambda}{\lambda}} \quad \text{(C-21)}$$

$$r^{BC} = -S^{\frac{2+3\lambda}{\lambda}} \cdot \frac{1}{\lambda} p_e \cdot S^{-\frac{1+\lambda}{\lambda}} \quad \text{(C-22)}$$

r^{BC} = product of k_{rw}^{BC} and $\partial p_c^{BC}/\partial S_w$ after Brooks and Corey (1964) [Pa]

Without explanation an empirical approach for the RPS the so-called power law is sometimes used:

$$k_{rw} = (S_w)^{\delta} \quad \text{(C-23)}$$

δ = empirical exponent at [-]

Closer inspection reveals a formal similarity between (C-23) and (C-20). Apparently, the exponent δ and the pore size distribution index λ are related. Applying the theory of Brooks and Corey provides a lower limit of 3 for the exponent δ which relates to the ideal uniform pore size distribution. Any deviation results in an increase of δ, or in other words, δ is proportional to the degree of non-uniformity of pore sizes. Note that Corey (1954, cited in Brooks and Corey 1964) had much earlier already suggested an exponent of 4 based on the observation of a large number of consolidated porous rock.

C4 Series 1 – CEs from literature

In Vidstrand et al. (2017), CEs are presented from Finsterle and Pruess (1995), Börgesson and Hernelind (1999), and Thomas et al. (2003), respectively. Favored there are the CEs from Finsterle and Pruess (1995) who derived van Genuchten parameters for the granite at the Grimsel site in Switzerland by inverse modeling (model A). Modeling of flow in the granite matrix at Äspö has been performed by Börgesson and Hernelind (1999) where a van Genuchten approach was used for the CPS and a power law for the RPS (model B). From modeling flow in the Canadian granite stem the van Genuchten parameters used in Thomas et al. (2003) (model C). The same rock is described empirically in Guo and Dixon (2006). This empirical retention curve ad hoc coupled with the van Genuchten formulation for relative permeability as in Thomas et al. (2003) was used in model D. Recent and provisional capillary pressure data for the granite at Äspö (Fransson et al. 2017) led to an ad-hoc set of CEs that is based on very few data points to which the van Genuchten approach from Finsterle and Pruess (1995) was fitted (model E).

A first series of models was run according to the five data sets. The used CEs are compiled in Table C-1. The resulting curves for relative permeability and capillary pressure with respect to saturation are depicted in Figure C-1. The "diffusion coefficient" D for the five models is shown in Figure C-2.

[10] According to the theory of Brooks and Corey the parameter λ can adopt any value greater than zero "being small for media having a wide range of pore sizes and large for media with e relatively uniform pore size" (Brooks and Corey 1964). For most porous media $0{,}2 \geq \lambda \geq 3$ holds (Helmig 1997).

Table C-1. CEs used for modelling unsaturated flow in granite; series 1.

	Model A	Model B	Model C	Model D	Model E
Source	Finsterle and Pruess (1995)	Börgesson and Hernelind (1999)	Thomas et al. (2003)	(ad hoc)[a)]	(ad hoc)[b)]
RPS model	van Genuchten	Power law	van Genuchten	van Genuchten	van Genuchten
m	0.6	–	0.35	0.35	0.6
δ	–	3	–	–	–
CPS model	van Genuchten	van Genuchten	van Genuchten	Empirical relation	van Genuchten
m	0.6	0.66	0.35	–	0.6
p_{c0} [MPa]	1.74	4.0	0.7	–	6.0

[a)] Based on Guo and Dixon (2006).
[b)] Based on Fransson et al. (2017).

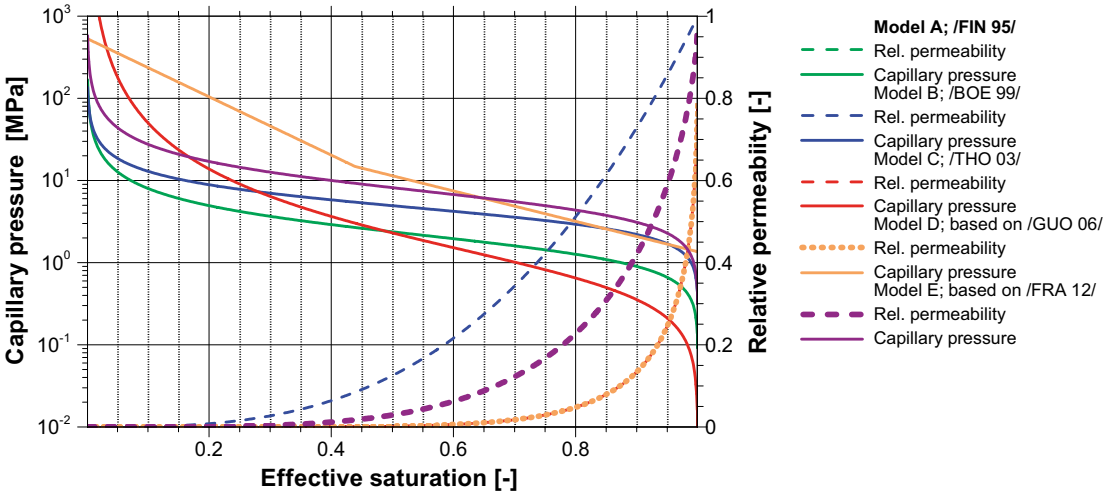

Figure C-1. *Equations of state for two-phase flow in granite; model series 1.*

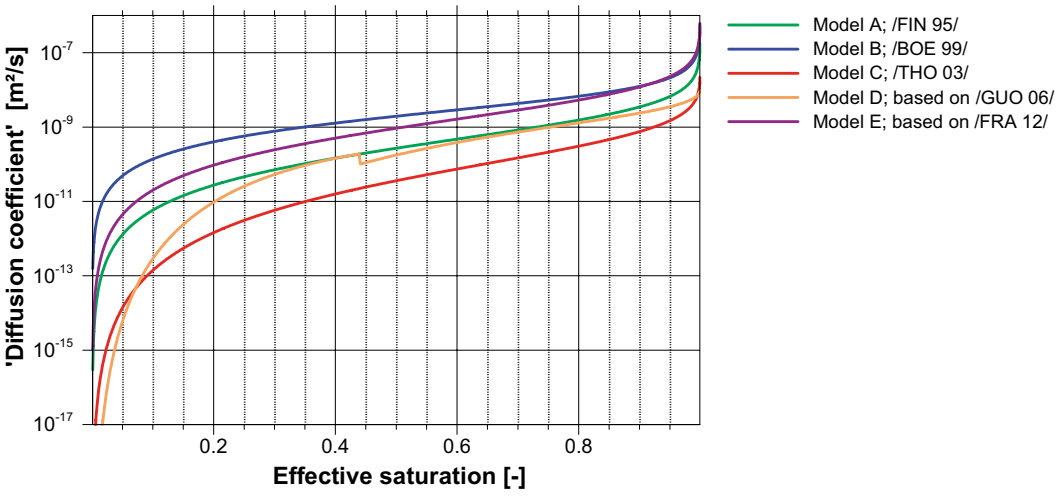

Figure C-2. *'Diffusion coefficient'; model series 1.*

An element size of 0.4 mm was chosen resulting in a grid of 100 elements. Contour lines were drawn for every hour and different colours were used to depict different days. The calculated saturation profiles for all models are shown in Figure C-3. Breakthrough times – the time required for the water to reach the other side of the sample – are listed in Table C-2.

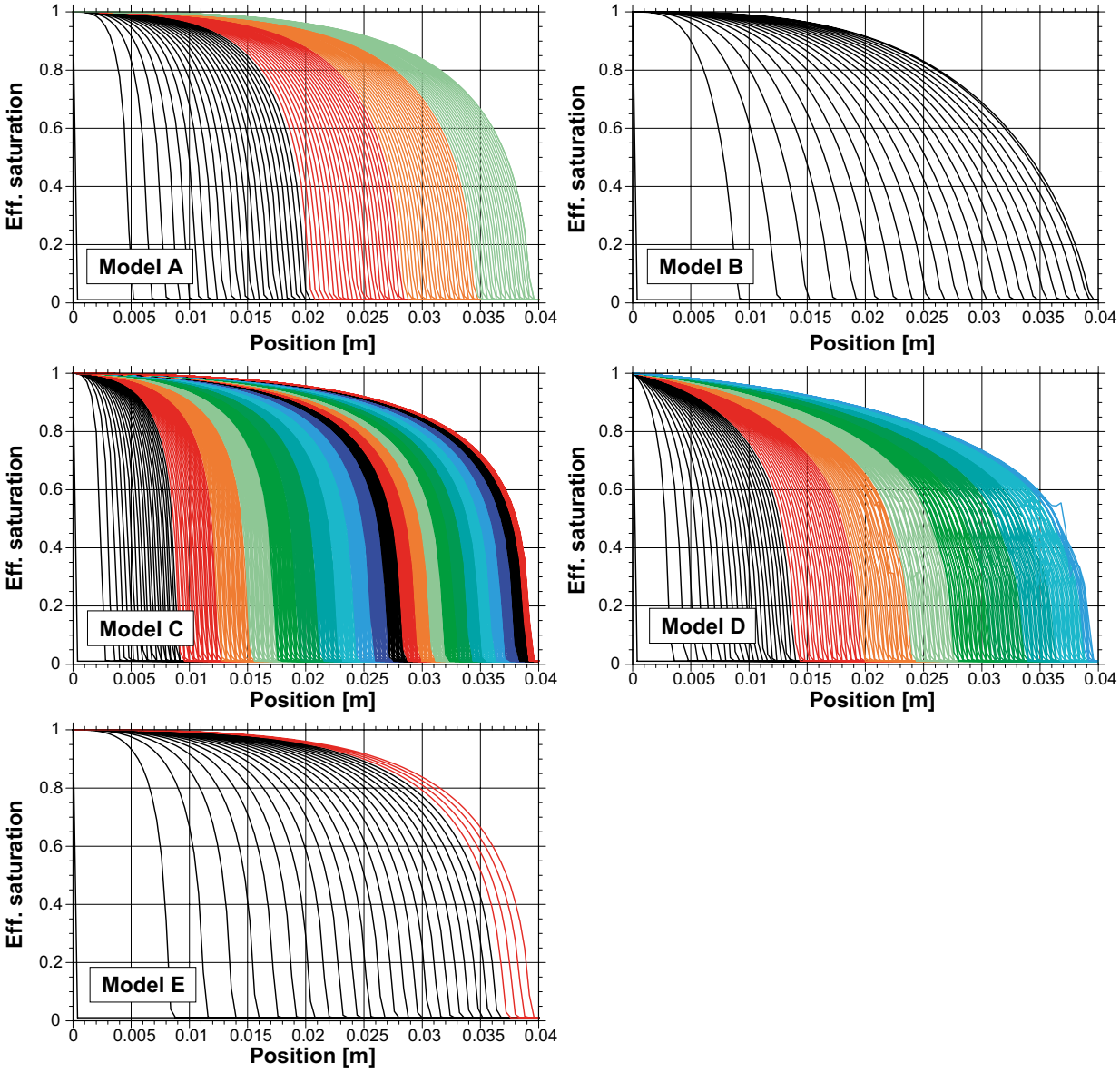

Figure C-3. *Transient saturation distributions; model series 1.*

Table C-2. Breakthrough times; model series 1.

	Model A	Model B	Model C	Model D	Model E
Breakthrough time	93 h	22 h	515 h	198 h	27 h

According to (C-10) water migration is only controlled by the 'diffusion coefficient' $\hat{D}$ and the curves for the 'diffusion coefficients' in Figure C-2 lie more or less on top of each other. In this situation a sorting of breakthrough times can be easily predicted. The sequence from shortest to longest time according to Figure C-2 – models C, D, A, E, B – is confirmed by the calculated data compiled in Table C-2.

The breakthrough times listed in Table C-2 show large differences. While the models based on Äspö data (models B and E) predict a breakthrough time of roughly one day the model based on Grimsel data (model A) yields almost 4 days and using the data from the Canadian granite (model C and D) even 21 and 8 days.

Figure C-1 and Figure C-2 suggest also that the CEs from Grimsel are better in line with the CEs for Äspö than the data for the Canadian rock. This is again confirmed by the calculated breakthrough times. Since the retention curve is an indication for the pore size distribution in the rock the Canadian granite appears

to differ distinctly from the rock at the two European sites. A posteriori this effect does not come as a surprise since the Canadian and the European granites are located on different tectonic plates and may thus differ considerably with respect to genesis, composition and other possible factors influencing the pore space geometry.

C5 Series 2 – scaled retention curves

Soils or rocks that are hydraulically similar especially with respect to the topology of the pore space have similar retention curves. According to Leverett (1941) these similar retention curves can be described by one dimensionless function which was later called J-function. This function can simply be scaled with the porosity and permeability of the material in question to provide the matching retention curve. Also included in the J-function is the surface tension of the fluid to account for different fluids:

$$J(S) = \frac{p_c}{\sigma}\sqrt{\frac{k}{\Phi}} \tag{C-24}$$

$J(S)$ = dimensionless J-function [-]

p_c = capillary pressure of the material in question [Pa]

σ = surface tension of the fluid in question

k = permeability of the material in question [m^2]

Φ = porosity of the material in question [-]

So, just one retention curve for a reference material must be determined. Capillary pressure for any similar material can then be calculated using the scaling factor f (e.g. Kröhn et al. 2009):

$$f = \sqrt{\frac{\Phi}{\Phi_0}\frac{k_0}{k}} \tag{C-25}$$

f = scaling factor [-]

k_0 = permeability of the reference material [m^2]

Φ_0 = porosity of the reference material [-]

Transfer of CEs that were developed for the granite at Grimsel or for the Canadian granite to the granite at Äspö would thus mean that with a change of permeability and porosity the measured retention curve must additionally be scaled with the factor f. This has not been done for the first series of models. The hydraulic data for the rock taken from Finsterle and Pruess (1995), Guo and Dixon (2006) and Vidstrand et al. (2017) as well as the resulting scaling factor f is compiled in Table C-3.

In the second series the models with CEs from Grimsel and Canada were run again with scaled retention curves. Referring variants of the CEs described in Finsterle and Pruess (1995), Thomas et al. (2003) and in Guo and Dixon (2006) were used for the models F, G, and H. These CEs are compiled in Table C-4. For comparison the CEs as well as the "diffusion coefficient" are depicted in Figure C-4 and Figure C-5, respectively.

The transient saturation can be seen in Figure C-6. Calculated breakthrough times are listed in Table C-5. Scaling of the retention curves has accelerated saturation in the models. However, while model F based on Grimsel data shows a breakthrough time in the order of the Äspö models B and E the breakthrough times of the models G and H based on data for Canadian rock are still way off. This adds to the suspicion stated in the previous subsection about substantial differences in the structure of the pore space between the Canadian and the two European granites.

Table C-3. Data for calculating the scaling factor *f*.

		Grimsel	Canada	Äspö
Permeability k	[m^2]	5.13×10^{-20}	5.00×10^{-20}	1.00×10^{-20}
Porosity Φ	[–]	0.01	0.005	0.005
Scaling factor f	[–]	5.07	1.41	1

Table C-4. CEs used for modelling unsaturated flow in granite; series 2.

	Model F	Model G	Model H
Source	Finsterle and Pruess (1995)	Thomas et al. (2003)	(ad hoc) [a]
RPS model	van Genuchten	van Genuchten	van Genuchten
m	0.6	0.35	0.35
δ	–	–	–
CPS model	van Genuchten	van Genuchten	Empirical relation
m	0.6	0.35	–
p_{c0} **[MPa]**	8.813	0.99	–
f	5.07	1.41	1.41

[a] based on Guo and Dixon (2006).

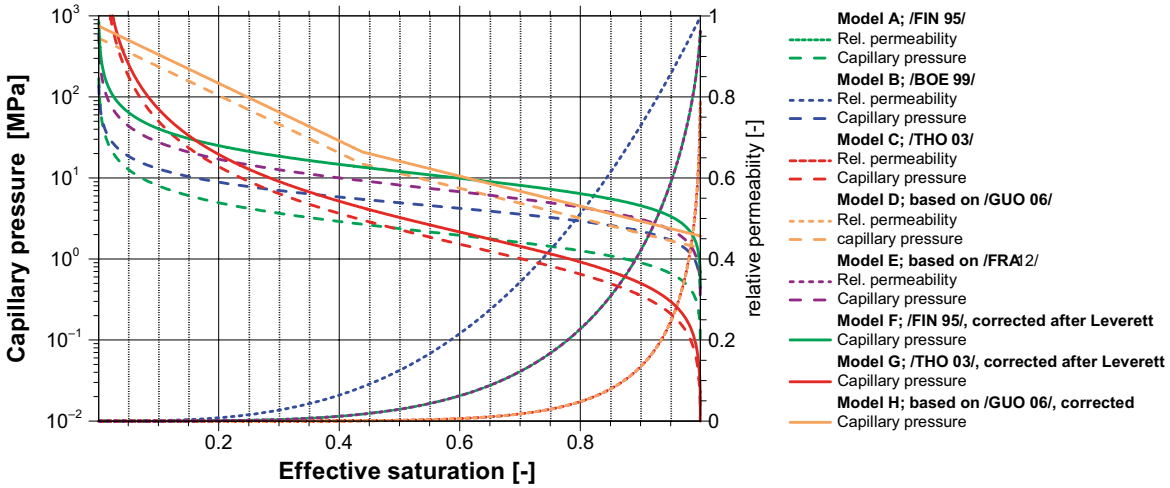

Figure C-4. *Equations of state for two-phase flow in granite; model series 2.*

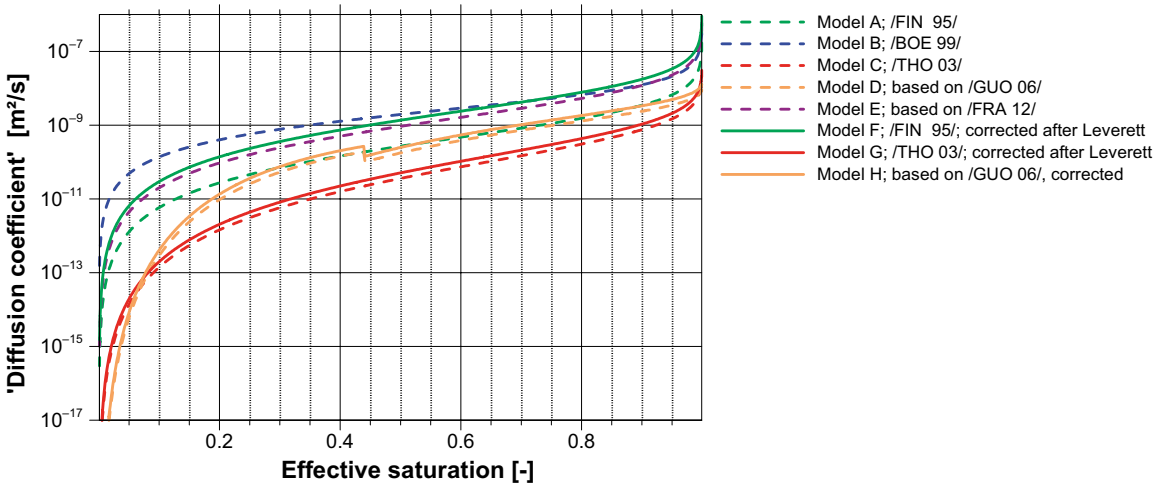

Figure C-5. *'Diffusion coefficient'; model series 2.*

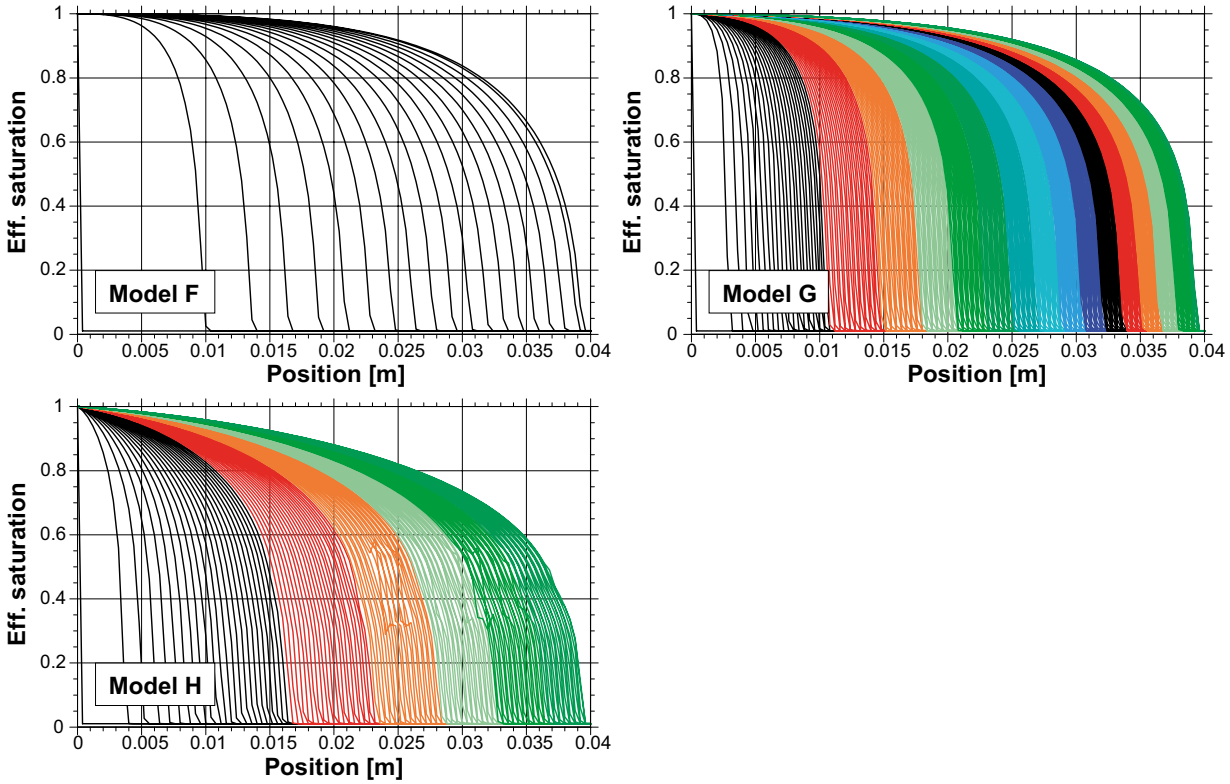

Figure C-6. *Transient saturation distributions; model series 2.*

Table C-5. Breakthrough times; model series 2.

Series 1	Breakthrough time		series 2
Model A	93 h	18 h	Model F
Model C	515 h	364 h	Model G
Model D	198 h	140 h	Model H

C6 Series 3 – Brooks and corey approach

The approach of van Genuchten is apparently more often used for modeling water flow in granite than the approach of Brooks and Corey. This may have to do with the fact that the retention curve after Brooks and Corey has a horizontal tangent at full saturation. A very small value of the term $\partial pc/\partial S$ can lead to difficulties solving the algebraic equation system of a numerical model and a zero on the principal diagonal of the equation matrix renders inversion mathematically impossible.[11]

From a physical point of view, however, this preference of the van Genuchten approach is peculiar because the retention curve after van Genuchten does not take the air entry pressure into account. Interestingly enough, van Genuchten's investigations were based partly on the same materials that Brooks and Corey had used being mainly sands, sandstone and silty soil. Both CEs are thus based on similar and partly even the same laboratory data. In case of these materials the air entry pressure is rather low, for sands a few hundred up to approx. 5 000 Pa (e.g. Brooks and Corey 1964, Helmig 1997) and for the other materials except for the clay sample up to 0.07 MPa.[12] The air entry pressure may therefore not play such an important role for this kind of material.

[11] A full discussion of this problem can be found in Helmig (1997).

[12] Van Genuchten could the CES for the clay sample not match as nicely with the data as for the other materials (van Genuchten 1980).

For granitic rock things look different, though. Since the air entry pressure is inverse proportional to the maximum diameter of the flow channels in the pore space of a porous medium it can be expected to be rather high in granite. And, indeed, it has been measured to lie between 0.5 and 0.8 MPa for the granite at Grimsel (Kull and Miehe 1995). Porosity as well as permeability at Äspö are lower than at Grimsel (see Table C-3) so the air entry pressure could be even higher there. To investigate the effect of the Brooks-Corey approach in general and the effect of an air entry pressure on breakthrough time in particular the van Genuchten approach used by Finsterle and Pruess (1995) and corrected after Leverett (1941) (model F) was transformed after Lenhard et al. (1989) into an equivalent Brooks and Corey formulation.

In the third series two variants of model F were investigated. Firstly, only the van Genuchten formulation for the retention curve was exchanged in favour of the Brooks and Corey formulation (model I). Then, the Brooks and Corey approach for relative permeability was also used (model J). The CEs are compiled in Table C-6. For comparison the CEs as well as the "diffusion coefficient" are depicted in Figure C-7 and Figure C-8, respectively. The transient saturation can be seen in Figure C-9. Calculated breakthrough times are listed in Table C-7.

From the CEs in Figure C-7 one would expect a significant impact of the RPS on the breakthrough time. The calculations show, however, that accounting for the air entry pressure lengthens the breakthrough time roughly by a factor of 3 while the difference due to the switch to the higher relative permeability values after Brooks and Corey amounts to less than 20 %. Note, that the choice of the set of CEs also influences steepness and height of the saturation front.

Table C-6. CEs used for modelling unsaturated flow in granite; series 3.

	Model I	**Model J**
Based on	Finsterle and Pruess (1995)	Finsterle and Pruess (1995)
RPS model	van Genuchten	Brooks and Corey
δ	0.6	–
λ	–	1.028
CPS model	Brooks and Corey	Brooks and Corey
m	–	–
p_{c0} [MPa]	–	–
λ	1.028	1.028
p_e [MPa]	5.597	5.597

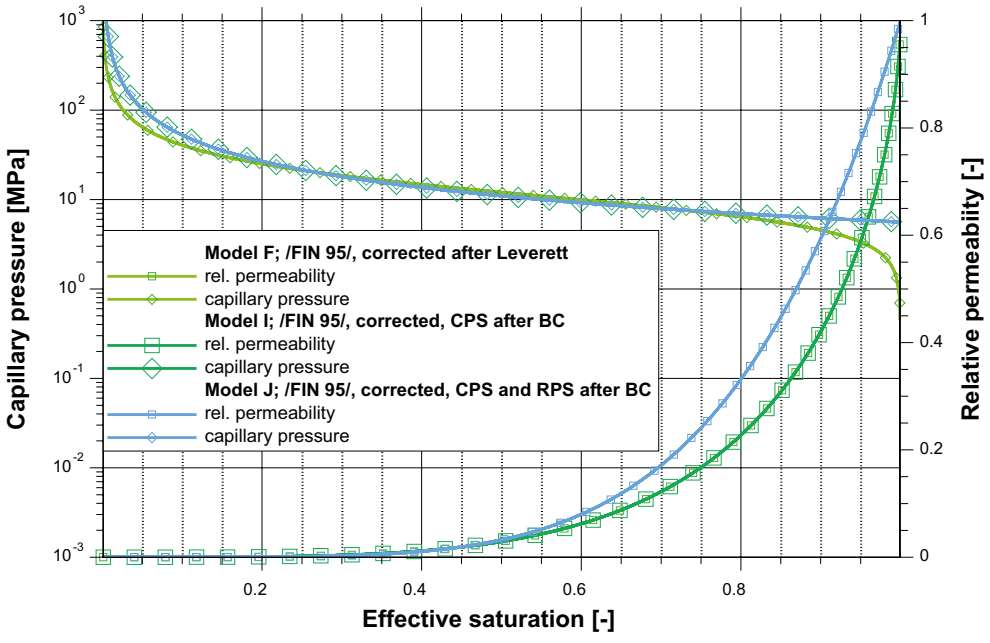

Figure C-7. Equations of state for two-phase flow in granite; model series 3.

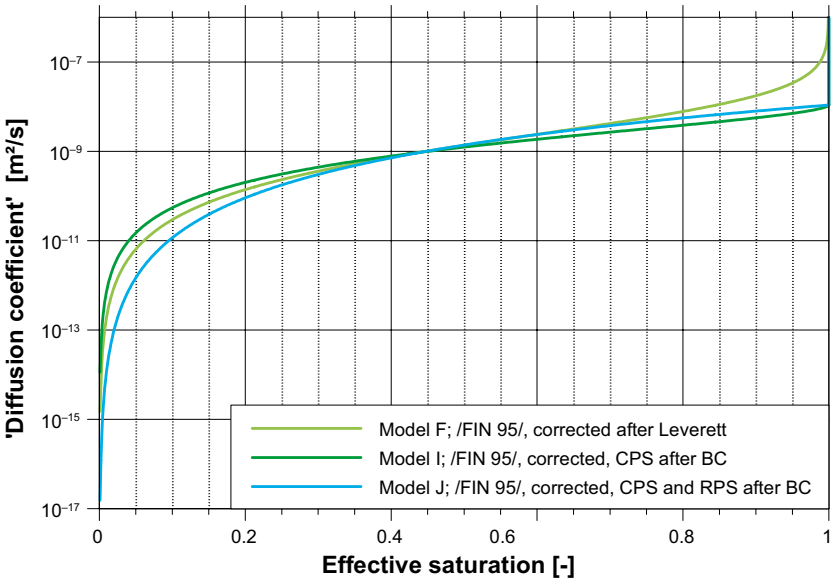

Figure C-8. 'Diffusion coefficient'; model series 3.

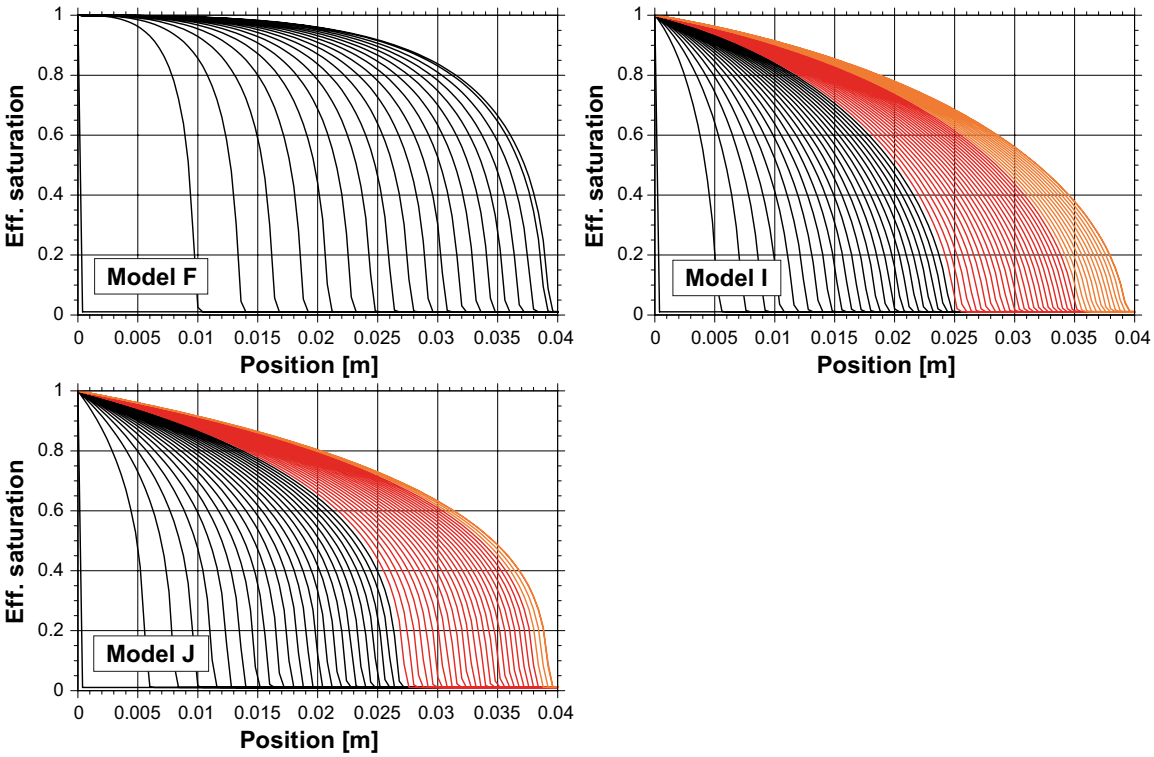

Figure C-9. Transient saturation distributions; model series 3.

Table C-7. Breakthrough times; model series 3

	Model F	Model I	Model J
Breakthrough time	18 h	59 h	50 h

C7 Series 4 – alternative RPS

As an alternative to the van Genuchten approach for the relative permeability a power law with an exponent of 3 as in Börgesson and Hernelind (1999) has often been used in the context of two-phase flow in granitic rock. In the framework of the theory by Brooks and Corey the exponent of 3 is equivalent to a uniform pore size distribution.

As a variant for models E, G, and H (based on Fransson et al. 2017, Thomas et al. 2003 and Guo and Dixon 2006) this simple approach is applied instead of the van Genuchten formulation (models K, L, and M). The referring CEs are compiled in Table C-8. For comparison the CEs as well as the "diffusion coefficient" are depicted in Figure C-10 and Figure C-11, respectively. The transient saturation can be seen in Figure C-12. Calculated breakthrough times are listed in Table C-9.

The change in the RPS from the Äspö-data based model E to the power law is much less dramatic than the change from the RPS for the Canadian rock to the power law as can be seen in Figure C-10. The acceleration of saturation in the models L and M is remarkably high. Also the curvature has changed the sign for most part of the saturation profiles.

Table C-8. CEs used for modelling unsaturated flow in granite; series 4.

	Model K	Model L	Model M
Based on	Fransson et al. (2017)	Thomas et al. (2003)	Guo and Dixon (2006)
RPS model	Power law	Power law	Power law
δ	3	3	3
λ	–	–	–
CPS model	van Genuchten	van Genuchten	Empirical relation
m	0.6	0.35	–
p_{c0} [MPa]	6.0	0.99	–
λ	–	–	–
p_e [MPa]	–	–	–
f	1	1.41	1.41

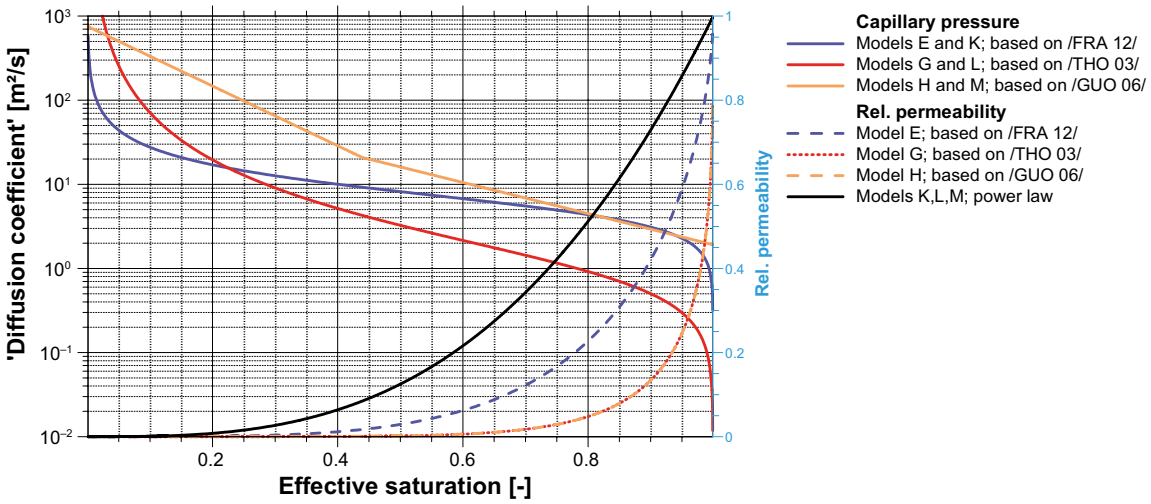

Figure C-10. *Equations of state for two-phase flow in granite; model series 4.*

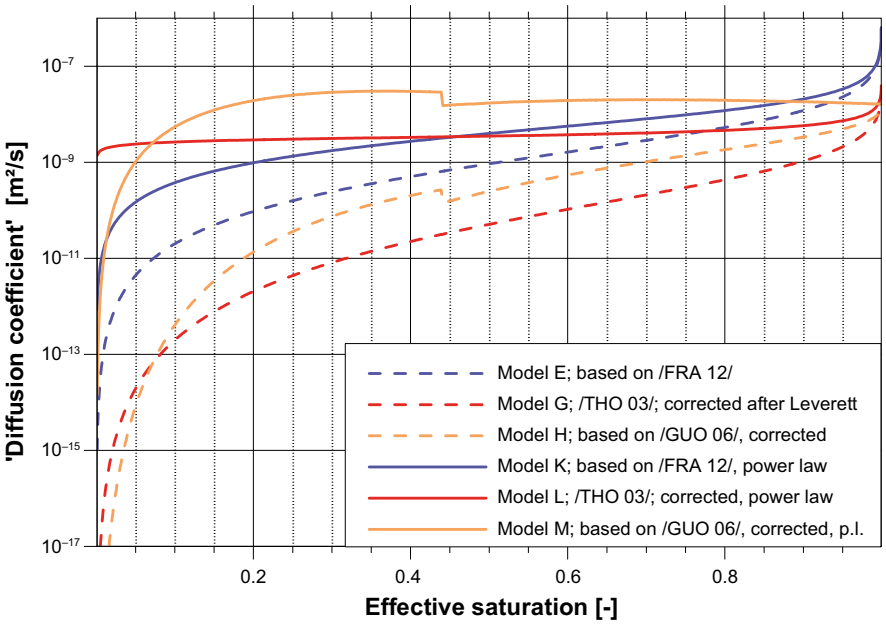

Figure C-11. *'Diffusion coefficient'; model series 4.*

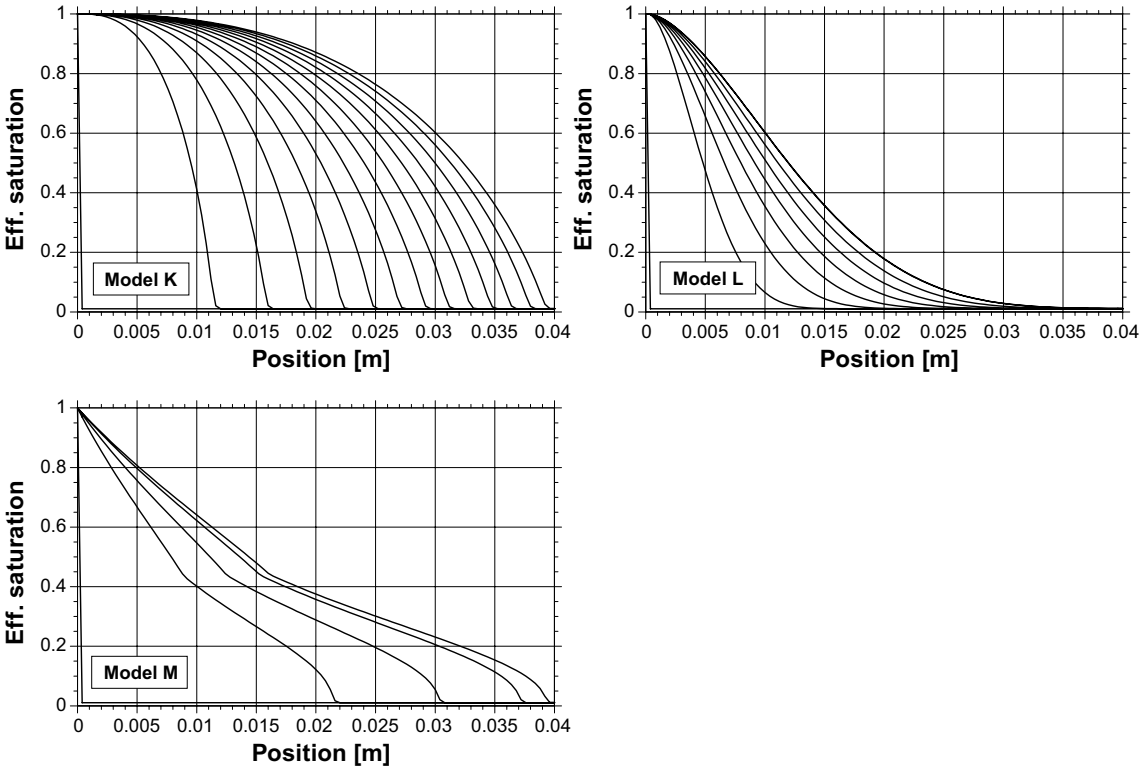

Figure C-12. *Transient saturation distributions; model series 4.*

Table C-9. Breakthrough times; model series 4.

Series 1/2	Breakthrough time		Series 4
Model E	27 h	13 h	Model K
Model G	364 h	7 h	Model L
Model H	140 h	3 h	Model M

C8 Series 5 – reduced model size

To get a feeling for the influence of model size on breakthrough time the calculations based on Äspö data (models B and E) as well as the calculations based on Leverett-corrected data from Grimsel and Canadian (models F, G, and H) were repeated for half of the model length (models N to R). The relations can also be taken from Table C-10. All five models were recalculated for a reduced model length of 2 cm but with the same element length as in the previous models. The results are depicted in Figure C-13. Breakthrough times can be found in Table C-11 along with the results from the larger models.

Table C-10. Relation of models; series 5.

Source/based on	Finsterle and Pruess (1995)	Börgesson and Hernelind (1999)	Thomas et al. (2003)	Guo and Dixon (2006)	Fransson et al. (2017)
4 cm length	Model F	Model B	Model G	Model H	Model E
2 cm length	Model N	Model O	Model P	Model Q	Model R

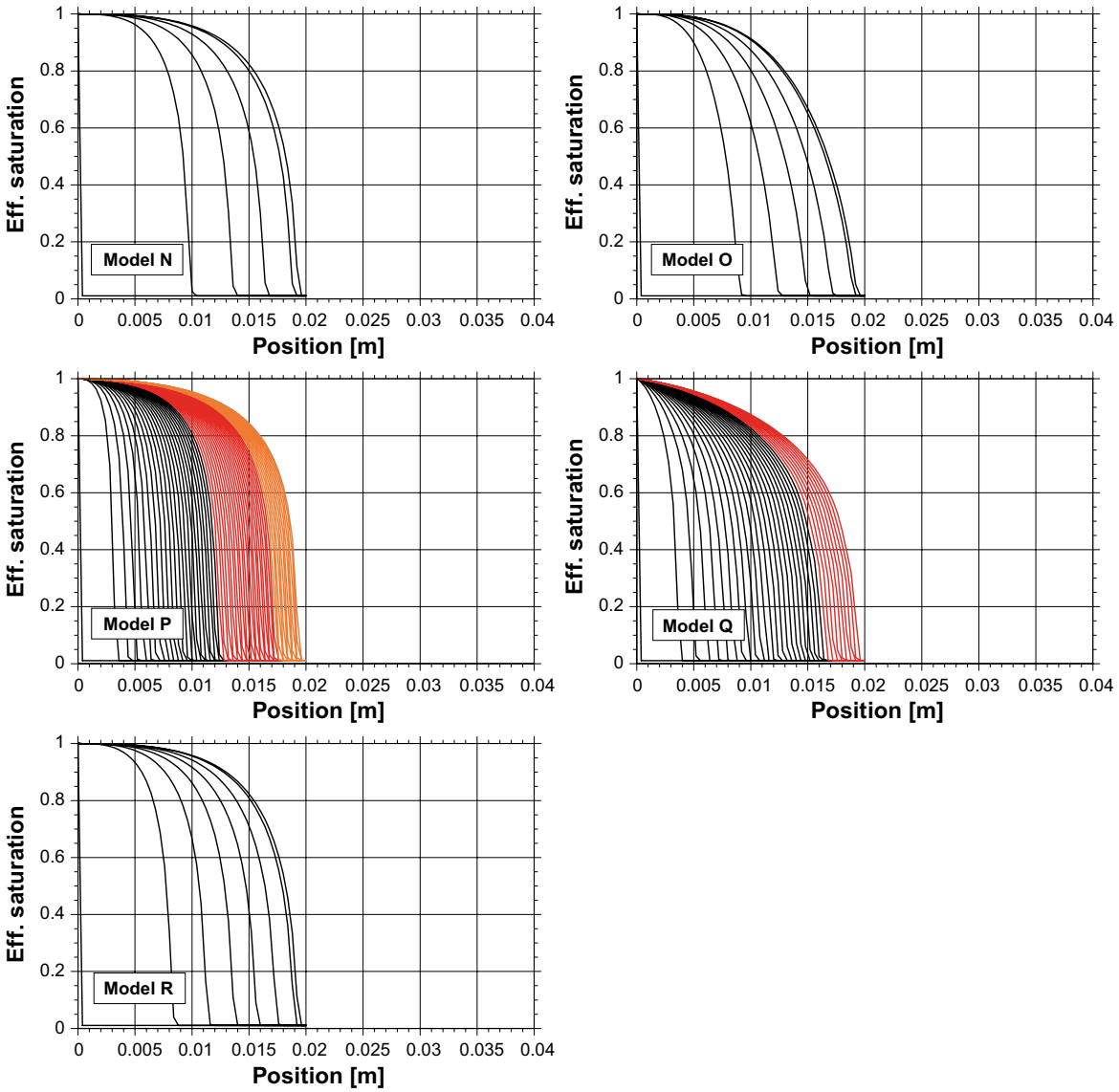

Figure C-13. Transient saturation distribution; reduced sample size, model series 5.

Table C-11. Comparison of breakthrough times.

Model	N/F	O/B	P/G	Q/H	R/E
Breakthrough time for the 2-cm model	4 h	5 h	60 h	33 h	6 h
Breakthrough time for the 4-cm model	13 h	22 h	364 h	140 h	27 h
Ratio	0.23	0.23	0.16	0.24	0.23

The ratio between breakthrough times from the 2-cm model and the 4-cm model varies between 0.16 and 0.24. This indicates that breakthrough time increases exponentially with the length of the model.

C9 Series 6 – grid convergence

To ensure that an adequate grid resolution was used calculation of model O was repeated with a grid of 100, 200, and 400 elements, respectively (models S, T, and U). As Table C-12 shows the calculated breakthrough time increased slightly with grid resolution. It amounted to 5 hours 9 min for 50 elements, 5 hours 35 min for 100 elements, 5 hours 46 min for 200 elements and 5 hours 51 min for 400 elements. Note that the breakthrough time increases theoretically slightly with grid resolution since the criterion for stopping the simulation depends on the value for the node next to the right hand side boundary.

Table C-12. Breakthrough times; model series 6.

Model	No. of elements	Breakthrough time
O	50	5 h 9 min
S	100	5 h 35 min
T	200	5 h 46 min
U	400	5 h 51 min

The results indicate that a grid with doubled resolution meaning 200 elements along the 4 cm model length would have been perceptively closer to the actual solution. However, the difference in breakthrough time for models O and U amounts to approx. 13 % which is acceptable for the purpose at hand.

C10 Summary and conclusions

Series 1 introduced the five different approaches for RPS and CPS that had been found in the literature. The calculated breakthrough times showed a spectrum between one and twenty-one days. Rather apparent was the relation between breakthrough time and the site for which the data was derived. The longest breakthrough times resulted from data from Canada (8 and 21 days), the shortest from data from Äspö (1 day) while breakthrough based on data from Grimsel lay in between (4 days).

Inspection of the retention curves reveals a similarity between Grimsel and Äspö granite in terms of pore size distribution while the Canadian rock is distinctly different in this respect. Since the Canadian and the European granites are located on different tectonic plates they may differ considerably with respect to genesis, composition and other possible factors influencing the pore space geometry. Contrary to that, permeability and porosity are almost the same for the Canadian and the Äspö rock while this data for the Grimsel granite deviates considerable. It can thus be concluded that breakthrough time for the model in question is much more dependent on the CEs than on permeability and porosity.

In series 1 the model descriptions followed the scheme suggested in the description of Task 8 (Vidstrand et al. 2017) where permeability and porosity values for Äspö granite was combined with the CEs for Grimsel granite. This procedure neglects the work of Leverett who found that the retention curve for similar rocks can be scaled according to permeability and porosity (Leverett 1941). Series 2 was thus concerned with scaling the CPS for models with non-Äspö CEs. It turned out that the scaled Grimsel CEs produced a rather similar breakthrough time to the original Äspö CEs in series 1. The results for the Canadian rock, however, were still way off (6 and 15 days) adding evidence to the conclusion from series 1 that the Canadian granite is structurally different from the European granites.

Series 3 looked into the generic approaches for the CEs namely the widely used formulations of van Genuchten (van Genuchten 1980) and the less favoured formulations of Brooks and Corey (Brooks and Corey 1964). The interesting difference lies in the way in which the capillary pressure is handled at high saturations. A retention curve after Brooks and Corey acknowledges the existence of an air entry pressure but it can lead to numerical difficulties while a retention curve after van Genuchten circumvents the numerical problems by letting the capillary pressure steeply dropping down to zero as full saturation is approached.

To allow a meaningful comparison the retention curve after van Genuchten was replaced by an equivalent retention curve after Brooks and Corey in the model with the scaled Grimsel CEs. This prolonged the breakthrough time by a factor of 3. In a second step also the RPS was replaced. This reduced breakthrough only by 20 %. The run of the retention curve at high saturations thus introduces significant differences in breakthrough time for the problem at hand. Also steepness and height of the saturation front are influenced by the choice of CEs.

If water and air coexist in the pore space the most difficult hydraulic quantity to measure is the relative permeability for water. Much easier is it to measure the retention curve, fit an approach for the retention curve to the data, and use the parameters to describe the relative permeability. However, usually it cannot be checked if this procedure is appropriate for a particular case.

This has led to the practice to vary the parameters for CPS and RPS independently from each other.[13] To investigate the consequences of this practice series 4 was concerned with exchanging the van Genuchten formulation for relative permeability with a power law that has been used modeling flow in the Äspö granite.

Obviously, the effect on the breakthrough time depends on the increase in relative permeability that comes with the switch of RPS. In case of the approach for the Canadian granite the ratio between the two RPS is considerable so a large acceleration of wetting the rock was determined (roughly by a factor of 50). The ratio for the van Genuchten formulation for Äspö granite was closer to the alternative power law amounted so only an acceleration by a factor of 2 was found. The choice of the RPS as well as the choice of the parameters for the RPS thus may have a strong impact on model calibration if the RPS are treated independently from the CPS. In the case investigated here even the curvature of the saturation distributions has changed the sign.

Series 5 confirmed what could already be suspected from the plots of the transient saturation distribution that progress of the water front slows down with time. This follows from the fact that the driving force, the capillary forces, remains more or less the same at the water front while resistance to flow increases with the progress of the water.

Series 6 demonstrated that grid convergence meaning the independence of numerical results from the mesh has almost but not quite been reached with the grid resolution used in this investigation. The ensuing error lay in the order of 13 % and is thus tolerable for the purpose at hand.

Having established that there is a similarity between the granites at Grimsel and at Äspö the models B, E, and F appear to be trustworthy to predict breakthrough time which was calculated as 22 h, 27 h, and 18 h, respectively, for a rock sample of 4 cm. The volumetric flow rates at breakthrough lie between 0.17 and 0.30 ml/d. Initially inflow may roughly be 10 times as high.

It should be noted here that these results formed the basis for designing an experiment at the geotechnical laboratory of GRS involving the wetting of dried disks of granite from Äspö. The disks used eventually in the experiments had only a length of 2 cm. However, no significant amount of water had passed through these disks within a time span of three weeks.

[13] So even if the referring formulations say of van Genuchten are used for a particular model it does not mean that a van Genuchten approach has been adopted in a strict sense.

Appendix D

Extraction of pressure boundary conditions

Atmospheric pressure was assigned to the surface of the drifts and boreholes in the models for Task 8. For the conditions on the outer surface of the model an excel-file with the results of a large-scale flow simulation for the HRL Äspö was provided with the task description. The relevant information about dynamic pressure, flow and salinity for the model could be extracted from this file. Note that dynamic pressure is defined here as the difference between absolute pressure and hydrostatic pressure. The data was given as pointwise information from the nodes of an irregular grid. The position of the nodes in space is depicted in Figure D-1.

Since no information about the connection of the nodes with their neighbouring nodes was given, the data could not simply be interpolated to derive values on the model boundary planes. Instead the following strategy – illustrated in Figure D-2 – was applied:

For each of the six boundary planes

- define the mathematical formula for the plane,
- find all nodes within a distance of Δl to the plane.

  For each of those nodes
  - find other nodes
    - o within a distance of 2 Δl,
    - o on the opposite side of the plane,
  - calculate coordinates for the interception of the connecting line with the plane,
  - interpolate the data for the interception.

The extraction process using a value of Δl = 20 m yielded enough data points to construct 2d-data fields in the six bounding planes. They are shown exemplarily for the dynamic pressure in Figure D-3. These planes had to be reduced to the boundary faces as indicated in Figure D-4. The whole model surface is shown in Figure D-5 including the interception of fractures as defined for Task 8b and the boundary faces.

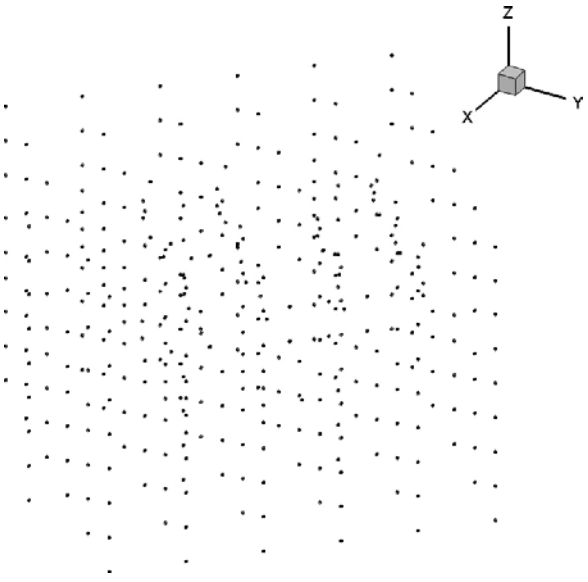

Figure D-1. *Location of the given nodes in space.*

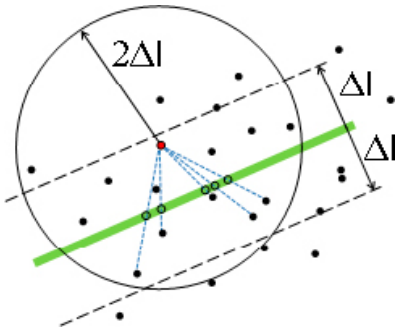

Figure D-2. *Extraction strategy for the boundary conditions.*

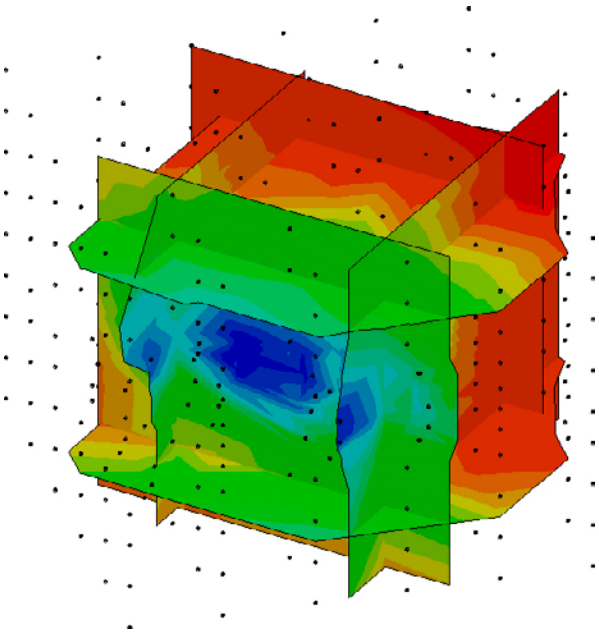

Figure D-3. *Six planes showing dynamic pressure.*

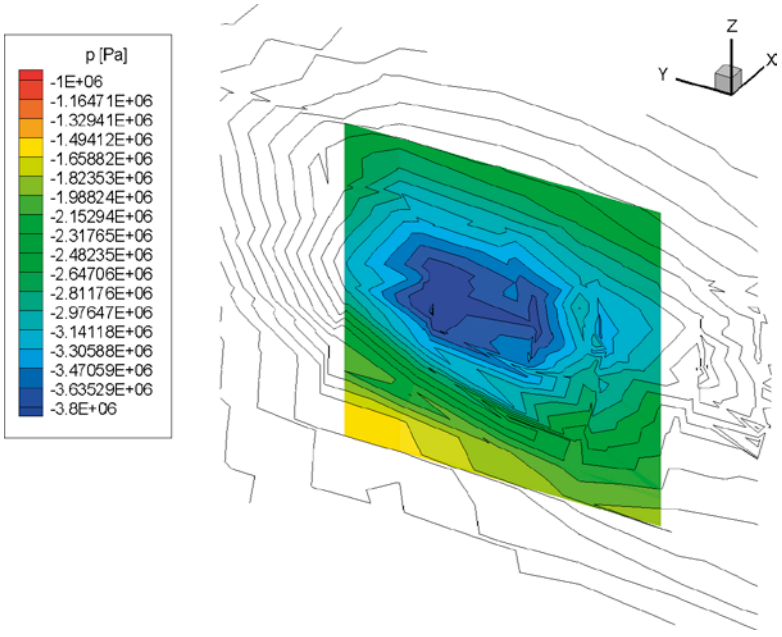

Figure D-4. *Clipping of a boundary plane.*

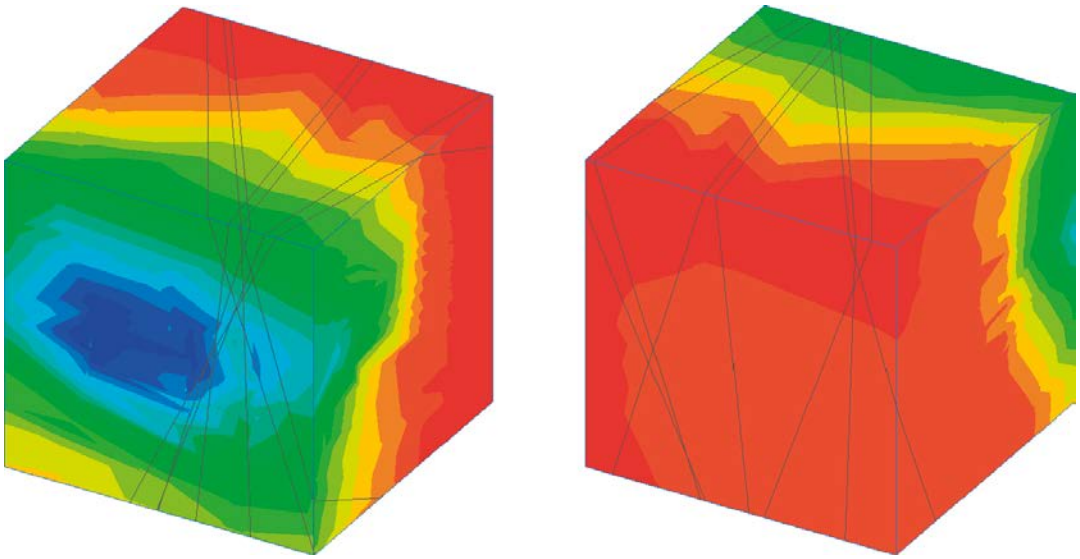

Figure D-5. *Dynamic pressure on the model boundaries.*

Figure D-5 shows a rather erratic pressure distribution that represents the original simulation results on this comparatively small scale probably quite poorly. Flow simulations based on these boundary conditions can be expected to show numerical difficulties and unphysical results.

On a larger scale, however, it shows also a certain pattern. It was therefore tried if the pressure distribution on the model boundary could be approximated by an analytical formulation. The quality of the approximation is depicted in Figure D-6, where the extracted data and the results from the analytical function can be compared.

$$p_{dyn} = \frac{d}{\left[\sqrt{(\xi + a)^2 + (\eta + b)^2 + (\zeta + c)^2}\right]^e} \tag{D-1}$$

p_{dyn} = dynamic pressure [Pa]
ξ,η,ζ = local coordinates [m] (q. v. (D-2))
a,b,c,d,e = constants (q. v. Table D-1)

$$\xi = \frac{1}{\sqrt{2}} x' + \frac{1}{\sqrt{2}} y' \tag{D-2}$$

$$\eta = -\frac{1}{\sqrt{2}} x' + \frac{1}{\sqrt{2}} y'$$

$$\zeta = z$$

x′, y′ = auxiliary coordinates [m] (q. v. (D-3))
z = vertical coordinate [m]

$$x' = x - 1\,551\,000 \tag{D-3}$$

$$y' = y - 6\,367\,000$$

x, y = horizontal RT90-coordinates [m]

Table D-1. Constants for Equation (D-1)

a	b	c	d	e
165	−926	413	−14 000 000	0.7

Note that the pressure distribution of the original simulation does apparently account for the influence of the open TASD-tunnel and the fractures only rather loosely. The boundary conditions with respect to pressure would therefore have been to be modified to avoid unrealistic flow rates. However, this development was later dropped in favour of the inverse distance weighing for the extracted data from the large-scale model.

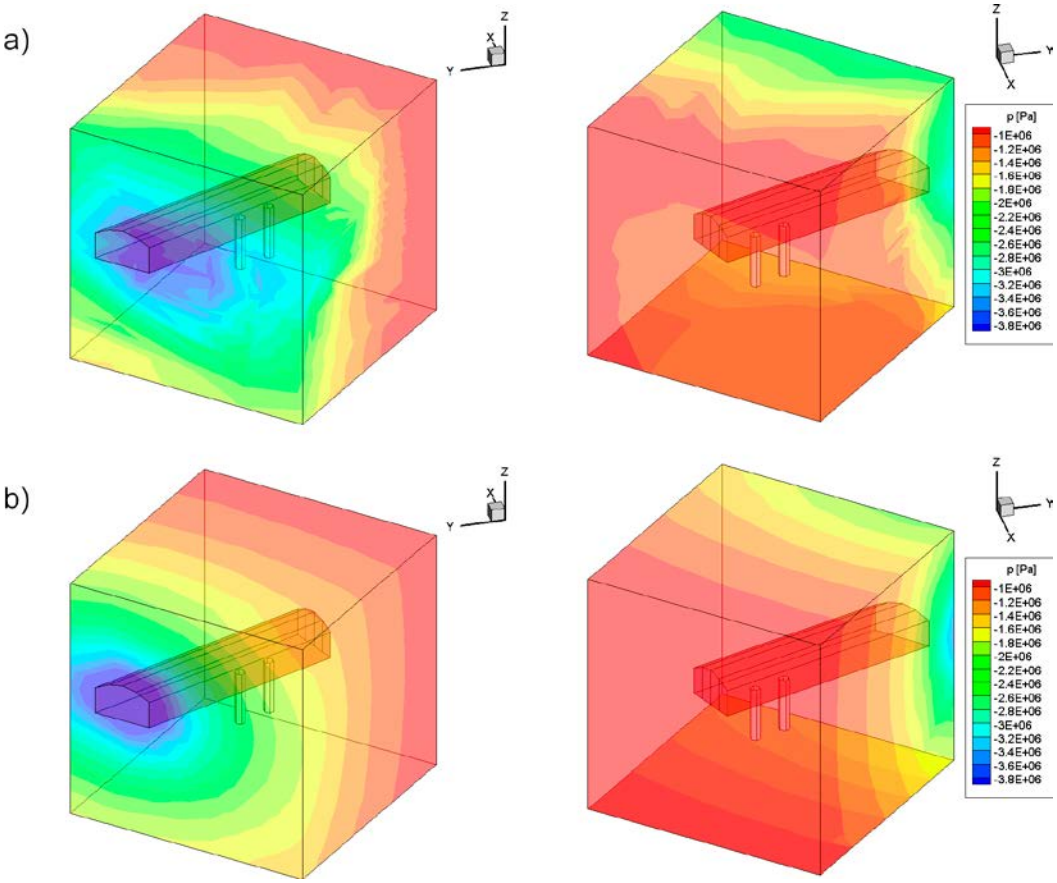

Figure D-6. *Comparison of the pressure distributions at the model boundary. a) from extracted data and b) from results of the analytical function.*

Appendix E

Evidence for the skin effect

Flow data from the Task 8c model concerning the outer boreholes (KG0018G01 and KG0020G01) were too high. A possible solution was seen in the option to include a skin-like narrow rock zone with reduced permeability around the geotechnical openings. Such a skin has been used time and again when calibrating of a flow model required a reduction of outflow rates. Used without any justification other than meeting a calibration target devalues such a model to a large extent. Without a physical explanation for this skin it is impossible to predict the reaction under different conditions. Skin as a sole concept is therefore no physical explanation of the observed phenomena but only means to meet the hydraulic data for a given flow problem.

The idea of the existence of such a skin appears to be rather widely spread among the fractured rock modeling community. Two examples corroborating the concept with observations from the field – namely Stripa (Olsson et al. 1992) and Äspö (Kull et al. 2002) – are described here shortly. It has to be noted though that the reasons for flow reductions close to tunnel and borehole walls are not pinpointed yet.

In Olsson et al. (1992) the Validation Drift Experiment at the Stripa mine in Sweden is described. From the face of the so-called "Validation Drift" six boreholes labeled "D boreholes" were drilled over a length of 100 m in the direction of the drift as depicted in Figure E-1.

Outflow from the rock flow into packered intervals of the boreholes was measured. After a certain period of time the Validation Drift was extended by 50 m (see Figure E-2) and outflow measurements at the new drift walls was repeated.

It was found that "The relative reduction in flow to the drift was greater for the 'averagely fractured rock' which was reduced by roughly a factor of 40 while flow through the fracture zone H was reduced by a factor of 8." As in the model of the BRIE-site total outflow was dominated by the fracture zone.

Furthermore, "Another significant observation concerns the high pressures which are generally observed close to drifts in the Stripa mine. For example, the water pressure in the H zone 10 to 20 m away from the drift … was 197–199 m, with no evident variation with distance. High pressures (160–180 m) were also observed within 10 m of the 3d-migration drift in the sealing experiments … and in the Macro-permeability experiment …". However "There are few exceptions …". It was therefore concluded that "High pressures are frequently observed close to drifts and indicate that a low permeability skin commonly occurs around drifts in the Stripa mine." (Olsson et al. 1992).

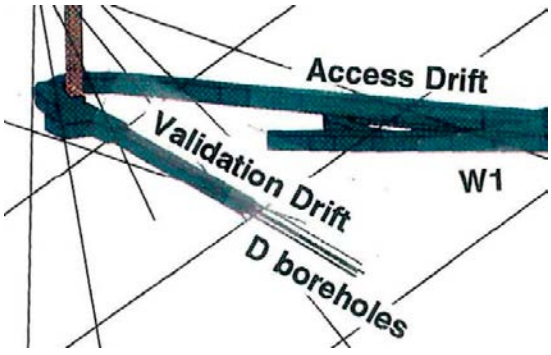

Figure E-1. *Setup of the Validation Drift Experiment; from Olsson et al. (1992).*

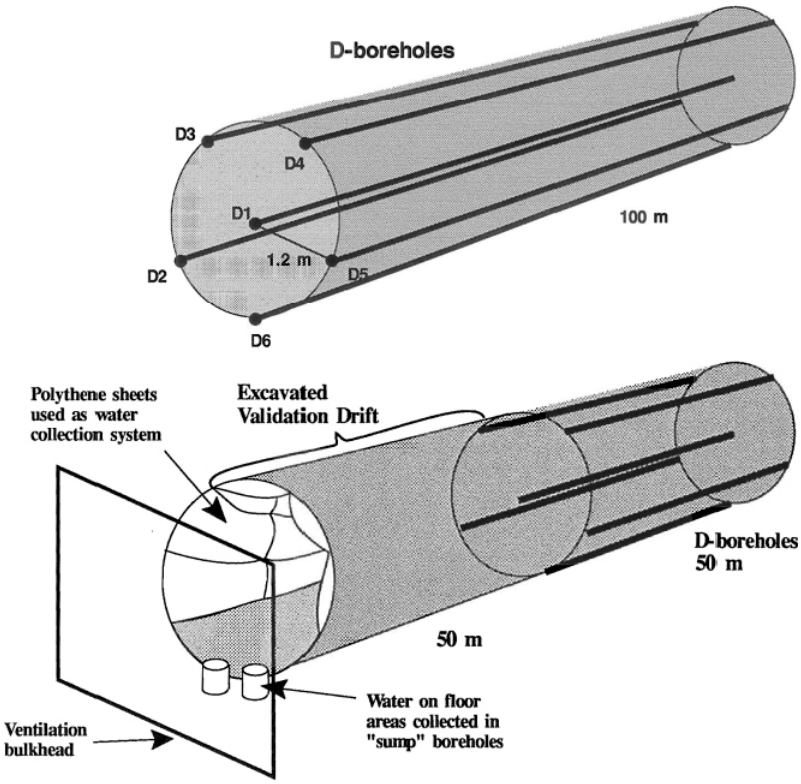

Figure E-2. *The two phases of the Validation Drift Experiment; from Olsson et al. (1992).*

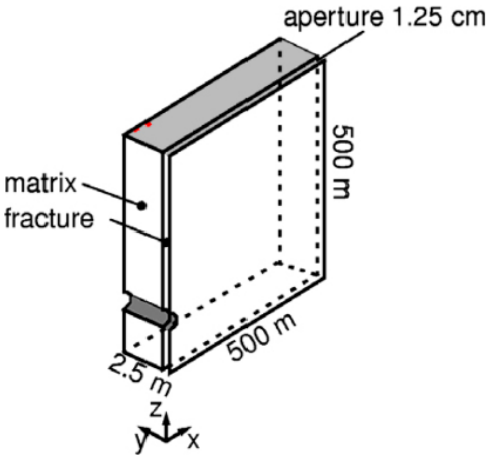

Figure E-3. *Principal sketch of the single-phase model; from Kull et al. (2002).*

Similar evidence for a low permeability skin was produced about 10 years later in the course of the Two-Phase-Flow Experiment at the Äspö HRL (Kull et al. 2002). It had been conducted in a fracture located at niche 2715 – see principal sketch in Figure E-3. In preparation several boreholes had been drilled to measure the undisturbed hydraulic pressure as shown in Figure E-4. A numerical single-phase flow model was then set up based on these data to provide the initial conditions for a two-phase flow model.

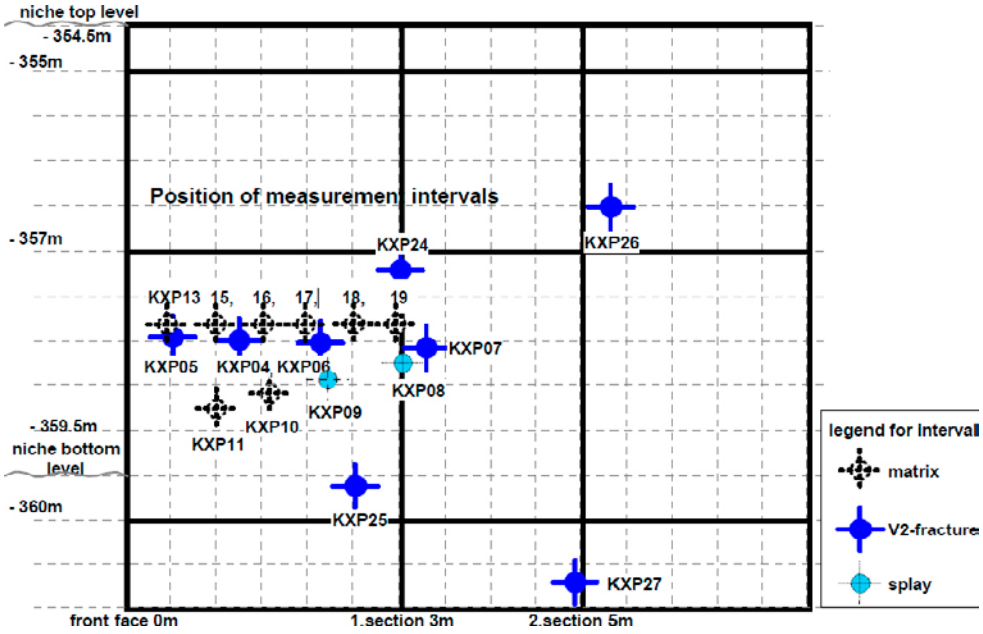

Figure E-4. *Setup of the Validation Drift Experiment; from Kull et al. (2002).*

The data showed an unexpected high pressure of about 1.8 MPa beyond a distance of approx. 1 m from the niche wall which remained almost constant over the following 4 metres that were investigated (see Figure E-5). In the framework of the single-phase flow model it was not possible to reproduce the abrupt pressure change with a homogeneous permeability distribution. "The most simple explanation … was the assumption of a narrow zone – probably less than one metre in thickness – surrounding the niche. This zone would have to be hydraulically much tighter than the neighbouring area …" (Kull et al. 2002). A permeability contrast of two orders of magnitude between the skin-zone and the adjacent zone lead to a good fit of measured and calculated pressure values which is also shown in Figure E-5.

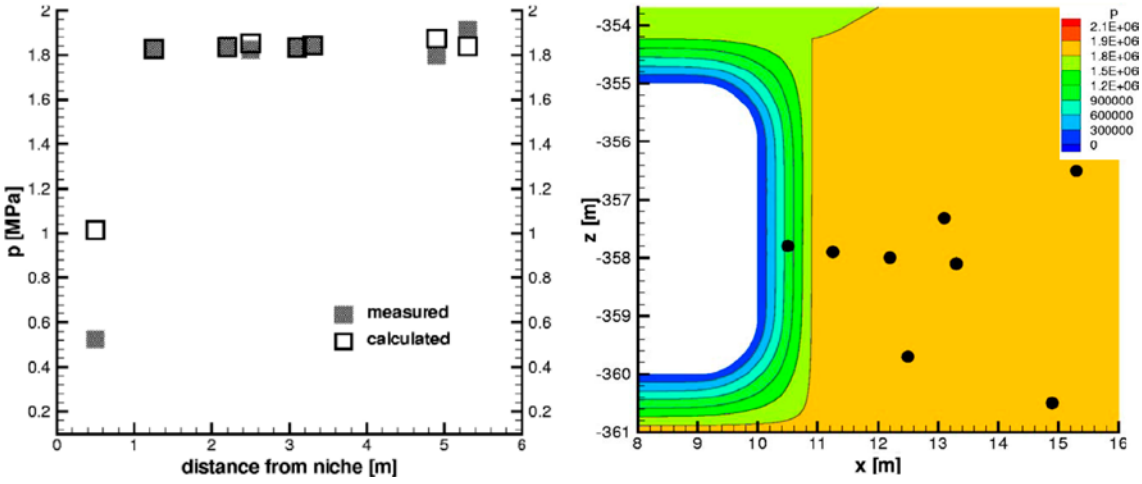

Figure E-5. *Measured and calculated pressure; from Kull et al. (2002).*

Several possible physico-chemical explanations for the low permeability skin were considered during the Drift Validation Experiment and discussed in Olsson et al. (1992):

- **Stress effects**
  Increase of normal stress on a fracture plane can cause a reduction of fracture transmissivity. Excavating a drift changes the stress field around the drift. Fractures being hit perpendicular to the drift should therefore not be strongly affected. However, 2d-HM-modelling of drift excavation showed high tangential stresses around the drift that closed "near radial" fractures intersecting the drift.
- **Shear displacement due to excavation**
  Excavation causes displacements towards the opening. In the presence of significant normal stresses to the fracture movement of one fracture wall relative to the other (shear displacements) could cause a reduction of transmissivity which are reported to account for a factor of 1/5 to 1/10.
- **Blast damage and dynamic loading**
  Several effects are related to blasting:
  - Creating new fractures preferentially in radial direction from the blast hole. As new pathways for water from the rock are formed this process would have the opposite effect to flow reduction.
  - Gases generated by blasting (mainly CO_2, water vapour and N_2) are forced into the fractures. As the gases would be flushed out of the fractures with time this process would only account for a temporary reduction. Reductions in the field had been observed for more than a year and remained "nearly constant" during this time.
  - Generating compressional and shear waves propagating through the rock. Related rapid displacements and increases in stress.
  - Fine-grained particles may be shaken loose and subsequently partly clogging the pathways for the water.
  - Debris from drilling the blast holes may be forced into the fractures blocking pathways for water flow.
- **Degassing and two-phase flow**
  Dissolved gas in the groundwater at Stripa (mainly nitrogen) was present at conditions that would lead to bubble forming at water pressures below 0.6 bar. These bubbles may form an impediment for water flow where pore diameters or fracture widths are small enough to keep the bubbles in place due to a sufficiently high capillary pressure. In the wider flow channels bubbles were expected to be carried away with the flow, accordingly. At steady-state a dynamic equilibrium would be reached where the gas flux via bubbles equals the amount of gas changing from dissolved state to a separate gas phase.
- **Chemical precipitation**
  Mixing of groundwater of different origins could lead to an oversaturation with respect to calcite at Stripa which made precipitation seem possible. This appeared to be contradicted by several observations in the field (Olsson et al. 1992).

The conclusion from the extensive discussion was that not just one process would be responsible for the observed flow reductions. While the effect of degassing could not be quantified at that time it was nevertheless considered to be a major contributor. Considerations on the pore scale were consistent with the observation on macro-scale that flow reduction was much more pronounced in the matrix than in the fracture. But also the different mechanical effects were thought to be relevant.

The evidence presented here indicates that a skin-like zone has to be considered in a single-phase flow model to account for the phenomena of flow reduction and pressure drop in the immediate vicinity of drift walls. This refers to the matrix as well as fractures opened by the drift. The observations suggest a skin thickness of one metre and a permeability decrease of 1 to 2 orders of magnitude.

There is apparently no information about the skin effect with respect to boreholes concerning size and strength of the effect. If degassing was the reason it can be speculated though that the permeability reduction would be greater in case of a borehole than in case of a drift wall. The curvature of the contour is much higher in a borehole than at the drift wall. Streamlines towards the contour of a borehole are converging faster than in case of a drift. The related pressure decrease is therefore more localized at a borehole. Due to the higher pressure gradient the effect of degassing becomes more localized and leads to a more effective impediment to water flow.

Appendix F

Advancing the boundary condition of VIPER

F1 Model concept for unrestricted access to water

Extending the model for water uptake of the buffer to re-saturation under restricted access to water requires insight into the conceptual background for the formulation of boundary conditions. The conceptual model behind code VIPER had been developed under the assumption that the bentonite in the immediate vicinity of the water-bearing rock fully re-saturates within a negligible amount of time. Later on, a dynamic equilibrium is formed between water migrating through the saturated zone and evaporation at the water-air interface in the pore space that feeds the diffusive vapour flux in the pore atmosphere. Parallel to that, the diffusive flow of interlamellar water also takes place. This concept is sketched in Figure F-1.

The fully water-saturated zone has a thickness of a few millimetres only[14] and is therefore not considered in the model. The boundary of the re-saturation model is consequently characterized by 100 % relative humidity in the pore space and the maximum water content of hydrated water. Such a boundary condition is conceptually rather simple and also easy to implement in a numerical model. It requires, though, that enough water is provided from the rock to keep up the narrow fully saturated zone. In other words inflow from the rock must be at least as high as the initial diffusive vapour flux at the location of evaporation.

F2 Model concept for restricted access to water

The concept for the originally adopted model boundary described in the previous section did not apply totally to the situation at the BRIE-site. The comparison of water outflow from the rock and water inflow into the bentonite (cf. Section 3.4.2) showed that the bentonite would demand more water than was freely accessible. In this case a constant flux density relating to the maximum outflow from the rock that is lower than the fluxes from the diffusive migration processes in the bentonite must be considered. This called for a modification of the implemented boundary condition.

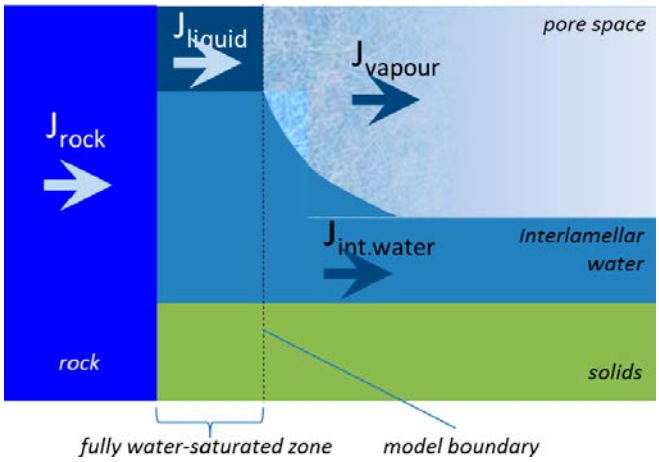

Figure F-1. *Model concept for re-saturation under unrestricted access to water.*

[14] For a more detailed discussion of the model concept see Kröhn (2011).

It is assumed here that all the water coming from the rock is taken up by the bentonite but inflow is not sufficient to build up the narrow fully saturated zone described in the previous section. Even if the bentonite hydrates immediately at the bentonite-water contact, the inflow is just sufficient for a partial water saturation. As all water coming from the rock is transported away from the bentonite-water contact a simple conditional equation holds

$$J_{rock} = J_{vapour} + J_{\mathrm{int}.water} \tag{F-1}$$

J_{rock} = water flux from the rock [kg/(m^2 s)]
J_{vapour} = diffusive flux of vapour into the benonite [kg/(m^2 s)]
$J_{\mathrm{int}.water}$ = diffusive flux of interlamellar water into the benonite [kg/(m^2 s)]

The two fluxes in the bentonite are defined as

$$J_{vapour} = -D_v \cdot \nabla \rho_v \tag{F-2}$$
$$J_{\mathrm{int}.water} = -\rho_d D_i \cdot \nabla w$$

D_v = vapour diffusion coefficient [m^2/s]
ρ_v = vapour partial density [kg/m^3]
ρ_d = bentonite dry density [kg/m^3]
D_i = diffusion coefficient fort he interlamellar water [m^2/s]
w = water content oft he bentonite [kg/kg]

Adding both equation results in one equation with two unknowns, vapour density and water content

$$J_{rock} = -D_v \cdot \nabla \rho_v - \rho_d D_i \cdot \nabla w \tag{F-3}$$

At this point it is not clear to which parts the water from the rock is divided into vapour flow and diffusion of interlamellar water. As a quick workaround the following procedure was installed. Instead of formulating appropriate Neumann boundary conditions with a priori unknown flow rates, a related set of boundary values for vapour density and water content was sought that would lead to the required gradients at the boundary and thus to the required inflow rates. Effectively, equivalent Dirichlet boundary conditions were formulated.

Finite differences for the differential expressions $\nabla \rho_v$ and ∇w at the boundary are introduced that are compatible with the finite element formulation applied in the framework of VIPER. As an explicit scheme is used for solving the differential equations numerically this provides an equation containing the looked for boundary values

$$\rho_v = f(w, J_{rock}) \tag{F-4}$$

Introducing the adsorption isotherm

$$w = g(\rho_v) \tag{F-5}$$

eliminates one of the unknowns

$$\rho_v = f(w(\rho_v), J_{rock}) \tag{F-6}$$

making this an implicit equation which is quickly evaluated iteratively. The resulting vapour density can then be used as a Dirichlet boundary condition for the next time step.

The bentonite at the boundary gets increasingly saturated with time in order to maintain the density gradient at the boundary and thereby the prescribed inflow J_{rock}. The boundary values must therefore be updated after each time step. The adjusting Dirichlet boundary condition is thereby mimicking the actually required Neumann boundary condition.

Given enough time the value for the adjusting Dirichlet boundary condition can reach full saturation. This is equivalent with the condition of free access to water. At the boundary the code switches then back to a constant boundary condition according to full saturation.

Appendix G

Questionnaire about model uncertainty

The questions were arranges in topical sections. The topics are printed in bold, the questions in italics. Statements added later for further clarification and were thus not submitted with the questionnaire are printed in blue.

G1 True system, reified model, and actual model

G1.1 True system

Describe in detail current system understanding, including hydrogeological features, processes, and conditions that are considered relevant to understand and predict the behaviour of the host rock, bentonite, and interface between them.

Basic observations

Compacted air-dry bentonite is a material ready to take up water at any rate up to a certain limit. This limit depends on the degree of saturation in the vicinity of the bentonite-rock contact.

The rock matrix is fully saturated except for an unsaturated zone adjacent to the borehole wall where evaporation removes water from the rock. The fact that the unsaturated zone has a depth of only a few centimetres in case of the BRIE suggests that evaporation and flow of pressurized water from the rock are in equilibrium because vapour diffusion is a rather fast process. Larger fractures, in contrast, produce an outflow of liquid water. In the following only the two hydraulically bounding cases for the rock of a rather tight matrix and of water producing fractures will be looked at.

Rock as well as bentonite is regarded as a porous medium. One of the few differences to a common layered soil system is the ability of bentonite to swell. While swelling under confined conditions primarily just reduces the porosity it changes the flow system a little bit by also swelling into the pores and fractures of the rock. However, it has been shown that this effect affects even larger fractures only on a centimetre scale so that much less influence can be expected on the pores of the matrix.

The second difference is that layered soil systems develop extremely slowly while the bentonite-rock system is created almost instantaneously. As a result, the air in the unsaturated zone at the borehole wall becomes entrapped. This is of no real consequence as long as there is also a connected air-filled porosity in the bentonite. In this case air from the unsaturated zone in the rock can be hydraulically squeezed out into the bentonite. Keeping in mind that the porosity contrast between the freshly installed bentonite and the granite amounts to more than an order of magnitude and that the unsaturated zone in the rock reaches only a few centimetres into the matrix the air from the rock would hardly change the gas pressure in the bentonite if it were transferred instantaneously.

In the framework of GRS' view of bentonite re-saturation there is a thin fully saturated zone in the bentonite at the bentonite-rock contact. This zone develops under sufficient water supply in a matter of minutes and its permeability is very low. Experiments with MX-80 under 6.5 bar hydraulic pressure have shown that after 3 minutes there is virtually no difference in the uptake behaviour whether it takes place under atmospheric pressure or increased hydraulic pressure. Only the saturated zone increases a bit. Beyond this zone only diffusion processes take place: vapour diffusion in the pore space and diffusion of interlayer water in the interlamellar space.

How extrusion of wetted bentonite into the fracture fits into this picture is presently unclear. Intuitively, it can be assumed that the dry density of the extruded bentonite in the fracture decreases with distance from the buffer and is thus posing less of a hydraulic impediment to flow in the fracture than in the compacted buffer. So the assumption might be justifiable that the extruded material can be seen either as an extension of the fully saturated zone in the buffer or as a sort of displacement of this zone into the fracture to an unknown extent. As a result the location of the water-air interface might shift for a few millimetres. This effect should be much less pronounced, though, in the pores of the matrix since the pore radius is substantially lower than the aperture of significantly water producing fractures. It can thus be expected to be negligible at the buffer-matrix contact.

Skin effect

Reduction of flow and transport of solutes from granitic rock across the surface of excavated drifts or drilled boreholes has been observed on different occasions. A generally valid explanation, though, has not been agreed on yet. Several mechanisms have been brought forward, among them

- changes in the pore geometry due to stress redistribution after excavation/drilling,
- sustained unsaturated flow due to degassing,
- local inhomogeneities in a sparse fractured rock,
- dewatering,
- clogging with very fine-grained excavation dust/rock flour.

The influence of these different mechanisms on the flow field is quite different regarding long-term evolution or increased temperatures. It is thus that a true system in the sense of this section cannot be defined at this point as the nature of the skin is still unclear.

Two basic flow scenarios

The hydraulic interplay of rock and bentonite depends on

- the considered flow regime in the rock meaning matrix or fracture because of the high contrast of flow rates, and
- the degree of saturation in the bentonite controlling the demand of water from the rock.

These differences can be abstracted to two principle flow modes in the buffer-rock system. Which one applies is controlled by a ratio r between the flow rates of water from the rock and the demand of the bentonite buffer for water.

In the very beginning of re-saturation the bentonite takes much water up in a rather short period of time. It can safely be assumed that the rock matrix with a permeability in the order of 10^{-20} m^2 cannot provide sufficient amounts of water fast enough to satisfy the demand of the bentonite. Outflow from the rock is thus lower than the potential uptake of the bentonite and ratio r is lower than 1 which will be referred to further on as mode or phase A. Note that up to now bentonite re-saturation has not been tested in the laboratory under these conditions. Mode A is thus highly interesting because no experimental evidence exists for the case of limited water supply in terms of flow rates.

The demand of water from the bentonite decreases with time, though. Assuming that water flow in the rock remains to be at quasi-steady-state as long as mode A applies ratio r exceeds the value of 1 after a certain period of time. More water is then offered by the rock than demanded by the bentonite reaching a phase of unrestricted water supply as far as the bentonite is concerned. This will be called mode or phase B further on. Flow in the bentonite-rock system comprises generally a phase in flow mode A at the beginning and later on a phase in flow mode B.

Flow mode A without flooding of the gap

During phase A water from the rock is taken up as it comes. An issue is the narrow unsaturated zone at the borehole wall, though. After installing the air-dry bentonite there is no ventilation anymore and thus a relative humidity prevails at the bentonite-rock contact that is controlled by the local water content. Vapour is therefor still drawn from the rock which continues to impede progress of the groundwater toward the buffer.

In case of the BRIE the initial water content of the bentonite was in equilibrium with a relative humidity in the pore space of about 60 %. Humidity in the TASD tunnel ranges between 65 % and 85 % due to seasonal changes. In the boreholes it might have been a little higher. Vapour flow from the water-air interface towards the borehole wall was therefore hardly influenced by the emplacement of the bentonite parcel, possibly even a little increased. Without impediment of outflow from the rock the whole flow field in the rock has initially been undisturbed by the installation of the bentonite.

It can be further speculated that without flooding of the gap between the parcel and the borehole wall the water uptake of the bentonite would have taken place via vapour diffusion for quite some time during which swelling of the bentonite would have filled the gap. Due to the much higher porosity of the bentonite than that of the rock the vapour flux density at the ensuing bentonite-rock contact is lower in the bentonite than in the rock thereby reducing the relative humidity across the contact plane, thus decreasing the gradient of the vapour partial density and resulting in a comparatively low re-saturation rate.

The water content of the bentonite close to the borehole would have risen continuously further on as well as the related relative humidity due to the continuing vapour flow from the rock. However, this relative humidity at the contact plane poses also a boundary condition for the vapour transport in the rock and an increase at the borehole wall means a decrease of vapour flow in the rock. Water uptake via vapour thus throttles the vapour flux feeding the uptake until liquid water reaches the borehole wall and can be taken up directly.

The air from the unsaturated zone in the rock is then slowly squeezed out by the progressing water front into the still unsaturated bentonite. Upon reaching the bentonite the water is drawn into the bentonite by suction. However, only limited tensile stresses can be borne by water. At a temperature of 14 °C – the one that prevails in the rock at the BRIE-site – the vapour saturation pressure amounts to 0.16 bar. Below that vapour evolves from the liquid phase and interrupts the continuous water phase.

Hydraulic pressure at the bentonite-rock contact thus cannot fall below 0.16 bar. This means that the influence of suction from the bentonite on the overall flow field in the rock is very limited as the undisturbed hydraulic pressure in the rock driving the flow amounts to approx. 4 MPa. As long as flow mode A prevails water is simply drained from the rock keeping the hydraulic pressure at the borehole surface somewhere close to atmospheric pressure. The outflow rate of liquid water from the rock which is then also the uptake rate of the bentonite remains more or less constant during phase A.

Flow mode A under BRIE conditions

In the actual test, though, the one millimeter gap between bentonite and rock was flooded with water. Since flooding was quick in comparison to flow in the rock this procedure temporarily entrapped the air in the unsaturated zone of the rock more or less instantaneously. By raising the humidity at the buffer-rock contact to full saturation this stopped also the vaporous water migration through the unsaturated zone. With no loss of water at the water-air interface this interface then started to move towards the borehole wall thereby compressing the entrapped air.

Meanwhile the water from the flooding had entered the bentonite and let is swell rather quickly until it filled the gap. Assuming that the pore volume of the bentonite adjacent to the gap would be fully filled up with the water from the flooding it could reach only 4 mm deep into the bentonite as the initial porosity of the bentonite amounted to about 25 %. After the relatively fast uptake of water from the gap interlamellar water as well as water vapour started to migrate inside the bentonite from the fully saturated zone towards the axis of the bentonite parcel due to the radial differences in water content and relative humidity.

What happened next depends on microstructural developments during the ensuing re-distribution process that are not well known but can be scientifically guessed. While the gas pressure increased in the rock the water in the saturated zone of the bentonite started to migrate away from the bentonite-rock contact thus starting to vacate the pore space in the bentonite again. It is envisaged that at a certain point during this development the entrapped gas in the rock could escape into the bentonite parcel where it mixed with the gas of the unsaturated bentonite. As the porosity of granite is much lower than the bentonite porosity it is assumed that the additional gas from the rock does not change the gas pressure in the bentonite significantly. Water from the rock would further migrate towards the bentonite as described in the previous section from then on. When the saturation front in the rock reached the bentonite either flow mode A or B could apply. In case of mode A suction from the bentonite had most likely exerted tensile stress in the pore water of the rock to the extent that the hydraulic pressure fell below vapour saturation pressure thus partly re-establishing the previously

prevailing unsaturated conditions in the rock. Movement of the saturation front is thus expected to have undergone cycles of slow advancement of the saturation front followed by a very quick retreat into the rock again until the pore air was terminally trapped between the pore water in the rock and the developing saturated zone in the bentonite. However, development of a saturated zone indicates the switch from flow mode A to mode B.

Flow mode B

Sooner or later the flow mode switches from A to B. In case of strongly water producing fractures the system might also start directly in mode B. When this happens water accumulates in the bentonite at the bentonite-rock contact and forms a thin fully saturated zone. This is confirmed for bentonite samples in case of unrestricted water uptake right from the beginning and is also assumed (for lack of deeper insight) to apply if the flow mode switches from A to B. The permeability of this zone is so low that it renders advective flow beyond this zone impossible leaving only vapour diffusion in the pore space and diffusion in the interlamellar space as possible migration processes.

Water flow across the bentonite-rock contact is now controlled by the demand for water by the bentonite which in turn is a function of the total water flow at the water-air interface inside the bentonite. Since this flow rate is lower than the potential outflow from the rock at atmospheric conditions, the bentonite acts as an impediment to flow from the rock so that hydraulic pressure builds up in the rock at the bentonite-rock contact.

Processes involved

For a certain period of time there are two flow domains in the rock depending on the distance to the bentonite-rock contact. In the outer domain the only relevant hydraulic process is pressure driven single-phase Darcy flow. Closer to the contact and shortly after installation of the buffer this changes to two-phase two-component flow including evaporation at the water-air interface and a possible phase change of dissolved gases. Since the buffer poses an increasing impediment to outflow from the rock the hydraulic pressure in the rock increases and the unsaturated domain shrinks until it vanishes. Dissolution of the residual gas and diffusion into the matrix come at the end of this development.

As long as rock and bentonite are unsaturated the gas phase is continuous across the bentonite-rock contact. Water leaving the pore space of the rock and entering the pore space of an unsaturated bentonite is in contrast quickly adsorbed in the interlamellar space of the clay particles. This process is called hydration and leads to swelling of the clay particles. Since the space for the buffer can be considered to be confined the swelling reduces the pore space of the bentonite.

Most of the water in the bentonite is hydrated in the interlamellar space or adsorbed at the surface of the clay particles. Only a very little fraction of water remains in vaporous form in the open pore space of the bentonite. The mass of hydrated water and the mass of water vapour are related by an isotherm. Local changes of the water content are thus reflected in a varying relative humidity in the pore space.

Binary diffusion of water vapour and air in the pore space as well as a diffusive spreading of the interlamellar water are the main water migration mechanisms in the bentonite.

Depending on the rate of water outflow from the rock this situation can prevail for some time which would relate to flow mode A. In case of flow mode B the bentonite becomes fully saturated at the bentonite-rock contact. In the evolving thin fully saturated zone, the interlamellar space as well as the pore space is completely water-filled thus excluding diffusive processes in this zone. However, suction at the water-air interface inside the bentonite would still draw a certain amount of water into the bentonite that could be moving by advection towards this interface. Evaporation at the water-air interface leads finally to the same conditions as at the bentonite-rock contact in flow mode A, meaning that gas diffusion and diffusion of interlamellar water take over from there.

Swelling of the bentonite exerts pressure on the bentonite as well as on the surrounding rock. If the skin effect proves to be caused by redistribution of mechanical stresses this might influence the hydraulic conditions in the rock.

Interface and transition zone

The descriptions given so far indicate that there is no real two-dimensional interface between rock and buffer. What can be found, though, are several more or less thin transition zones located at both sides of the bentonite-rock contact. In the rock there is the unsaturated zone either from previous evaporation or from degassing. Additionally, there might be significant changes in the pore space geometry due to stress redistributions after excavation. In the bentonite another thin zone is formed if water outflow from the rock is sufficiently rapid (flow mode B). This leads to a thin fully saturated zone at the bentonite rock contact beyond which the diffusion processes take over.

So in a sense there is a bentonite-rock interface between the domain of single-phase flow in the rock and the diffusive migration processes in the bentonite. It has a small but finite extension and the thickness as well as the influence on the flow system is transient. It is therefore rather called a transition zone here.

Coupling of flow domains

The discussion about flow modes suggests that flow in the rock and flow in the bentonite can be seen as rather loosely coupled processes. In case of flow mode A the flow field in the rock does not change significantly from the conditions before installation of the buffer while water uptake of the bentonite is controlled by the outflow rate from the rock. During flow phase B the rate of flow across the bentonite-rock contact is controlled by the demand for water by the bentonite which is then less than the rock can provide. The buffer becomes therefor an increasingly effective impediment to outflow from the rock.

G1.2 Reified model

Describe a hypothetical model that best represents the true system behaviour, specifically model features that are considered influential.

As pointed out in the previous section, not all aspects are known in sufficient detail that knowledge of the “true behaviour” can be claimed. Deriving influential model features thus becomes easily speculative.

In general the flow mechanisms in the rock and in the bentonite appear to be rather simple and clear: single-phase flow in the rock and diffusion of vapour and interlamellar water in the bentonite. However, since fluxes across the bentonite-rock contact play a significant role in the interplay between rock and buffer the properties and the behaviour of the transition zone are of high interest. Unfortunately, this zone includes the influence sphere of the skin effect with its hardly known true impact on the mechanical and hydraulic system. This concerns the immediate effects as well as their long-term evolution.

G1.3 Actual model

Describe in detail the features, processes, and conditions implemented in the actual model used to predict the behaviour of the repository subsystem, including assumptions, simplification, limitations, restrictions and constraints.

The actual model consists of two separate parts, one part dealing with the flow in the rock and one part taking care of the bentonite re-saturation.

Flow in the models takes place in a piecewise homogeneous, isotropic 3D-continuum that is interrupted by the geotechnical openings (drifts and boreholes) as well as three large discrete fractures which in turn represent lower- or equal-dimensional continua (depending on the grid resolution in the model). The effect of background fractures on the flow field is accounted for by an increase of the matrix permeability. Around the geotechnical openings the model includes a flow impeding skin zone in which the permeability of the large discrete fractures as well as the rock matrix is reduced. The thickness of the skin around the drifts amounts to about 1 m and round the boreholes to about one borehole radius. The highly heterogeneous outflow rates into the probing and test boreholes are believed to be caused by background fractures intersecting the boreholes. To account for the resulting differences the

permeability of some borehole skins is lowered by one order of magnitude. The steady-state single-phase flow is controlled by the pressure at the boundaries which is either interpolated between pointwise data from a large-scale flow model or assigned to be atmospheric at the boundaries of the tunnels and the open boreholes where applicable. The wall of sealed-off boreholes was considered to be a no-flow boundary.

Bentonite re-saturation is calculated with a 1D-radially symmetric model representing a disk-like section at mid-height of the test boreholes. The model physics comprise vapour diffusion in the pore space, diffusion of interlamellar water and instantaneous hydration as a coupling process between the two diffusive migration processes. Water flux from the matrix was found to be quite low making flow mode A applicable where the outflow rate from the flow model was used as a boundary condition. Flow from single productive fractures was simulated according to flow mode B. After it became clear that there was no horizontal fracture crossing the test boreholes the axisymmetric geometry was not appropriate anymore. As a rough approximation a model with a constant cross-section was used instead.

G1.4 Alternative model

Describe alternative conceptual models considered viable to explain and predict true system behavior, or to question or disprove the hypotheses examined with the actual model.

The transition zone including the skin is not really understood. Almost any model can thus be calibrated to account for the observed data. Discussing viability of conceptual models appears to be ambitious considering that the physics of the true system are not known yet.

G2 Input and prior uncertainties

G2.1 Prior uncertainties

Describe and – if possible – quantify the state of knowledge or uncertainty about features that are included or excluded from the actual model.

Included features

- **Single-phase flow in the rock including the network of background fractures**

  Bordering cases for the permeability of the so-called undisturbed rock can be found in the laboratory. The uncertainty lies in the range of at least ± one order of magnitude. If merged with the network of background fractures, though, this uncertainty is insignificant in case of the BRIE because the effective permeability is dominated by the background fractures. Their true hydraulic behaviour can only be tested in the field.

- **Single-phase flow in the large deterministic fractures**

  Requires also hydraulic testing in the field. Uncertainties arise from possible inhomogeneities in the fracture as well as from size or, if intersected by model boundaries, by the boundary conditions.

- **Increased flow resistance in the skin around the geotechnical openings**

  While the effect on flow into a drift as well as the influence sphere in the rock can be quantified loosely by observation the same is largely unknown for boreholes with a small diameter. Due to a lack of a reliable physical explanation this effect is particularly difficult to quantify.

- **Vapour diffusion in the pore space of the bentonite**

  The process itself can be considered to be common knowledge. The effect on bentonite re-saturation is fairly well understood by means of measurements of uptake from vapour-saturated air.

- **Diffusion of interlamellar water**

  Accuracy of related data from the literature cannot be evaluated.

- **Instantaneous hydration according to the isotherm/retention curve**

  This hypothesis might be not correct as it takes quite some time in the laboratory to reach an equilibrium between water content and relative humidity. This is already known to be the case with the retention curves for common soils. A final word on that matter is still pending.

Excluded features

- **Discrete description of flow in background fractures**

  That would require the network geometry which is only known in terms of statistics.

- **Unsaturated flow**

  Would have made sense with a good grip on the constitutive equations for capillary pressure and relative permeability. Otherwise almost anything can come from a model even with only slightly wrong mathematical models.

- **Degassing**

  Since degassing is a consequence of a drop in hydraulic pressure the flow field must be known to a rather high degree of accuracy so the comments on unsaturated flow apply here as well.

- **Mechanical effects in the rock**

  No really good idea about mechanical influence on flow. Included as the skin if applicable at all.

- **Mechanical effects in the bentonite**

  Laboratory tests have shown that the displacement of clay particles due to swelling is rather little under confined conditions and can thus be neglected.

- **Flow in the fully-saturated zone in the bentonite**

  Not well known yet but also not heavily relevant as it occurs only in the very narrow zone at the bentonite-rock contact.

- **Hydration kinetics**

  This effect is apparently quite differently pronounced depending on the actual situation. Appeared to be negligible in case of uptake under confined conditions.

- **Hysteresis of the isotherm/retention curve**

  Neglected so far. Might become of interest if precise predictions are required. The water content at equilibrium can differ in the order of 5 % for the adsorption and the desorption path.

G3 Sensitivities

G3.1 Impact on understanding

Describe potential impact of model features on overall system understanding.

From more to less sensitive:

- **Conceptual treatment of buffer-rock interaction**

  The concept of the buffer-rock interaction is closely related to the conceptualisation of bentonite re-saturation and to groundwater flow in the rock. As such it should be derivable from those two concepts. For the model discussed here they indicate the possibility of decoupling both processes to a high degree. Since the interaction of buffer and rock depend on the flow mode in the bentonite the two cases must be considered separately.

  In case of flow mode A all water coming from the rock is assumed to be taken up by the buffer. The outflow rate from the rock is thereby assumed to be constant and in the order of the outflow into the open borehole. Fitting boundary conditions at the buffer-rock interface would therefore be a constant hydraulic pressure for flow in the rock and the resulting outflow rate for the water uptake in the bentonite. The re-saturation model for the buffer would thus require data from the groundwater flow model but not vice versa. As a result, coupling of codes for groundwater flow and buffer re-saturation is neither necessary nor advisable.

  In flow mode B permanent full saturation in the bentonite is assumed at the buffer-rock interface. Full water saturation and vapour pressure are thus assumed here for the re-saturation model. Outflow from the rock is not required for the uptake model and flow in the rock is only of secondary interest as it simply decreases with time. Since the bentonite takes up less and less water with time flow would eventually come to a standstill and the undisturbed pressure field would prevail in the pore space of the rock. The groundwater flow model is only used in this case to identify regions where flow mode B for the re-saturation model is applicable. No further coupling is required.

This conceptualisation is radically different from models where flow and re-saturation are described both in terms of two-phase flow. The results from different approaches might not be so different, though. One way or the other, the impact on the overall system understanding would be quite high because either one concept can be rejected or both concepts leave room for decisive improvement.

- **Nature of low permeable skin – flow reduction by the skin**

  Not knowing the nature of the skin and thus not the referring influence factors means that this phenomenon can only be modelled on a highly empirical basis. Since no long-term observations have been made yet the predictive capacity of any model for long-term behaviour is equal to zero.

- **Treatment of the background fractures**

  In the far-field at a not highly resolving scale something like an REV might apply to a fracture network especially if it is not sparse. Independent modelling from at least three different teams has shown that this concept leads to reasonable results at closely resembling permeability values for the effective matrix continuum. A direct comparison of this continuum with a DFN that is based on the available geostatistical data performed in terms of overall flow rates would be quite revealing.

  In the near-field of geotechnical openings, homogenisation does not work, though, because even in the highly fractured rock at Äspö the related REVs are too big on the scale of single boreholes. So either a system of single background fractures and an undisturbed matrix have to be considered as in Task 8c or the hydraulic effects of fractures and matrix have to be combined and subsequently also smeared over a skin zone as in Task 8d.

  Note: it has to be kept in mind that these considerations apply to flow simulation only. In case of transport phenomena this conceptualisation requires extreme care, if it can be used at all.

- **Assumption about reduction or missing narrow saturated zone in the bentonite in case of limited water supply for the bentonite from the rock**

  The assumption about water being buffered in a possibly vanishing saturated zone controls the dynamics of water distribution in the bentonite and consequently also the uptake from the rock. It is consistent with the uptake concept of GRS but it has not been supported by laboratory evidence. Related experiments are presently under development.

- **Boundary conditions for the large fractures**

  Fractures cutting through the geotechnical openings provide a powerful hydraulic shortcut for the groundwater on its way to tunnels and boreholes. If they are completely contained in the model domain they lead to a considerable pressure decrease in the surrounding matrix as they are drawing water from the matrix. In principle, this effect must be captured by the boundary conditions if the fractures are larger than the model domain. This was not the case in Task 8, though, as the pressure field provided by the large-scale flow model did not show such features as if the fractures had not been there. Flow from the fractures as well as from the matrix is therefore too high in the model. However, in the light of all other uncertainties this might still be tolerable.

- **Boundary conditions for the matrix**

  According to the large-scale flow model the pressure at the model boundaries varies considerably. In the light of all the other uncertainties the analytical formulation presented in Appendix D of this report could have been used, though. Even the error by introducing constant pressure conditions appears to be tolerable.

- **Matrix permeability**

  Measured and suggested values for the matrix permeability cover a range of two orders of magnitude. Among the possible explanations for this uncertainty are the different locations from where the samples had been taken, different types of rock and the inhomogeneity of the rock. Often, such a high uncertainty has as strong impact on modelling results. But in case of the system of matrix and background fractures at the BRIE the latter appear to be dominant rendering this uncertainty irrelevant.

- **Assumption of two diffusive processes in the bentonite outside the transition zone**

  While the conceptual models based on diffusive processes and based on THM-approaches are radically different it could be shown that the resulting mathematical models are quite similar (Kröhn 2017). This casts therefore no additional light on system understanding.

- **Single-phase flow in the rock outside the transition zone**

  Since single-phase flow or unsaturated flow at residual gas saturation are hardly discernible the impact on system understanding is low.

- **Omission of the narrow saturated zone in the bentonite**

  This zone has a thickness of just a few millimetres in comparison to the radius of 15 cm of the bentonite parcel. The error on the calculated transient water content distributions is little and thus the relevance to system understanding.

G3.2 Impact on predictions

Describe and – if possible – quantify impact of model features on specific model predictions.

(See Section G3.1.)

G4 Ranking

G4.1 Ranking of features

If possible, rank model features, omissions, simplifications, and assumptions according to their potential impact on overall system understanding and numerical model predictions.

(See Section G3.1.)

G4.2 Weighting of features

If possible, assign weights to the ranked model features, omissions, simplifications, and assumptions.

High relevance

- Conceptual treatment of buffer-rock interaction.
- Nature of low permeable skin – flow reduction by the skin.

Meso relevance

- Treatment of the background fractures.
- Assumption about reduction or missing narrow saturated zone in the bentonite in case of limited water supply for the bentonite from the rock.
- Boundary conditions for the large fractures.

Low relevance

- Boundary conditions for the matrix.
- Matrix permeability.
- Single-phase flow in the rock outside the transition zone.
- Assumption of two diffusive processes in the bentonite outside the transition zone.
- Omission of the narrow saturated zone in the bentonite.

G5 Prediction uncertainty

G5.1 Uncertainty in understanding

Describe the degree of confidence you have about the overall system understanding given conceptual uncertainties and their impact on that understanding.

The main sources of uncertainty can be found on a small scale. They are the stochastic layout of the system of background fractures and the lack of knowledge about the nature of the skin. Both lead to problems describing the system below a resolution of the BRIE test range because fracture location and appropriate process understanding in the skin are required in this case.

G5.2 Uncertainty in predictions

Describe the degree of confidence you have in your model predictions given conceptual uncertainties and their impact on these predictions.

It depends on the scale of interest as described above. For instance, the REV for the network of background fractures appears to be larger than the boreholes at the BRIE-site. Outflow from the rock into such a borehole can therefore only be taken as sort of a mean value. The actual outflow will exceed or fall below that mean depending on the outline of the fracture network. Total outflow into a tunnel system in contrast should be comparatively well predictable.

G6 Calibration and prediction

G6.1 Data uncertainty

Assess the quality of the BRIE and water uptake test (WUT) data, i.e., uncertainties and potential systematic errors.

The data of the WUT is of course less uncertain than the data from the BRIE since a laboratory experiment is usually better controlled than the conditions in the field. Inflow in case of the laboratory experiment can be monitored quite precisely while flow from the rock had proved to change over time without any obvious reason. Also the sheer size of the bentonite parcels does not allow the degree of spatial resolution especially in terms of the water content as in the lab. With a view to reproducing the basic uptake mechanisms under unrestricted water supply for the bentonite the data from the WUT are excellent. In case of Test 3 concerning the flooding of the 1 mm gap this cannot be said with as much confidence, though, since there appears to be a fundamental gap in understanding the persistent increase in water content at the outer boundary.

G6.2 Expected residuals

Describe which component of the measured data the model is expected to reproduce and predict (e.g., order-of-magnitude behaviour, average value, general trend, low-frequency fluctuations, high-frequency fluctuations, all details except measurement error, all details including systematic component of measurement error).

Concerning groundwater flow the modelling exercise aims at the mean outflow from the rock into the boreholes and the TASO-tunnel. Also the spatial distribution over the tunnel floor of the measured total outflow rates into the boreholes was looked at. Finally the trend in the hydraulic pressure in the range of the boreholes was compared with the model. With respect to buffer re-saturation the uptake dynamics in terms of the transient development of the water content were sought. Only simple cases could be addressed, though, because of the geometric restrictions of code VIPER.

G6.3 Prediction of BRIE

Describe how well your model predicted the system behaviour observed during the BRIE experiment.

No predictions for transient data were performed.

G6.4 Calibration to BRIE

Describe how well your model reproduced the system behaviour observed during the BRIE experiment.

Concerning groundwater flow there are two criteria for checking the related model: hydraulic pressure and outflow. The calculated pressure for the vertical boreholes was generally a bit too high while the results for the horizontal boreholes deviated in both directions from the measured values. Maximum deviation was by a factor of 3.

Outflow from the boreholes is met satisfyingly from KO0017G01 if deviation by a factor of 5 can be tolerated. Towards the face the match becomes worse as measured pressure and outflow are apparently not related anymore. This was taken as an indication of the influence from the not resolved background fractures.

The uptake model for the wet section of KO0017G01 matched the measurements of the outer sensor very well. Beyond that, the limits of the very simple model were passed. No statements can be given with respect to the dry sections as no conclusive model could be set up.

According to the low ambitions described in the section “Expected Residuals” the models did thus quite well.

G6.5 Prediction of WUT

Describe how well your model predicted the system behaviour measured during the water uptake test.

The prediction was qualitatively excellent.

G6.6 Calibration to WUT

Describe how well your model reproduced the system behaviour measured during the water uptake test.

The tortuosity in the water uptake model required a moderate correction which led to a very satisfactory fit of measured data and model results.

G7 Specific predictions

G7.1 Predictions

Provide the model-predicted best-estimate value of inflow into the open probing holes KO0017G01 and KO0018G01. Provide the model-predicted best-estimate value of the time for bentonite re-saturation to 95%.

Since outflow from the rock was used as means for calibration there was naturally no prediction of that flow rate. In case of bentonite re-saturation two cases were considered: unrestricted water supply from a fracture and initially restricted water supply from the matrix based on data from the flow model. In the first case 232 days were calculated and 535 days in the second case.

G7.2 Uncertainty

Provide the uncertainty (range or distribution) of these predictions based on parametric uncertainties in the actual model used for these predictions. Describe which parametric uncertainties are considered in this assessment.

The conceptual model for bentonite re-saturation applied here leaves by and large only two sources of uncertainty since it is based on well-known established processes. One is the shape of the adsorption isotherm/retention curve which has been extensively investigated and well established for the bentonite used at SKB. The other is the hardly measurable tortuosity of the pore space and the interlamellar space. However, as modelling the WUT had shown the tortuosity needed to be adjusted only from 0.8 down to 0.28 to provide a very satisfying fit.

G7.3 Conceptual uncertainty

Describe the uncertainty of these predictions accounting for conceptual model uncertainties. Describe which conceptual uncertainties are considered in this assessment.

The two cases predicting the bentonite re-saturation time were influenced each by a certain shortcoming. The model for a bentonite bar reproducing uptake from the fracture could not account for lateral water migration and thus provides only a lower limit for the re-saturation time. The model for limited water supply from the matrix was based on data from the flow model where the outflow rate was a mean including the contribution of background fractures (cp. Section G5.2). It therefore provides also only a lower limit for the re-saturation time.

G8 General assessment

G8.1 Understanding

Describe the main improvement in system understanding gained by performing Task 8.

Highly interesting is the relevance of the different scales of the features involved, most notably the background fractures. While the rock at Äspö is known to be highly fractured, the network of background fractures appears to be sparse on the scale of the BRIE. Of these fractures some are known to exist from the drilling, some became only apparent from the bentography. But in all cases the fracture size was not known. And very little came to light concerning connectivity of these fractures. This means that it makes only very limited sense to put up a stochastic fracture model in order to describe the flow field at BRIE-scale. However, there is also far too little data for a deterministic flow model that accounts deterministically for discrete background fractures.

On a much larger scale with less spatial resolution, though, it appears that treating the background fracture network as a continuum for simulating groundwater flow is viable. Blind predictions of outflow from the rock at specific locations thus become increasingly unreliable with a decreasing size of the area of interest.

Another important lesson learned concerns the bentonite re-saturation. Working on Task 8 brought up the fact that a limited access to water during re-saturation has not been investigated in the laboratory, yet, and had not been considered in the re-saturation model of GRS before.

Less a matter of direct understanding than a matter of identifying a topic for further investigation is the unresolved problem of the skin-effect. Once for all it should be settled what processes are behind this long known but little investigated phenomenon.

G8.2 Change in uncertainty

Describe how uncertainty has changed as new data from BRIE were incorporated into the model.

An important reliance limiting factor was the little data for calibration that were available until Task 8d. Especially the additional outflow data from the new boreholes as well as the effort to acquire some total outflow data were very helpful to set up the flow model. It has to be noted, though, that the preliminary outflow from the new probing boreholes data were unfortunately not confirmed later on.

During the course of Task 8 the value of the so-called undisturbed matrix was corrected several times until a range of possible values was defined that covered 2 orders of magnitude. If the matrix permeability had had a significant influence on the combined continua of matrix and background fractures it would have introduced a high uncertainty for the resulting flow field.

G8.3 Conceptual uncertainty

Describe the degree to which the current conceptual understanding is believed to represent the behaviour of the true system.

The processes that are relevant outside the transition zone (c.f. Section G1.1) in the rock and in the bentonite are believed to be quite well understood. Inside, however, especially the skin related processes are still to be determined. A skin zone where simply the permeability is reduced does not qualify as understanding of the true system at all.

G8.4 Model uncertainty

Describe the degree to which the current numerical model is believed to represent the behaviour of the true system.

While the system might not be understood a model can nevertheless represent its behaviour very well. As elaborated on in Section G8.1 there is an inherent problem setting up a working model for the sparse background fracture network. On the average, though, the current model appears to do a good job to reproduce flow in the rock and re-saturation. The main problem for the model seems to

be the little outflow rate from the rock which could not be established. And of course the long-term behaviour of the skin is presently unknown.

G8.5 Key uncertainty

Describe which aspect of the conceptual or numerical model is the main source of insufficient system understanding and predictive uncertainty.

There appear to be two main fields. While the immediate influence of the skin-effect on the flow field can be estimated from observations, the long-term consequences are totally unknown. And, secondly, water-uptake from a flow-restricted source remains to be looked after in terms of outflow rates from the rock matrix as well as in terms of the re-distribution dynamics in the bentonite.

G8.6 Research plan

Describe how uncertainty in this main aspect could be reduced in general, and what specific changes to the actual model could be made to improve system understanding and to reduce predictive uncertainty.

The highest uncertainties stem from a lack of process understanding (skin, water uptake under limited water access). Improvement of understanding can thus not come from mere model modifications but requires intensive experimental studies.

Arkitektkopia AB, Bromma, 2018

SKB is responsible for managing spent nuclear fuel and radioactive waste produced by the Swedish nuclear power plants such that man and the environment are protected in the near and distant future.

skb.se